JAIME DANIEL BUSTOS VANEGAS

CHARCOAL COOLING KINETICS: COMPUTATIONAL SIMULATION AND INDUSTRIAL APPLICATIONS

Thesis submitted to the Agricultural Engineering Graduate Program of the Universidade Federal de Viçosa in partial fulfillment to the requirements for the degree of *Doctor Scientiae*.

VIÇOSA
MINAS GERAIS – BRASIL
2018

Ficha catalográfica preparada pela Biblioteca Central da Universidade Federal de Viçosa - Câmpus Viçosa

T
B982c
2018

Bustos Vanegas, Jaime Daniel, 1982-
Charcoal cooling kinetics : computational simulation and industrial applications / Jaime Daniel Bustos Vanegas. – Viçosa, MG, 2018.
xiii, 93f. : il. (algumas color.) ; 29 cm.

Texto em inglês.
Orientador: Marcio Arêdes Martins.
Tese (doutorado) - Universidade Federal de Viçosa.
Inclui bibliografia.

1. Carvão - Propriedades térmicas. 2. Carvão vegetal - Resfriamento. 3. Pirólise. 4. Fluidodinâmica computacional. 5. Simulação (Computadores). I. Universidade Federal de Viçosa. Departamento de Engenharia Agrícola. Programa de Pós-Graduação em Engenharia Agrícola. II. Título.

CDD 22. ed. 662.74

JAIME DANIEL BUSTOS VANEGAS

CHARCOAL COOLING KINETICS: COMPUTATIONAL SIMULATION AND INDUSTRIAL APPLICATIONS

Thesis submitted to the Agricultural Engineering Graduate Program of the Universidade Federal de Viçosa in partial fulfillment to the requirements for the degree of *Doctor Scientiae*.

APPROVED: December 17, 2018

_____	_____
Álvaro Messias Bigonha Tibiriça	Jane Sélia dos Reis Coimbra
_____	_____
Jochen Mellmann	Angélica de Cássia Oliveira Carneiro (Co-advisor)

_____

Marcio Arêdes Martins
(Advisor)

This thesis is dedicated…

To my beloved mother Gloria Yolanda,

To my father Jaime,

To my brother Pedro,

To my sister Magda Jhoana,

To my nephew Juan Sebastian.

ACKNOWLEDGMENTS

To my parents, Jaime and Gloria Yolanda, to my brothers Pedro Alfonso and Magda Jhoana, to my nephew Juan Sebastian, for being always united like family, still in the distance. For being my driving force in this and in all my ways.

To my advisors Prof. Marcio Arêdes Martins and Prof. Angélica Cassia de Oliveira Carneiro for their valuable teachings and constant support.

To Dr. Jochen Mellmann for the guidelines and welcome at the ATB in Germany.

To the colleagues of the drying group, for the partnership and good chat at lunch.

To Debora and her family for her love, company and welcome in Viçosa.

To all my family and friends in Colombia, because I know they were cheering for me.

To my colleagues and friends at the Biofuels Laboratory, for their help, partnership and laughter. My respect and admiration for each one of you.

To my friends in Viçosa, for so many times shared. Friendship to the whole life.

To the Universidade Federal de Viçosa and to the Departament of Agricultural Engineering, for the opportunity granted to me.

To CNPq for the scholarship and financial support to carry out my research.

BIOGRAFHY

JAIME DANIEL BUSTOS VANEGAS, son of Gloria Yolanda Vanegas and Jaime Bustos, was born in Ibagué-Tolima (Colombia), on November 9, 1982.

In February of 2000 initiated an undergraduate course in Agroindustrial Engineering at the Universidad del Tolima (Colombia), graduated in April of 2007. Since then, he has worked in the production, quality control, and research and development areas in the food industry.

In April of 2013 began the Master's degree studies in Agricultural Engineering Graduate program at the Universidade Federal de Viçosa, concentrating his studies in the area of storage of agricultural products. In February of 2015 concluded the dissertation entitled “Mathematical modeling of physical properties and heat and mass transfer in coffee beans during roasting”.

In March of 2015 initiated the doctorate in Agricultural Engineering Graduate Program at the Universidade Federal de Viçosa, focusing his studies in the area of Energy in Agriculture. From March to November, 2018, he was Visiting Scholar at Leibniz-Institut für Agrartechnik und Bioökonomie e.V. (ATB), Potsdam, Germany. The thesis has been submitted to the committee in December of 2018, to obtain the *Doctor Scientiae* degree in Agricultural Engineering.

CONTENTS

LIST OF ABREVIATIONS AND SYMBOLS

a	Absorption coefficient
l	Characteristic length, m
γ	Emissivity
C	Constants in the turbulence model
S	Coordinate along the path of radiation
ρ	Density, kg m^{-3}
D	Diameter, m
ε	Dissipation rate of the turbulent kinetic energy, m^2 s^{-2}
L_c	Dome height, m
μ	Dynamic viscosity, Pa s
σ_ε	Equivalent Prandtl number for dissipation of the turbulent kinetic energy
σ_k	Equivalent Prandtl number for the turbulent kinetic energy
β	Expansion coefficient, K^{-1}
$\vec{v}$	Gas velocity vector, m s^{-1}
R_0	Gas universal constant, J mol^{-1} K^{-1}
U	Global heat transfer coefficient, W m^{-2} K^{-1}
Q_r	Heat of oxidation reaction, J kg^{-1}
h	Heat transfer coefficient by convection, W m^{-1} K^{-1}
hr	Heat transfer coefficient by radiation, W m^{-2} K^{-1}
R	Heat transfer resistance, m^2 K W^{-1}
Gr	Grashof number
g	Gravity, m s^{-2}
A_s	Interfacial area, m^{-1}
δ_{ij}	Kronecker delta
Nu	Nusselt number
C_{0x}	Oxygen concentration, kg m^{-3}
ϕ	Phase function for scattering
d_p	Pore diameter, m
φ	Porosity
Pr	Prandtl number
A_0	Pre-exponential factor, s^{-1}

i	Radiation intensity, W m^{-2}
Pk	Rate production of the turbulent kinetic energy, Pa s^{-1}
Ra	Rayleigh number
τ	Reynolds stress tensor
σ_s	Scattering coefficient
ω	Solid angle
C_p	Specific heat, J kg^{-1} K^{-1}
σ	Stefan-Boltzmann constant
T	Temperature, K
k	Thermal conductivity, W m^{-1} K^{-1}
t	Time, s
k^T	Turbulent kinetic energy, m^2 s^{-2}
q'''	Volumetric heat source, W m^{-3}
L_w	Wall height, m
λ	wavelength

Subscripts

$surf$	External surface
ext	External side
b	Floor
f	Fluid phase
HE	Heat exchanger
is	Insulation
i	Interfacial
$s\text{-}i$	Internal surface
m	Overall
s	Solid phase
t	Turbulence
w	Wall

ABSTRACT

BUSTOS VANEGAS, Jaime Daniel, D.Sc., Universidade Federal de Viçosa, December, 2018. **Charcoal cooling kinetics: Computational simulation and industrial applications**. Advisor: Marcio Arêdes Martins. Co-Advisor: Angelica de Cássia Oliveira Carneiro.

Brazil is the largest producer of charcoal from planted forests with 5.5 million tons in 2016. The Brazilian steel industry consumes 85% of the national production of charcoal from eucalyptus. The common-use technology for large-scale charcoal production in the country consists of masonry kilns. Its walls and floor are built using isolation materials that minimize heat losses during the wood carbonization stage. However, the thermal inertia of these components represents additional heat that must be removed during the charcoal cooling stage, as reflected in the extended process time. The long cooling time is also due to the heat generation in oxidation reactions at low temperatures. The intensity of this reactions depends on complex interactions between the interstitial gas and the solid matrix of charcoal. Natural and forced convection heat exchangers have been developed by some companies in an attempt to reduce cooling times. However, there is still a lack of knowledge regarding the dynamics of gas flow inside the kiln and physical-chemical reactions occurring in the charcoal bed, which constitutes a limitation for its optimization. In this scenario, in the first part of this study are presented and discussed the main technologies developed for cooling of carbonization kilns, identifying the challenges for its optimization and the possible impacts on charcoal quality. In the second part, aims to evaluate the effect of the thermal inertia of the kiln structural elements, a typical industrial kiln with a capacity of 700 m^3 was modeled and validated using a set of experimental measurements of temperatures during a 4-day carbonization stage and 8-day cooling stage. A CFD (Computational Fluid Dynamics) analysis was performed to simulate the heating and cooling of the system composed of wood, carbonization gases, brick walls, and floor. In the third part, a laboratory-level experiment was conducted with the objective of evaluating the kinetics of charcoal oxidation at low temperatures by quantifying the heat generated and the oxygen consumed in the reaction. Finally, two and three-dimensional CFD analysis were performed to evaluate the effect of an insulation layer covering the floor and a buoyancy-driven heat exchanger on the cooling time. With the results of this research, it can be concluded that there is still a great opportunity for improvement and optimization of cooling systems for carbonization kilns. The temperature profile in the walls approaches to a pseudo-steady state, allowing to model

this domain as a boundary condition. The heat transfer at the floor is extensive; therefore, the adiabatic boundary condition cannot be imposed at the bed – floor interface. A 3 cm layer of insulation concrete over this interface could reduce the energy requirement for the carbonization stage in 6% and could reduce the cooling time in almost 2 days. The use of a buoyancy-driven flow heat exchanger can reduce the cooling time between 27 and 59%, increasing productivity per kiln per year up to 65%. The rate of oxygen consumption increases with charcoal temperature at rates that depend on the initial concentration of O_2. The beginning of the oxidation reactions was observed at 67 °C in atmospheres with 20.9% O_2. The overall activation energy for the self-heating phenomenon was 17790 J mol^{-1} and its intensity was increased with the temperature and O_2 concentration. Our findings provide important information for the improvements in the kiln operation and allow the establishment of consistent initial conditions of temperature and heat flux for kinetics models for charcoal cooling in kilns.

RESUMO

BUSTOS VANEGAS, Jaime Daniel, D.Sc., Universidade Federal de Viçosa, dezembro de 2018. **Cinética de resfriamento de carvão vegetal: simulação computacional e aplicações industriais**. Orientador: Marcio Arêdes Martins. Coorientador: Angelica de Cássia Oliveira Carneiro.

O Brasil é o maior produtor de carvão vegetal de florestas plantadas, com 5,5 milhões de toneladas em 2016. A indústria siderúrgica brasileira consome 85% da produção nacional de carvão vegetal produzido a partir de eucalipto. A tecnologia de uso comum para a produção de carvão em larga escala no Brasil consiste em fornos de alvenaria. Suas paredes e piso são construídos usando materiais isolantes que minimizam as perdas de calor durante a fase de carbonização da madeira. No entanto, a inércia térmica desses componentes implica uma carga térmica adicional que deve ser removida durante a etapa de resfriamento, resultando em longos tempos de operação. A baixa taxa de resfriamento também é devido à geração de calor em reações de oxidação a baixas temperaturas. A intensidade dessas reações depende de interações complexas entre o gás intersticial e a matriz sólida do carvão. Trocadores de calor por convecção natural e forçada foram desenvolvidos por algumas empresas na tentativa de reduzir os tempos de resfriamento. No entanto, ainda há falta de conhecimento sobre a dinâmica do fluxo de gás no interior do forno e reações fisico-quimicas ocorrendo no leito de carvão, o que constitui uma limitação para sua otimização. Neste cenário, na primeira parte deste estudo são apresentadas e discutidas as tecnologias atualmente desenvolvidas para resfriamento de fornos de carbonização, identificando os desafios para sua otimização e os possíveis impactos na qualidade do carvão vegetal. Na segunda parte, foi avaliado o efeito da inércia térmica dos elementos estruturais do forno. Um forno industrial retangular com capacidade de 700 m^3 de madeira foi modelado e validado usando um conjunto de medidas experimentais de temperaturas durante um período de 4 dias de carbonização e 8 dias de resfriamento. Uma análise CFD (Computational Fluid Dynamics) foi realizada para simular o aquecimento e resfriamento do sistema composto de madeira, gases de carbonização, paredes e piso. Na terceira parte, um experimento ao nível de laboratório foi conduzido com o objetivo de avaliar a cinética de oxidação do carvão vegetal a baixas temperaturas quantificando o calor gerado e o oxigênio consumido na reação. Finalmente, foram realizadas análises CFD em duas e três dimensões objetivando avaliar o efeito de uma camada de isolamento térmico cobrindo o piso e de um trocador de calor acionado por convecção natural no tempo e homogeneidade do resfriamento. Com os resultados

desta pesquisa pode se concluir que ainda existe uma grande oportunidade de melhora e otimização de sistemas de resfriamento para fornos de carbonização. O perfil de temperatura nas paredes se aproxima de um estado pseudo-estacionário, permitindo modelar este domínio como uma condição de contorno. A transferência de calor no piso é extensa; portanto, a condição de fronteira adiabática não pode ser imposta na interface leito-piso. Uma camada de 3 cm de concreto isolante sobre essa interface poderia reduzir a demanda de energia para o estágio de carbonização em 6% e reduzir o tempo de resfriamento em quase 2 dias. O uso de um trocador de calor de fluxo acionado por convecção natural pode reduzir o tempo de resfriamento entre 27 e 59%, aumentando a produtividade por forno por ano em até 65%. A taxa de consumo de oxigênio aumenta com a temperatura do carvão a taxas que dependem da concentração inicial de O_2. O início das reações de oxidação foi observado a 67 °C em atmosferas com 20,9% de O_2. A energia de ativação global para o fenômeno de auto-aquecimento foi 17790 J mol^{-1} e sua intensidade aumentou com a temperatura e a concentração de O_2. Nossas descobertas fornecem informações importantes para melhorias na operação do forno e permitem o estabelecimento de condições iniciais consistentes de temperatura e fluxo de calor para modelos cinéticos de resfriamento de carvão vegetal em fornos de alvenaria.

1. GENERAL INTRODUCTION

Perhaps renewables saw the highest growth rate of any energy source in 2017 (now account for 25% of global electricity generation), the global economic growth, lower fossil-fuel prices, and weaker energy efficiency efforts, result in an increase of 460 million tons of energy-related CO_2 emissions in the same year (IEA 2017). In order to meet the goals of the Paris Agreement on climate change, greater efforts should be directed towards energy efficiency and reduction of greenhouse gases, mainly CO_2 emissions (Tanaka and O'Neill, 2018).

The iron and steel industry is responsible for more than 5 % of the anthropogenic CO_2 emissions worldwide (Fick et al., 2013) and approximately 27% of CO_2 emissions from the global manufacturing sector (Hasanbeigi et al., 2014). This fact is basically due to the use of coal as a source of carbon for the reduction of iron ore. In this context, research points to biomass as an alternative source of carbon (Kokonya et al., 2013; Fick et al., 2013; Montiano et al., 2014; Nakahara et al., 2015), which, because of its renewable character, contributes to cleaner production. Abreu et al. (2015) concluded that replacing 50% of coke by charcoal in iron ore sinter production, productivity remains the standard level and may result in a 50% reduction in greenhouse gas emission.

Brazil stands out as the largest producer and consumer of charcoal. In the last decade, the national pig iron industry consumed in average 6.9 million tons per year, representing a 25-35% share of charcoal as a reducer (CGEE 2015). Charcoal presents quality characteristics suitable for use as a reducer in the steel industry, but its limited use is due in part to the higher cost when compared to coke from coal. In this scenario, the producing companies and in some cases aligned with the academic has been developing technologies that aim at a more efficient and sustainable production. Research has focused on the use of the enthalpy of carbonization gases for wood drying or power generation (Coelho 2013; Pereira et al., 2017) and the optimization of the production cycle.

The common-use technology for large-scale charcoal production in Brazil consists of masonry kilns. The production cycle takes an average of 4 days for the carbonization step (reaching a final temperature between 350 and 400 °C) and 8 days for the cooling stage (reaching a final temperature of about 60 °C). During the carbonization stage, the insulation characteristics of this structure minimize energy losses. In contrast, during cooling, the energy accumulated in the mass of charcoal is hardly dissipated through the walls and floor, which reflects in long operating times and consequently, low productivity

per kiln. Some systems using forced convection heat exchangers have been developed and tested achieving reductions of up to 50% of the cooling time (Santos 2013; Martins 2014; Oliveira et al. 2015). During cooling, the atmosphere inside the kiln undergoes a depressurization. Then, the tension exerted on the walls tends to generate small cracks through which the outside air can infiltrate. Oxygen in the air reacts with the charcoal particles reactivating pyrolysis reactions, generating heat and making cooling even more difficult. Knowledge of the kinetics and intensity of these reactions is key to the planning and optimization of cooling systems.

In view of the above, this research was focused on the understanding of the physical-chemical phenomena associated with the charcoal cooling stage in masonry kilns looking for the optimization of cooling systems. The study was divided into four parts in the form of articles. In the first part, as a review, the state of the art of cooling systems, the challenges for its implementation and the possible effects on the quality of the charcoal are presented. In the second part, a mathematical model to quantify the thermal inertia of the kiln structure during the carbonization and cooling stages was formulated and validated with experimental data.

In the third part, a laboratory-level experiment was conducted with the objective of evaluating the kinetics of charcoal oxidation at low temperatures. The energy released in the reactions and their relation with the oxygen concentration was quantified.

Finally, using the mathematical model previously validated in the second part, a 2D CFD study was performed aiming to quantify the effect of an insulation layer over the floor. Then, a three-dimensional CFD study was carried out pointing at the optimization of a buoyancy-driven heat exchanger.

1.1 REFERENCES

Abreu G C, Andrade J, da Silva B, Pedrini R. Operational and environmental assessment on the use of charcoal in iron ore sinter production. Journal of Cleaner Production. (2015), doi: 10.1016/j.jclepro.2015.04.015.

CGEE Centro de Gestão e Estudos Estratégicos. Modernização da produção de carvão vegetal no Brasil: subsídios para revisão do plano siderurgia – Brasilia. 2015. 150p.

Coelho, M P. Desenvolvimento de metodologia para o dimensionamento de câmaras de combustão para gases oriundos do processo de carbonização de madeira. Viçosa, Brasil. [dissertation]: Universidade Federal de Viçosa. 2013.

Hasanbeigi A, Arens M, Price L. Alternative emerging ironmaking technologies for energy-efficiency and carbon dioxide emissions reduction: A technical review. Renewable and Sustainable Energy Reviews. 2014;33:645-658.

IEA International Energy Agency. Global energy & CO2 status report 2017. https://www.iea.org/publications/freepublications/publication/GECO2017.pdf (accessed November 2018).

Konkonya S, Castro-Díaz M, Barriocanal C, Snape C. An investigation into the effect of fast heating on fluidity development and coke quality for blends of coal and biomass. Biomass and Bioenergy. 2013;56:295-306.

Martins, M. A., 2014. Desafios da implementação de periféricos na produção de carvão vegetal. In: I SEMINARIO DE CARVÃO VEGETAL. Aperam Bioenergia. Universidade Federal de Viçosa.

Montiano M G, Díaz-Faes E, Barriocanal C, Alvarez R. Influence of biomass on metallurgical coke quality. Fuel. 2014;116:175-182.

Nakahara T, Yan H, Ito H, Fujita O. Study on one-dimensional steady combustion of highly densified biomass briquette (bio-coke) in air flow. Proceedings of the Combustion Institute 35 (2) (2015) 2415-2422.

Oliveira, A. C., Carneiro, A. de C., Barcellos, D. C., Rodriguez, A. V., Amaral, B. M., Pereira, B. L., 2015. Resfriamento artificial em fornos retangulares para a produção de carvão vegetal. Revista Árvore Viçosa-MG 39 (4), 769-778.

Pereira, E. G., Martins, M. A., dos Santos, L. F., Carneiro, A. de C., 2017. Energy Assessment of Wood Pyrolysis Coproducts for Drying and Power Generation. Energy & Fuels 31(12), 13815-13823. DOI: 10.1021/acs.energyfuels.7b02998

Santos I. Resfriamento artificial de carvão vegetal em fornos de alvenaria [dissertation]. Universidade Federal de Viçosa; 2013.

Tanaka K and O'Neill B. The Paris Agreement zero-emissions goal is not always consistent with the 1.5 °C and 2 °C temperature targets. Nature Climate Change. 2018;8:319-324.

2. CHAPTER I: ARTIFICIAL COOLING OF CARBONIZATION KILNS: CHALLENGES IN PRODUCTIVITY AND QUALITY

ABSTRACT. Brazil stands out as the largest producer and consumer of charcoal from planted forest, being the iron and steel industries the main consumer. The producers face challenges to maximize productivity and minimize environmental impact while maintaining the quality of the charcoal produced. Charcoal is produced in masonry kilns which by its insulating characteristics benefits the carbonization stage but makes cooling difficult. The cooling stage consumes between 60 and 70% of the total process time, reflecting in a low productivity per kiln. This scenario has encouraged companies to develop artificial systems based mainly on evaporative cooling and forced convection. However, there is still a void in the knowledge of process kinetics, addressing self-heating reactions as well as the impact on the yield and quality of the charcoal produced. In this review are presented and discussed the main technologies developed for cooling of carbonization kilns, identifying the challenges for its optimization and the possible impacts on charcoal quality.

KEY WORDS: *charcoal, modeling, pyrolysis, heat transfer*.

2.1 INTRODUCTION

Charcoal is a type of biomass of high energy density resulting from the process of wood carbonization (for industrial purposes, mainly of eucalyptus wood). Although there was a fall in production of 16% between 2010 and 2015, as a result of the fall in the steel production sector, Brazil stands out as the largest producer and consumer, reaching 6.1 million tons in 2016 (EPE, 2017). 85% of the production is destined for industrial consumption, mainly as a bio-reducer of iron ore in the pig iron and steel companies (EPE, 2017). In the internal market, the state of Minas Gerais stands out as the largest producer and consumer with an average consumption of 2.6 million tons in 2016 (IBA, 2017).

The main thermo-reducers sources of iron ore used by the pig iron industry are coke (from coal) and charcoal. The latter presents comparative advantages in reference to its lower content of sulfur, nitrogen, and heavy metals, elements that may adversely affect the quality of the steel (Nakahara et al., 2015), and in reference to its renewable character, contributing to the reduction of CO_2 emissions.

In industrial scale the production of charcoal is carried out in rectangular masonry kilns, that varies between 50 and 2000 m^3 of capacity. The insulating characteristics of the wall's kiln are suitable to the carbonization stage, but inconveniences to its cooling. Therefore, the cooling process involves in addition to the charcoal bed, the stagnant gases and the structural elements of the kiln, that is, floor and walls.

The production cycle in a 700 m^3 kiln extends on average for 12 days. Of these, 4 days correspond to the pyrolysis stage (drying and carbonization) and 8 days to the cooling stage. The long cooling time reflects in a low productivity per kiln. In order to accelerate this step, artificial cooling systems using heat exchangers and water in liquid form and steam, have been developed (França and Campos, 2002; Oliveira et al., 2010; Santos, 2013; Martins, 2014; Oliveira et al., 2015). In some cases, these systems have been able to reduce the cooling time by up to 50%.

The technologies currently available for artificial cooling were mostly developed by the steel companies and did not have extensive scientific documentation. It is worth noting that these technologies despite the advances already achieved, need to be optimized, deepening in the knowledge of the reactions that may occur during the process, gas flow patterns inside the kiln and possible impacts on charcoal quality. In this sense,

this work will be presented in the format of a literature review related to technologies currently implemented or tested for artificial cooling of carbonization kiln, addressing their advantages and disadvantages and possible impacts on product quality.

2.2 CHARCOAL PRODUCTION PROCESS

The charcoal production is based on a thermochemical process known as slow pyrolysis. The quality of the charcoal produced depends on the wood quality and the carbonization parameters (final temperature and carbonization rate). This process occurs initially in an endothermic phase characterized by drying the wood (150 °C - 180 °C) followed by the degradation of hemicelluloses (180 °C - 270 °C). Soon the process enters an exothermic phase with degradation of cellulose (270 °C - 350 °C) and carbon concentration above 350 °C (Figure 1) (Peláez-samaniego et al., 2008; Rezende, 2006, Souza, 2016). Carbonization of wood consists basically of concentrating carbon and expelling oxygen through the action of heat, with consequent increase in the energy content of the product (Vale and Gentil, 2008; Carneiro et al., 2013). On average, at the end of the process the products obtained are charcoal (30%), condensable gases (42%) and non-condensable gases (28%) (Carneiro et al., 2013). The condensable gases are a mixture of steam and pyrolignous liquid, composed mainly of acetic acid, methanol and aromatic compounds. The non-condensable gases correspond to N_2, CO_2, CO, CH_4, H_2 and hydrocarbons. Some researches have been conducted looking for the use of the high energy content of these gases in wood drying or power generation (Coelho, 2013; Pereira et al., 2016), resulting in an economically and ecologically sustainable operation.

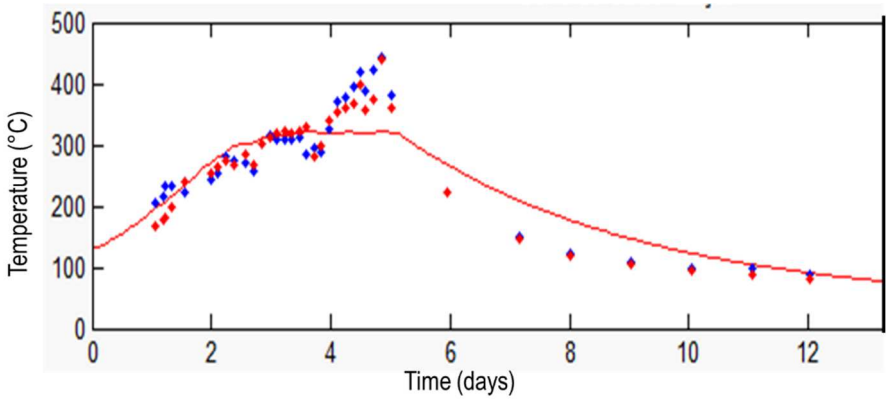

Figure 1. Standard carbonization curve. Souza, 2016.

The average time of the carbonization stage in a rectangular kiln with 700 m^3 of nominal capacity is approximately 4 days, while the cooling by natural convection last between 8 and 13 days depends on the environmental conditions (Oliveira et al., 2010). The thermal degradation of the wood during its carbonization reduces its volume by more than 50% creating a headspace in the upper part of the kiln. The hot gases in this space direct the carbonization front from top to bottom. Similarly, during cooling, the gases in the headspace cool faster than the charcoal bed and direct the cooling front from the top down. The cooling rate decreases exponentially due to gas stagnation, as a consequence of the lower buoyancy force when temperature difference decrease. Therefore, the cooling stage consumes most of the time in the production cycle since it must guarantee an average bed temperature (safety temperature) that prevents ignition breakouts when opening the kiln. From field experience, this temperature has been set between 50 and 60 °C in the upper region of the kiln.

The usual practice for the kiln cooling is the manual and mechanical application of mortar (a mixture of clay and water) on the walls (Figure 2). This is done one to five times a day during the first days of cooling. The objectives are to seal any air infiltration that could reactivate the pyrolysis reactions, reheating the charcoal bed (Vital et al., 2013, Oliveira et al., 2015), and to increase the heat transfer rate between the walls and the environment by evaporative cooling. In this way, the charcoal mass and the stagnant gases inside the kiln exchange heat with the walls by conduction, convection, and radiation, and these, in turn, transfer heat to the environment by natural convection and radiation. In this configuration, due to the low thermal conductivity of the wall material and poor advection of gases in the headspace, the cooling takes a long time (Fig. 1), leading to a low productivity per kiln. In addition, charcoal particles with high-ignition risk remain in the lower part of the bed, and a common practice at the time of opening the kiln is the spray of water over the bed, which may result in a decrease in the mechanical strength of the charcoal.

Figure2. Application of mortar over the carbonization kiln in the cooling stage. PAM Bioenergy (2016).

2.3 ARTIFICIAL COOLING SYSTEMS

Forced convection systems using gas-air and gas-water type heat exchangers and natural convection heat exchangers (Figure 3) have been tested on pilot and industrial scale achieving significant gains in cooling time. Furthermore, water in liquid form and steam has been used directly as refrigerant fluid. It should be noted that these technologies, so far, have been developed mostly by the producing companies, so few results have been published in scientific journals.

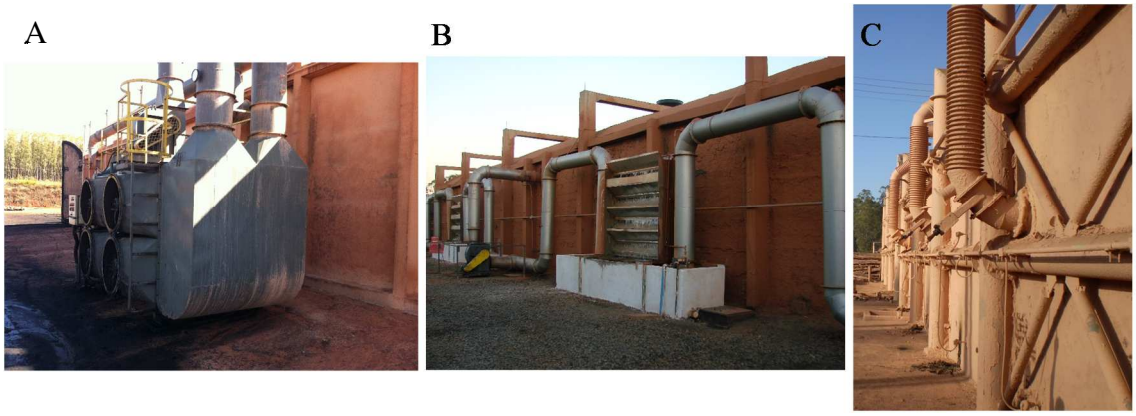

Figure 3. Heat exchanger tested by charcoal companies. A) gas/air type. B) gas/water type. C) Natural convection type. Martins (2014).

2.3.1 State of the art of technologies for artificial cooling of carbonization kilns

The Vallourec company using water foggers on the charcoal bed during the first day of cooling, was able to reduce the cooling time of rectangular furnaces from 12 to 6 days. A total of 10,000 L of water was consumed and the excess water in the bed resulted in a decrease in the mechanical strength of the charcoal (France and Campos, 2002). Although this technique is efficient in reducing cooling time, it presents operational limitations in regions with water deficit, and results in charcoal which may not meet the quality requirements of the metallurgical industry.

Oliveira et al. (2010) tested the cooling of a kiln with a capacity of 3.5 ton of wood using steam at 112 °C as refrigerant. The steam was generated in an aquatubular boiler and was injected at the bottom of the charcoal bed from the beginning of the cooling and for 12 h. At this point, the average bed temperature reached the temperature of the steam, so its injection was stopped and the cooling continued for 12 hours more by natural convection. Although a reduction of 50% in total cooling time was achieved, the quality parameters of the charcoal produced were changed. The volatile content increased from 21 to 27% and fixed carbon fell from 77 to 72%. The true porosity increased from 70 to 78%, the friability from 45 to 52% and the moisture content remained constant.

The reduction of the fixed carbon content, compensated by the volatile content increase, may be related to the shorter contact time between the solid carbon matrix and the gases inside the kiln. The increase in friability may be a consequence of the rapid evaporation of water droplets within the solid matrix of the charcoal particles. The sudden increase in pressure caused by this rapid evaporation can break the charcoal matrix, generating cracks and pores that weaken its structure.

Santos (2013) analyzed the influence of a forced gas flow on the cooling dynamics of the charcoal bed and on the quality of the charcoal produced. A heat exchanger of the shell-and-tube type was coupled to a 3.5-ton capacity kiln. To force air and gas flow, two centrifugal fans were used: one blowing air into the heat exchanger and the other at the exchanger outlet, injecting the cooled gas into the kiln (Fig. 4).

Three gas velocities were tested obtaining reductions in the cooling time ranging from 50 to 63% (Table 1). The fans operated during the first 12 h of cooling. The largest reduction was obtained using the lowest flow velocity (0.034 m s^{-1}) percolating the charcoal mass. The increase in the gas flow had an adverse effect on the cooling due to

the occurrence of combustion points in the areas near the gas suction, as a consequence of the air infiltration caused by the pressure drop between the suction and the gas injection. To avoid that problem, the author suggests increasing suction and injection areas and keeping the pressure drop below 140 Pa. The author verified that the fast cooling did not cause significant variation of the charcoal quality parameters.

Table 1. Operating parameters of the cooling system proposed by Santos (2013)

Frequency (Hz)	Gas flow ($m^3\ s^{-1}$)	Superficial velocity ($m\ s^{-1}$)	Saved time	Pressure drop (Pa)
30	0.1243	0.034	63.0 %	139
45	0.2196	0.060	56.6%	238
60	0.3981	0.108	50.0%	353

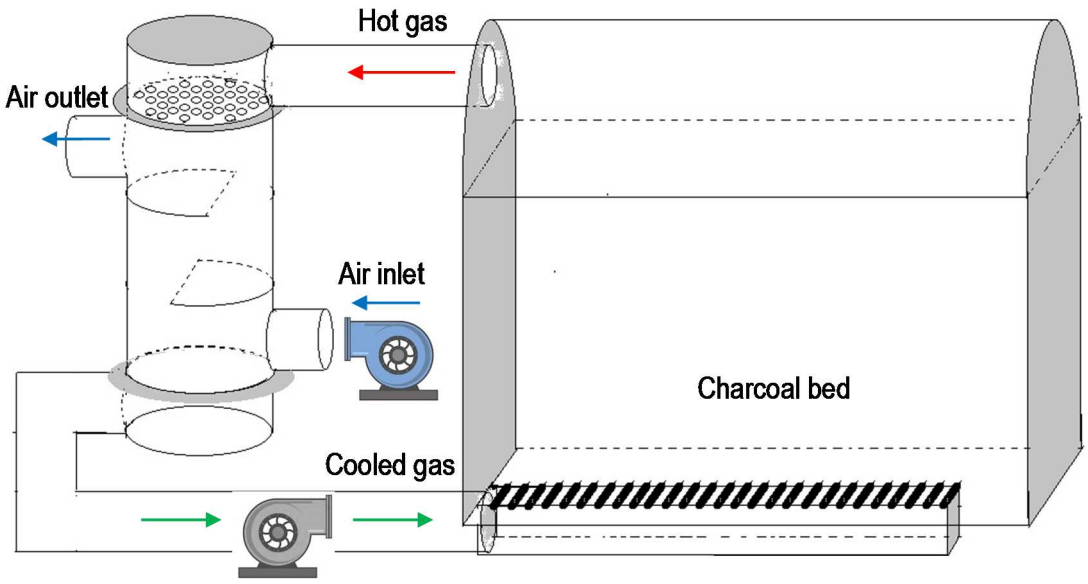

Figure 4. Heat exchanger coupled to the carbonization kiln (Santos, 2013).

Martins (2014) carried out a study on energy consumption in heat exchangers (gas/air type) aiming at the optimization of its operation. Using a centrifugal fan, the hot gases were sucked from two points (close to the doors) in the top of the kiln and forced through the heat exchanger (Figure 5). The cooled gases were injected on the opposite side of the kiln at four equidistant points. Four gas velocities defined by the fan frequency (15, 20, 30 and 60 Hz) and two injection height (top and bottom) were tested.

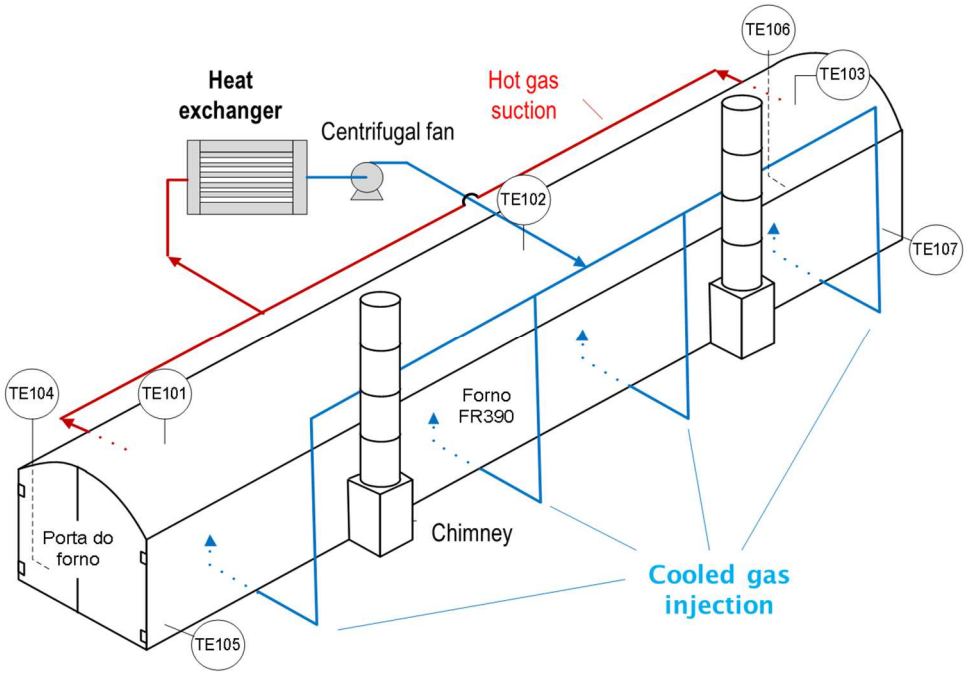

Figure 5. Cooling system tested by Martins 2014.

Cooling time reductions of 43 and 71% were achieved with gas injection in top and bottom, respectively. Due to the resistance exerted by the charcoal bed, a higher frequency was required when injecting into the bottom. The optimum performance of the heat exchanger was achieved using a frequency of 30 Hz in the cooling from top and 40 Hz in the cooling from the base. Cooling from the bottom resulted in shorter times and more homogeneous temperatures within the charcoal mass. However, the higher ventilation power required results in higher operating costs. Besides that, due to greater pressure drop between the injection and suction lines, the risk of air infiltration could increase.

Oliveira et al. (2015) evaluated the reduction of the cooling time in rectangular masonry kilns of 320 m^3 wood capacity using three models of heat exchangers. The equipment specification and results are summarized in Table 2. Steel ducts of 0.8 mm thick and 400 mm diameter were used to conduce the hot gases through the heat exchangers. The suction and injection points were located at 3.8 m height. Figure 6 shows the lateral view of the three models tested. In Model 1 the external wall of the duct was exposed to natural convection with the environment. In the other models a portion of the heat exchange area was keep in water immersion.

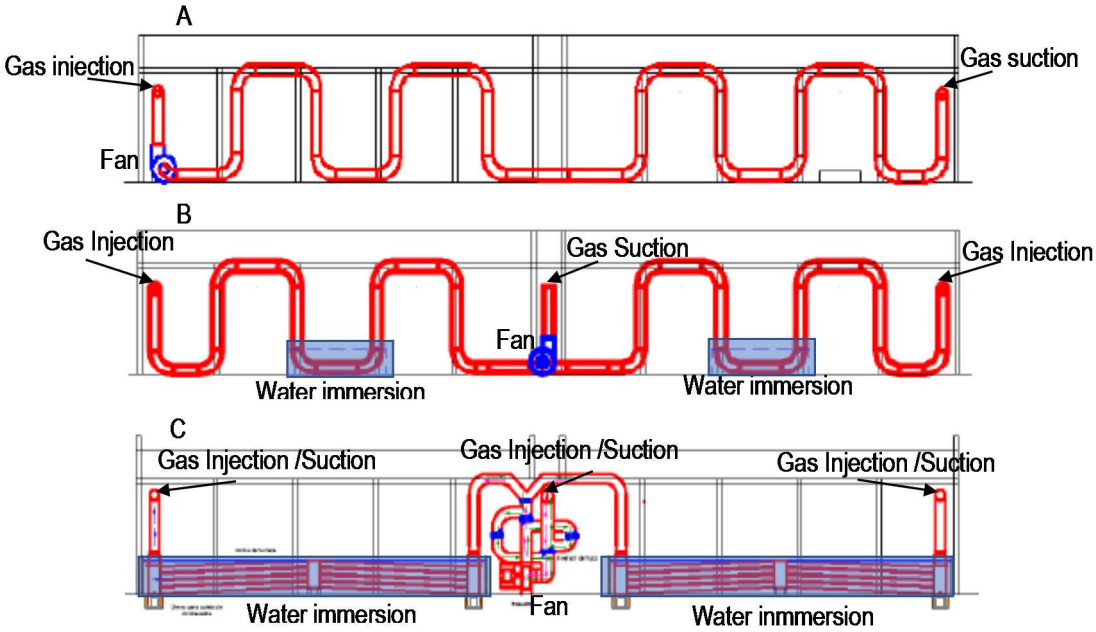

Figure 6. Lateral view of the carbonization kiln with coupled heat exchangers. A) Model 1. B) Model 2. C) Model 3. (Oliveira et al., 2015).

Table 2. Heat exchangers tested by Oliveira et al. (2015)

Model	Heat exchanger type	Heat exchange area (m^2)	Fan Power (HP)	Saved time
Model 1	Gas/air	125	5	12.5%
Model 2	Gas/air-water	gas/water : 35 gas/air : 90	5	38.0%
Model 3	Gas/air-water	gas/water : 330 gas/air : 30	10	43.0%

In model 1 the fan remained on during the entire operation. The suction at one point at the end of the kiln created a pressure drop that caused air infiltration in this region, and foci of combustion were detected during the opening. An inhomogeneous cooling was achieved with this model. As expected, due to the higher heat transfer coefficient of water, the use of gas/water exchangers resulted in shorter cooling times. In model 2 the combustion foci were detected in the central region of the kiln, where gas suction is located. In model 3 the fan was equipped with a frequency inverter, which allowed to change the points of injection and suction. In this configuration the heat exchange area

was increased in 300%, reflecting in a high heat flow rate and minimum cooling time. The homogeneity of the cooling was improved by injecting the gases at the center of the kiln. Despite the best results obtained with model 3, the 50% increase in ventilation power can be a limitation for its implementation.

2.3.2 Technological challenges of artificial cooling of carbonization furnaces

There are several technical challenges to be overcome for the successful implementation of artificial cooling systems in carbonization kilns:

- Residual pyrolysis as a consequence of the air infiltration resulting from the pressure drop between suction and injection of the cooled gases;
- The increase of the charcoal moisture when it is cooled with water;
- The insulation characteristics of the construction materials of the kilns;
- The mathematical modeling of the cooling phenomenon, due to the anisotropic condition of the charcoal bed and to constitute a conjugated problem of heat and mass transfer.

It should be noted that the first challenge to solve should be the mathematical modeling, since a validated model could be used in computational simulation to test the possible solutions to the other challenges, minimizing time and experimental cost.

2.3.2.1 Residual pyrolysis

Carbonaceous materials like wood, wood sawdust, pulp chips, hay, straw, charcoal, among others, tend to self-heating and spontaneous combustion when its surface reacts exothermally with oxygen in the air even at normal temperature (Perdochova et al., 2015). Besides energy, the reaction release hydrocarbons, carbon monoxide, carbon dioxide, water, and, in lower amounts, nitrogen and hydrogen (Wang et al., 2003). In the oxidation reaction, the consumption of 1 mole of O_2 can generate 1 mole of CO_2 and approximately 0.1 moles of CO.

The intensity of the reaction, measured as the amount of energy released, depends on the oxygen concentration (Perdochova et al., 2015; Yuan and Smith, 2013). Spontaneous combustion occurs when the heat withdrawn to surroundings is less than the heat generated in the reaction and the substance reaches its ignition point. We call “residual

pyrolysis" the oxidation reactions at low temperatures that continue to occur in the charcoal bed after the completion of the carbonization stage.

The study of the kinetics of residual pyrolysis becomes of vital importance since the artificial cooling of carbonization kilns will only be effective if the heat dissipated by the system is greater than the heat generated in the reactions of residual pyrolysis. Although these reactions have been studied in the storage of coal (Xuyao et al., 2010, Yuan and Smith, 2012, Taraba et al., 2014, Xia et al., 2015, Zhang et al., 2016), knowledge and quantification of the heat generated by these reactions in the charcoal bed remains an unsolved problem.

As observed by Santos (2013), Martins (2014), and Oliveira et al. (2015), forced convection inside the kiln create pressure gradients between the suction and the injection of the cooled gases, allowing the infiltration of air by the cracks in the walls. When the charcoal comes into contact with the air, an exothermic heat flux proportional to the concentration of oxygen diffusing in the charcoal will be generated due to the oxidation reactions (Wang and Yan, 2008; Cocchi, 2014). Carbonization gases contain oxygen at varying concentrations depending on the carbonization phase (14 - 19%) (Coelho, 2013), and the oxidative exothermic reactions can be activated at specific locations depending on the [O_2]-temperature binomial. The energy released in these reactions causes an increase in temperature, reaching the flash point and generating breakouts of combustion in scenarios where the convection is not enough to dissipate the heat generated.

According to Uhart (1972), the flammability temperature is related to the percentage of oxygen absorbed by the charcoal during its production and this in turn, is a function of the final carbonization temperature. The concentration of O_2 absorbed by the charcoal tends to increase to a maximum value of 31% at the carbonization temperature of 430 °C, resulting in a minimal flammability temperature of 150 °C (Uhart, 1972).

2.3.2.2 Construction materials of carbonization kilns

The function of the carbonization kilns is to maintain the mass of wood in a confined environment, so that the carbonization parameters can be controlled. The kiln structure must withstand the pressure increase during the carbonization phase due to the production of gases, and likewise, withstand the pressure drop at the beginning of the cooling, when

the furnace is completely closed. This pressure drop is responsible for the formation of cracks in the walls, which allow the air infiltration making it difficult to cool.

Therefore, the kilns are designed and constructed in such a way as to minimize thermal losses and gas exchange with the environment. Cost, functionality and durability are parameters that guide the choice of construction materials. The bricks used in the construction of the walls are made of clay and joined with mortar, this configuration being of low cost and with insulating characteristics appropriate for the carbonization phase, but it makes difficult the heat dissipation during the cooling.

The tendency among companies is to use a clay brick 11 cm wide, 5 cm high and 23 cm long. Some companies tested larger size bricks (21x10x22 cm and 21x10x40 cm) that facilitate construction and improve sealing, but there are no documented results on the advantages or disadvantages of this configuration.

The floor of the masonry furnaces generally corresponds to the soil of the region in which the company was established. In general, they are clayey soils and depends on its thermal properties, it can have a significant thermal inertia. This is related to the amount of energy in the form of heat that is "retained" in the kiln floor once the carbonization stage is finished. During cooling, this energy could return to the charcoal bed increasing the thermal load that must be dissipated. This condition reflects in longer cooling time. Some producers tested the application of a layer of concrete on the floor, but there is still no scientific documentation about the effect on the carbonization and cooling stages. It could be expected that a layer of insulation concrete on the floor would minimize the reheating of the charcoal bed during the cooling step. This hypothesis could be tested in a simulation study.

2.3.2.3 Cooling using water

Cooling of a hot body through the forced flow of a fluid over its surface is known as forced convection cooling. This heat exchange mechanism is based on Newton's cooling law, where the heat flux being withdrawn from the body is proportional to the temperature gradient between the fluid and the body surface, and to the heat transfer coefficient by convection (h). This coefficient depends on the properties of the fluid and the flow conditions, being up to 100 times higher for liquids than for gases (Bergman et al., 2011). In addition, liquid water has a high latent heat of vaporization, 2257 kJ kg^{-1} at 100 ºC

(Bergman et al., 2011). Therefore, the use of water in the cooling of charcoal can be a good alternative from the technical point of view.

However, one of the limitations of the use of water is its availability, in addition to being able to decrease the charcoal resistance, altering its quality parameters. The charcoal moisture is directly related to its friability (Vital et al., 2013), thus, wetter charcoal may have lower mechanical strength, which is an undesirable characteristic for the iron industry. According to SBRT (2014), the hygroscopicity of charcoal varies according to the carbonization temperature: the higher the temperature, the lower the water absorption capacity (approximately 4% for charcoal obtained at 450 ºC). Research carried out at the company Vallourec Florestal tested the cooling of kilns by sprinkling liquid water on the surface of the charcoal bed. They verified that the thermal exchange was increased reflecting in a lower cooling time, however, the quality of the charcoal was reduced due to the increase of its friability (França and Campos, 2002).

One way to minimize the problem of increasing charcoal moisture due to the use of liquid water as a refrigerant is the use of saturated or superheated water vapor. The steam, with a temperature above 100 °C, comes into contact with the charcoal bed, initially at a temperature close to 400 °C. Thus, the bed transfers heat to the steam and this reaches the overheating condition, which ensures that there will be no condensation on the bed. Another advantage of the use of steam as a refrigerant is the ease of percolating the charcoal bed, leading to a more homogeneous cooling.

Among the main limitations of the use of steam for kiln cooling are its generation cost and the lowest potential cooling when compared to liquid water. An alternative to overcome the problem of generation cost is proposed by the DPC (Drying-Pyrolysis-Cooling) technology, making use of water, in the form of steam that is removed from the wood itself during the drying stage. DPC carbonization technology processes the drying, carbonization and cooling stages simultaneously and independently in three interconnected reactors. The carbonization gases are burned, providing energy for drying and ignition of the wood pyrolysis. The steam generated during drying is conducted to the reactor in the cooling stage, improving the thermal exchange and reducing the process time. Although this technology is less polluting and more efficient in energy use, its cost of implementation is still limiting in the current scenario for charcoal producers in Brazil (CGEE, 2015).

The operating principle of the DPC system could be implemented in companies with masonry kilns. At present, companies try to optimize the burning of the gases by means of the kiln synchronization. The objective is to provide the combustion chamber of the burner with high-power gases, maintaining the combustion without auxiliary fuel (wood or semi-carbonized wood). In the same way, the gas generated in the initial stage of carbonization, rich in water vapor and low calorific value, could be directed to the kilns in the cooling stage, accelerating the process. The above is a great technological challenge because this gas also contains oxygen at concentrations that could activate residual pyrolysis reactions, creating an adverse effect.

In this scenario, mathematical modeling and simulation assisted by computational fluid dynamics, is emerging as a tool for the planning of cooling systems and to support decision-making in the sustainable production of charcoal.

2.3.2.4 Mathematical modeling

Mathematical models are developed with the objective of predicting or estimating responses to a variable or set of independent variables acting on a given phenomenon. In order to be valid and applicable, mathematical models must be able to represent the physical fidelity of the phenomenon. The cooling of charcoal in masonry kilns involves the cooling of the charcoal mass, the gases contained, and also the cooling of the walls and floor, which have insulating characteristics.

Finished the carbonization stage, the kiln is completely sealed, closing the air inlets in the chambers and closing the exhaust gases to the chimney. Thus, the cooling start by the gases percolating the charcoal bed by natural or forced convection, supporting the thermal exchange and, under certain conditions, favoring exothermic reactions (residual pyrolysis). The conduction and radiation mechanisms also act in the heat transfer between the charcoal pieces and between it and the walls. The heat diffuses through the walls to finally be transferred by convection and radiation to the environment. Thus, the charcoal cooling phenomenon can be approached as a conjugated heat and mass transfer problem with heat generation in a porous medium. Thus, the mathematical model will be governed by the energy conservation equations and the Navier-Stokes equations. The initial and boundary conditions must be specified in accordance with the kiln configuration and the coupled cooling system.

The initial conditions for the floor and walls of the kiln must be taken into account, since the thermal inertia of these components will be of importance in the performance of the model. It should be noted that, in the actually proposed models, the simplifications of adiabatic floor and the walls with a homogeneous temperature distribution, could be deviate from the reality. The walls, depending on the physical properties of their components, especially the thermal diffusivity, can present a thermal response that allow the use of the resistance method. This condition is useful for modeling it as a boundary condition.

However, the heterogeneity of the charcoal bed makes difficult its homogeneous cooling and it is a challenge when it comes to the mathematical modeling of the phenomenon. The bed of charcoal to be cooled presents pieces of different size due to the advancement of the carbonization front (from top to bottom) and to the higher temperatures reached in the ignition points and in the combustion breakouts. Thus, smaller pieces and fines particles can be found in the vicinity of these points. Broken parts can be found in the base due to the pressure exerted by the bed mass, along with semi-carbonated parts when the carbonization front does not reach all the volume into the kiln.

The mathematical approach to the charcoal cooling phenomenon considering all the above variables is still an unsolved problem. Few studies have addressed them, in addition to using several simplifications that facilitate numerical calculations, but which may not faithfully represent the physics of the phenomenon.

França and Campos (2002) modeled the natural convection cooling of a rectangular kiln by means of a 2D analysis using the Finite Difference Method with implicit formulation. The main assumptions were the porous medium in thermal equilibrium condition, adiabatic boundary condition at floor, and neglected advective term in the energy equation. To define the thermal conductivity of the charcoal bed, the authors analyzed different models proposed in the literature, including the radiation between particles. Although the model presented a good fit to the in-bed temperature experimental data, the simplification of heat transfer solely by diffusion reflected a loss of accuracy at the start of the process in the above-bed region where the carbonization gases cooled rapidly due to natural convection. The authors simulated the effect of the wall thickness and wind velocity outside the kiln. Wind speed did not have a significant effect on cooling. The reduction of wall thickness resulted in cooling time reduction between 18 and 27%.

Santos (2013) considered a lumped approach to estimate the temperature of the charcoal bed during the cooling. This approach has as limiting the fact of estimating a homogeneous temperature for the charcoal mass, making it impossible to detect regions with a risk of ignition. In the model validation, the author verified a good adjustment to the experimental data only in the lower part of the bed (thermocouple located at 0.5 m height inside the bed). For other locations inside the oven, the model did not show a good fit.

Several numerical models have been proposed to simulate the flow and heat transfer in porous domains applying simplifications that facilitate the solution of the system of equations. From the geometric point of view, uni, bi, and three-dimensional analyzes and the consideration of homogeneous porosity can simplify the problem. Solving the problem of heat and mass transfer coupled in one or two dimensions minimizes computational time, but such an approach must agree with the physical model conditions.

Moraga et al. (2009) and Agnetti et al. (2016) through a 2D analysis, modeled the generation and heat transfer in a stack of organic waste from wastewater treatment. The two-dimensional simplification was made considering the typical length of a waste stack, which can exceed 150 m. In this condition, an infinite length stack can be assumed, where the temperature variation along the length is negligible when compared to the temperature variation in width and height (cross-section).

The fluid dynamics analysis of the porous media can be done in terms of pore or microscale scale considering the internal porosity of the particles, as well as the macro level, considering a homogeneous porosity, represented by the large porosity of large-scale beds (Das et al., 2016). The heterogeneity of the shape and size of the particles in porous media, results in an anisotropic porosity that raises the complexity of the gas flow and the process of heat and mass transfer between the solid and fluid phases, making difficult the mathematical representation of the physical model (Feng et al., 2016).

In the micro approach, the transport equations are solved by means of direct numerical simulation, but with the disadvantage of needing a greater computational resource for the modeling (Khan and Straatman, 2016). On the other hand, in the macro analysis, the need for modeling at the particle scale is eliminated, which reduces the computational requirement (Khan and Straatman, 2016). In the macro approach, since the porous medium is considered continuous, the transport equations are expressed in terms of mean

volume. The difficulty of this analysis is to achieve a coupling at the interface of the fluid-porous domains that guarantees physically reasonable results in the vicinity of the interface (Degroot, 2012).

Several authors have modeled porous media by applying a macro approach achieving acceptable results. Feng et al. (2016) used a macro analysis in modeling the cooling of a sinter bed in a vertical tank for the sintering process in the steel industry. The authors adopted a mean porosity for the bed and the porosity of the sintered particle (micropores) was not considered. The air and sinter output temperatures simulated by the model were validated with experimental data, obtaining an acceptable fit. Moraga et al. (2009), Zambra et al. (2011, 2012), and Agnetti et al. (2016), modeled by means of a macro analysis the diffusion of heat and oxygen, as well as the heat generated by the biological and oxidative activity in stacks of organic solid waste.

It is worth noting that the simplification of local thermal equilibrium, characterized by a homogeneous temperature in the porous domain, is valid when the thermal conductivities of the fluid and solid phases are very close. In this approach, a single energy equation is formulated for the porous domain in terms of effective properties. Several authors have considered the thermal equilibrium condition to model fluid dynamics and heat generation in organic solid waste deposits (Moraga et al., 2009; Zambra et al., 2011 and 2012; Agnetti et al., 2016) and to evaluate the influence of flow conditions, Reynolds number and incident angle on permeability, pressure drop and heat transfer coefficient in a 2D pipe arrangement (Alshare et al., 2010).

The thermal non-equilibrium condition, which in most cases best represents the process physics, has been used in recent years to model the cooling of porous beds (Taherzadeh and Saidi, 2015, Feng et al., 2016). Das et al., (2016) also considered the non-equilibrium condition for a hydrodynamic and heat transfer study in complex geometries using direct numerical simulation and the immersed boundary method.

Although the thermal conductivity of charcoal and carbonization gases show close values (Santos, 2013), the thermal non-equilibrium approach represents better the charcoal cooling phenomenon. Due to the advective mechanism (natural or forced convection) acting on the gas phase, temperature gradients are created along the entire volume of gas. The resulting density differences promote the movement of the gas phase through and above the bed, creating currents that improve thermal exchange. On the other

hand, the exothermic oxidation reactions taking place on the solid matrix lead to an increase in the temperature of the charcoal pieces.

Other considerations that could be adapted to the mathematical formulation of the cooling of carbonization kilns, namely:

- Conduction, convection, and radiation acting as heat transfer mechanisms inside the furnace. Diffusion and convection acting as mechanisms of mass transfer within the bed.

- Buoyancy force acting on the carbonization gases inside the kiln.

- The heat source in the solid phase of the porous medium modeled as an Arrhenius type reaction, proportional to the concentration of oxygen (Moraga et al., 2009; Zambra et al., 2011 e 2012; Aganetti et al., 2016).

- Carbonization gas is a mixture of varying concentrations of O_2, CO_2, CO, CH_4, H_2 and CnHn (Coelho, 2013). Because they are involved in the oxidation reaction, the oxygenated gases (CO_2, CO, and O_2) can be considered as diffused compounds in the porous bed.

- Physical properties of charcoal are constant (Larfeldt et al., 2000).

2.4 FINAL CONSIDERATIONS

For the successful implementation of artificial cooling systems using steam as refrigerant fluid, as proposed by Oliveira et al. (2010), a thermodynamic analysis of the cooling process should be conducted to determine the mass flow requirements and operating conditions, like pressure and temperature. Further studies should evaluate the real impact of the use of steam on the quality of the charcoal produced, considering its physical, chemical and mechanical properties.

Using the maximum surface velocity (0.1 m s^{-1}), Santos (2013) observed self-heating inside the furnace after 12 hours from the start of the cooling. One possible solution to the combustion breakouts could be tested, operating at higher gas flow rates at the beginning of the cooling, before the charcoal mass begins to react with the infiltrated oxygen, and progressively decreasing the gas flow during the rest of the cooling.

The use of refractory bricks, which have better insulating properties, would optimize the kiln operation during the carbonization stage and could result in better performance during the cooling phase. A thermal analysis should be conducted to determine if the best seal (and consequently lower breakouts of combustion by air infiltration) achieved with this type of brick has an effect superimposed on the effect of the higher heat transfer resistance due to the refractory material. The feasibility of using this type of brick in the construction of carbonization kiln should be determined through a CAPEX-OPEX analysis.

2.5 CONCLUSIONS

Although few studies have analyzed the effect of artificial cooling on quality parameters of the charcoal, it can be affirmed that the artificial cooling using the carbonization gases itself is a technique that keeps the charcoal quality with significant gains in the time of the production cycle. Research should be developed to overcome the technological challenges for its implementation: residual pyrolysis, building materials, and mathematical modeling.

Cooling using water in its liquid and vapor forms may affect the quality of the charcoal produced, especially in terms of its mechanical strength. There is still a vacuum in the knowledge regarding the optimum operation conditions (temperature, pressure, mass flow) of the steam used for cooling, aiming a homogeneous cooling without condensation on the charcoal bed. The high cost of steam generation could be reduced through the cogeneration, by burning of the carbonization gases. The use of the water removed in the wood drying stage to be used as cooling fluid, as done in the DPC technology, constitutes a great challenge because of its oxygen content, which can activate the exothermic reactions in the charcoal causing an adverse effect on the cooling.

In order to develop efficient cooling systems, is necessary a deep knowledge of the physical and chemical phenomena occurring simultaneously within the charcoal bed. Mathematical modeling addressing the complex physicochemical phenomena as well as the thermal inertia of the structural elements of the kiln, could be implemented in computer simulation software to evaluate different scenarios. The use of CFD for modeling and simulation would allow the analysis of the operation parameters in different configurations, being a useful tool for planning and optimization of cooling systems.

2.6 REFERENCES

Aganetti R, Lamorlette A, Guilbert E, Morvan D, Thorpe G R. Advection and self-heating of organic porous media. International Journal of Heat and Mass Transfer. 2016;93:1150-1158.

Alshare A A, Strykowski P J, Simon T W. Modeling of unsteady and steady fluid flow, heat transfer and dispersion in porous media using unit cell scale. International Journal of Heat and Mass Transfer. 2010;53:2294-2310.

Barcellos D C. Avanços tecnológicos da produção de carvão vegetal. In: II FÓRUM NACIONAL SOBRE PRODUÇÃO DE CARVÃO VEGETAL. Sete Lagoas, 2010.

BEEMG. 30 Balanço Energético do Estado de Minas Gerais. Companhia Energética de Minas Gerais. Belo Horizonte: Cemig, 2015.

Bergman T L, Lavine A S, Incropera F, Dewit D P. Fundamentals of heat and mass transfer. 7th ed. New York: John Wiley & Sons; 2011.

Carneiro A de C O, Vital B R, Oliveira A C, Pereira B L. Pirólise lenta da madeira para produção de carvão vegetal. In: Santos F, Colodette J, Queiroz J, editors. Bioenergia e Biorrefinaria: cana de açúcar e espécies florestais. Viçosa: UFV; 2013. p. 429-458.

Centro de Gestão e Estudos Estratégicos CGEE. Nota técnica: Metodologia de estudo e analise de escoamento de gases com transferência de calor por médio de simulação computacional em CFD para otimização do processo de carbonização da madeira em tecnologia DPC. Plano siderurgia MDIC: Modernização de produção de carvão vegetal. 2014.

Centro de Gestão e Estudos Estratégicos CGEE. Nota técnica: Carvão vegetal sustentável. 2015.

Cocchi, G. Estimating the activation energy of exothermic reactions in substances that undergo self-heating processes with the Heat Release method: Use of sub critical data. Fuel. 2014;125:152–154.

Coelho M. Desenvolvimento de metodologia para o dimensionamento de câmaras de combustão para gases oriundos do processo de carbonização de madeira [dissertation]. Universidade Federal de Viçosa; 2013.

Das S, Deen N G, Kuipers J A M. Direct numerical simulation for flow and heat transfer through random open-cell solid foams: Development of an IBM based CFD model. Catalysis Today. 2016;273:140-150.

Degroot C T. Numerical modelling of transport in complex porous media: metal foams to the human lung [dissertation]. The University of western Ontario. London, Ontario, Canada. 2012

EPE Empresa de Pesquisa Energética. Balanço Energético Nacional. 2017. 70-1.

Feng J, Dong H, Gao J, Li H, Liu J. Numerical investigation of gas-solid heat transfer process in vertical tank for sinter waste heat recovery. Applied Thermal Engineering. 2016;107:135-143.

França G A C, Campos M B. Análise teórica e experimental do resfriamento de carvão vegetal em forno rectangular. IV Encontro de Energia no Meio Rural; 2002 Oct 28-31; Campinas (SP), Brazil.

IBÁ. Industria brasileira de árvores. Relatório 2017

Khan F A, Fischer C, Straatman A G. Numerical model for non-equilibrium heat and mass exchange in conjugate fluid/solid/porous domains with application to evaporative cooling and drying. International Journal of Heat and Mass Transfer. 2015;80:513-528.

Khan F A and Straatman A G. Closure of a macroscopic turbulence and non-equilibrium turbulent heat and mass transfer model for a porous media comprised of randomly packed spheres. International Journal of Heat and Mass Transfer. 2016;101:1003-1015.

Larfeldt J, Leckner B, Melaaen M. Modelling and measurements of heat transfer in charcoal from pyrolysis of large wood particles. Biomass & Bioenergy. 2000;18:507–14.

Martins M A. Desafios da implementação de periféricos na produção de carvão vegetal. In: I SEMINARIO DE CARVÃO VEGETAL. Aperam Bioenergia. Universidade Federal de Viçosa, 2014.

Moraga N O, Corvalán F, Escudey M, Arias A, Zambra C. E. Unsteady 2D coupled heat and mass transfer in porous media with biological and chemical heat generations. International Journal of Heat and Mass Transfer. 2009;52:5841-5848.

Nakahara T, Yan H, Ito H, Fujita O. Study on one-dimensional steady combustion of highly densified biomass briquette (bio-coke) in air flow. Proceedings of the Combustion Institute. 2015;35(2):2415-2422.

Oliveira D, Teixeira C A, Silva J, Reis H O, Vorobieff C L. Resfriamento rápido de fornos de carbonização. Engenharia Agrícola, Jaboticabal. 2010;30(6):1023-1032.

Oliveira A C, Carneiro A de C, Barcellos D C, Rodriguez A V, Amaral B M, Pereira B L. Resfriamento artificial em fornos retangulares para a produção de carvão vegetal. Revista Árvore. 2015;39(4):769-78. Portuguese.

Oliveira J B, Vivacqua F A, Mendes M G, Gomes P A. Produção de carvão vegetal – Aspectos técnicos. In: Pinedo W R et al. Eds. Produção e Utilização de Carvão Vegetal. Belo Horizonte: CETEC, 1982. p. 60-73

Pereira E G, Martins M A, Pecenka R, Carneiro A de C. Pyrolysis gases burners: Sustainability for integrated production of charcoal, heat and electricity. Renewable and Sustainable Energy Reviews. 2016;75:592–00.

Perdochova M, Derychova K, Veznikova H, Bernatik A, Pitt M. The influence of oxygen concentration on the composition of gaseous products occurring during the self-heating of coal and wood sawdust. Process Safety and Environmental Protection. 2015;94:463-470.

Santos I. Resfriamento artificial de carvão vegetal em fornos de alvenaria [dissertation]. Universidade Federal de Viçosa; 2013.

Santos M A S. Parâmetros de qualidade do carvão vegetal para uso em alto-forno. In: FORUM NACIONAL SOBRE CARVÃO VEGETAL, 1., 2008, Belo Horizonte. Anais... Belo Horizonte: UFMG, 2008.

Souza L C. Aspectos técnicos e econômicos da produção de carvão vegetal em fornos retangulares de alvenaria. In: FORUM NACIONAL SOBRE CARVÃO VEGETAL, IV., 2016, Belo Horizonte. Anais... Belo Horizonte: UFMG, 2016.

SBRT – Serviço Brasileiro de Respostas Técnicas. 2014. Produção de carvão vegetal. Disponível em: http://www.sbrt.ibict.br. Acesso em: 29 agosto 2016.

Sindicato da Industria do Fero no Estado de Minas Gerais SINDIFER. Anuário 2015. Disponível em http://www.sindifer.com.br/institucional/anuario/anuario_2015.pdf

Taherzadeh M and Saidi M S. Modeling of two-phase flow in porous media with heat generation. International Journal of Multiphase Flow. 2015;69:115-127.

Taraba B, Michalec Z, Michalcová V, Blejchar T, Bojko M, Kozubková M. CFD simulations of the effect of wind on the spontaneous heating of coal stockpiles. Fuel. 2014;118:107–112.

Uhart E A. Floresta amazônica – fonte de energia. Relatório técnico – Convênio Sudam-C.T.F.T./França. Belém: SUDAM, 1972, 144p.

Vale A T and Gentil L V. Produção e uso energético de biomassa e resíduos agroflorestais. In: Oliveira J T S, Fiedler N C, Nogueira M (Ed.). Tecnologias aplicadas ao setor madeireiro III. Jerônimo Monteiro-ES; 2008. p. 196-246.

Wang H, Dlugogorski B, Kennedy E. Coal oxidation at low temperatures: oxygen consumption, oxidation products, reaction mechanism and kinetic modelling. Progress in Energy and Combustion Science. 2003;29:487–513.

Wang Y and Yan L. CFD studies on biomass thermochemical conversion. International Journal of Molecular Sciences. 2008;9:1108-1130.

Xia T, Wang X, Zhou F, Kang J, Liu J, Gao F. Evolution of coal self-heating processes in longwall gob areas. International Journal of Heat and Mass Transfer. 2015;86:861-868.

Xuyao Q, Deming W, Xiaoxing Z, Junjie G, Tao X. Characteristics of oxygen consumption of coal at programmed temperatures. Mining Science and Technology. 2010;20:372-377.

Yuan L and Smith A. C. CFD modeling of spontaneous heating in a large-scale coal chamber. Journal of Loss Prevention in the Process Industries. 2009;22(4):426-433.

Yuan L and Smith A. The effect of ventilation on spontaneous heating of coal. Journal of Loss Prevention in the Process Industries. 2012;25(1).

Yuan L and Smith A. Experimental study on CO and CO2 emissions from spontaneous heating of coals at varying temperatures and O2 concentrations. Journal of Loss Prevention in the Process Industries. 2013;26(6):1321-1327.

Zambra C, Rosales C, Moraga N O, Ragazzi M. Self-heating in a bioreactor: Coupling of heat and mass transfer with turbulent convection. International Journal of Heat and Mass Transfer. 2011;54:5077-5086.

Zambra C E, Moraga N O, Rosales C, Lictevout E. Unsteady 3D heat and mass transfer diffusion coupled with turbulent forced convection for compost piles with chemical and biological reactions. International Journal of Heat and Mass Transfer. 2012;55:6695-6704.

Zhang J, Liang Y, Ren T, Wang Z, Wang G. Transient CFD modelling of low-temperature spontaneous heating behavior in multiple coal stockpiles with wind forced convection. Fuel Processing Technology. 2016;149:55-74.

3. CHAPTER II: THERMAL INERTIA EFFECTS OF THE STRUCTURAL ELEMENTS IN HEAT LOSSES DURING THE CHARCOAL PRODUCTION IN BRICK KILNS

(Bustos-Vanegas J D, Martins M A, Carneiro A de C, Freitas A G, Barbosa R C. Thermal inertia effects of the structural elements in heat losses during the charcoal production in brick kilns. Fuel. 2018;226:508-515.https://doi.org/10.1016/j.fuel.2018.04.024)

ABSTRACT. Brazil is the largest producer of charcoal from planted forests with 5.5 million tons in 2016. The Brazilian steel industry consumes 85% of the national production of charcoal from eucalyptus. The walls and floor of industrial brick kilns are built using isolation materials that minimize heat losses during the wood carbonization stage. However, the thermal inertia of these components represents additional heat that must be removed during the charcoal cooling stage, as reflected in the extended process time. This study aims to evaluate the effect of the thermal inertia of the kiln structural elements for the charcoal production. A CFD (Computational Fluid Dynamics) analysis was performed to simulate the heating and cooling of the system composed of wood, carbonization gases, brick walls and floor. A typical industrial kiln with capacity of 700 m^3 was modeled and validated using a set of experimental measurements of temperatures during a 4-day carbonization stage with final temperature of 400 °C and an 8-day cooling stage. The temperature profile in the walls was linear, corresponding to a pseudo-steady state, where the thermal load increases with the pyrolysis time. The heat transfer at the floor is extensive; therefore, the adiabatic boundary condition cannot be imposed at the wood bed – floor interface. Our findings provide important information for the improvements in the kiln operation and allow establishment of consistent initial conditions of temperature and heat flux for kinetics models for charcoal cooling in kilns.

***Keywords**: biomass, heat transfer, modeling, simulation, CFD*

3.1 INTRODUCTION

Brazil is the largest producer and consumer of charcoal from planted forests, with production reaching 5.5 million tons in 2016 (EPE 2017). In terms of Brazil's market share, 85% of the production is destined for industrial use, mainly as a bio-reducer of iron ore in the pig iron and steel industries (EPE 2017). Charcoal is a renewable product with advantages over coal because of its higher carbon content, which contributes to the reduction of CO_2 emissions. However, the implicit production cost of charcoal is a limiting factor of its use.

In the current scenario, where global warming is a reality, production systems should be designed with consideration of not only economic gain but also, reducing environmental impacts. In the charcoal process, efforts are focused on the reduction of the emissions of pollutant gases via burning the outlet stream and extraction of the released energy (Coelho, 2013; Pereira et al., 2016) and on the process optimization, via reduction of the cooling time.

Charcoal production is based on a thermochemical process known as slow pyrolysis. The quality of the charcoal is a function of the wood quality and carbonization rate. The process occurs in four stages governed by the temperature: wood drying, up to 110 °C; roasting, up to 250 °C; carbonization, up to 350 °C; and carbon fixation, up to 450 °C (Peláez-samaniego et al., 2008; Carneiro et al., 2013). After the last stage, the charcoal mass into the kiln should be cooled prior the discharge. The carbonization time in typical rectangular kilns, that varies between 50 and 2000 m^3 of capacity is approximately 4 days, with the cooling time via natural convection of 9 and 14 days, respectively.

The carbonization process is performed in brick kilns. The bricks have insulating characteristics adequate for the carbonization phase, but unfavorable for the cooling, resulting in a long process time and therefore low productivity. Cooling the charcoal bed involves cooling the inner gases, the walls and even the floor of the kiln, which is usually composed of compacted clay. The thermal properties of those structural elements affect the overall heat transfer and needs to be well known.

Artificial cooling systems via forced heat convection have been developed by companies in an attempt to reduce the cooling time and consequently to increase the productivity (Santos, 2013; Oliveira et al., 2015). Some prototypes using evaporative

cooling have also been tested (Reis, 2009), although without thorough knowledge of the carbonization and cooling kinetics, thus limiting their implementation on an industrial scale.

Modeling and simulation are tools for use in analysis, design and project optimization. Some previous research focused on modeling the process of charcoal cooling and charcoal carbonization (França &Campos, 2002; Reis, 2009; CGEE, 2014) with adoption of simplifications that sometimes do not consider physical phenomena of importance, e.g., time-dependent boundary conditions. Computational fluid dynamics (CFD) allows the evaluation of different scenarios and configurations of cooling and carbonization systems in simulated prototypes, saving both costs and time of experimentation.

This study is the first report in the literature of a mathematical model for simulation the carbonization in a rectangular brick kiln. The model was used to investigate the thermal inertia of the structural components and to provide information for formulation of mathematical models that include the heat transfer during the charcoal cooling.

3.2 METHODOLOGY

3.2.1 Experimental setup

The carbonization kiln under study corresponds to the industrial model 390 from Vallourec Florestal, with wood load capacity of 700 m^3, internal dimensions of 32 m in length, 4 m in width, 4 m in height, with a1.2 m high dome (Fig 1). The walls are built with 0.24-m thick clay brick and doors at each end are constructed of concrete with a thin metal structure. Four chambers located below the kiln provide the energy required for ignition and for starting the pyrolysis. The ignition chambers are four structures located just below the floor surface (Fig 1B) and equidistant throughout the kiln. In this chambers, wood is burnt at the beginning of the process (first 5 hours of the carbonization stage). The gases resulting from this combustion process are conducted along the kiln by a channel located just below the floor (Fig 1D). These hot gases circulate the bed of wood providing the energy for starting the pyrolysis. The two energy sources at the base of the wood bed (Fig 1C) represents the energy provided for the combustion gases, which are responsible for the natural convection flow into the porous section and the gas head space over the bed. Its implementation into the model will be described further on.

The carbonization stage takes 4 days with a final temperature of 400 °C. The further cooling stage lasts for 8 days in natural convection condition with a final temperature of 50 °C. The carbonization gases flow through a duct to a central burner.

Three production cycles were monitored via a data acquisition system consisting of 17 J-type shielded thermocouples 4 AWG, three data acquisition modules (ICP CON 7018) and one interface module (ICP CON 7520) connected to a computer. At 1 m high, the thermocouples recorded the average of 11 measuring points of temperature of the inner wall face during the carbonization and cooling stages. At 3.8 m high, the average of 6 measuring points of temperature of the inner wall face were registered.. The average temperatures recorded during the three cycles were used to validate the proposed model.

3.2.2 Model and simulation

The carbonization cycle was modeled to quantify the thermal effects of the thermo-chemical conversion of the wood bed to charcoal. It is important to remark that the focus of this work was not the modeling of pyrolysis reactions. Therefore, the overall heat generated by the wood drying and subsequent pyrolysis was modeled as an energy source in the heat transfer governing equations. This source was calculated based on a thermal balance and adjusted for typical values of reaction heat of pyrolysis in literature.. A typical carbonization cycle of 12 days (4 days for the carbonization stage and 8 days for the cooling stage) was modeled and simulated with the CFD technique using ANSYS CFX v11.0 software.

3.2.2.1 Physical model

The computational domain is defined by the kiln brick wall, the clay floor and the inner porous material (Fig. 1). Because the length of the kiln is significantly greater than its width, the heat transfer to the external environment occurs mainly in the cross-section. Thus, a two-dimensional approach can be performed, creating two solid subdomains (walls and floor), and one porous domain to represent the wood and charcoal inside the kiln (Fig. 1C). The porous medium corresponds to the wooden bed with logs positioned horizontally. Initially, the bed occupies the total space of the kiln, and as the pyrolysis progresses, the wood degrades and shrinks. The bed height was then defined as a function dependent on the process time, decreasing up to 1.8 m at the end of the carbonization stage (4th day) and remaining constant during the cooling.

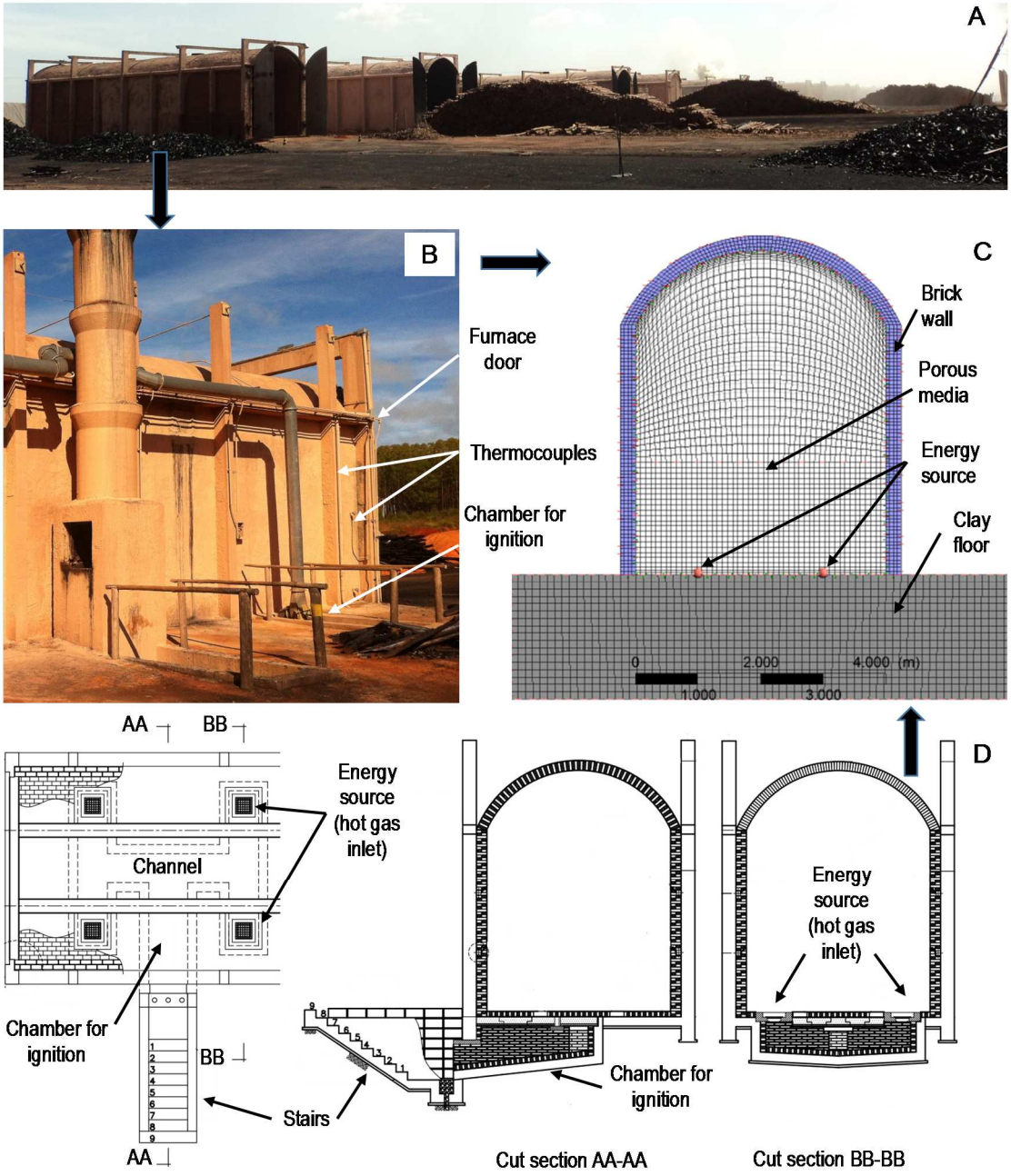

Figure 1. Typical Brazilian charcoal plant (A). Brick kiln with thermometry system and ignition chamber (B). Computational domain detailing a two-dimensional approach for the kiln cross-section (C). Top and side view of brick kiln showing detail of combustion chamber and hot gas inlet (D).

In order to investigate the heat diffusion effects through the floor, this subdomain was extended up to 4 m depth and 2 m on each side, as depicted in Fig. 1.

The computational domain was discretized for each subdomain, which allows a set of meshes with good orthogonality. After a previous spatial and temporal convergence testing, a mesh of 13740 elements (8820 for the porous subdomain, 888 for the wall subdomain and 4032 for the floor subdomain) and a time step of 60 minutes were chosen. A mesh refinement was applied at the bed-walls and bed-floor interfaces to improve the heat flux conservation and temperature continuity.

3.2.2.2 Governing equations

Because the aim of this research was to understand the heat transfer and its inertia in the structural components of the kiln, the following assumption were adopted:

a) The intergranular gas inside the kiln is an ideal mixture of CO_2 and N_2.
b) Buoyant force modeled using the Boussinesq approach.
c) Low-Mach number: density changes only associated with temperature variations.
d) Charcoal bed is considered as an isotropic porous medium in the condition of local thermal non-equilibrium.
e) Thermal radiation intensity is isotropic.

The governing equations of the transient model were based on the continuity, momentum and energy equations. For the porous medium:

$$\varphi \frac{\partial \rho_f}{\partial t} + \nabla \cdot \left(\rho_f \vec{v}\right) = 0 \tag{1}$$

$$\frac{\partial \left(\rho_f \vec{v}\right)}{\partial t} + \frac{1}{\varphi} \nabla \cdot \left(\rho_f \vec{v} \vec{v}\right) = -\varphi \nabla P + \mu \nabla^2 \vec{v} + \rho_f \vec{g} - \frac{\varphi \mu}{K} \vec{v} - \frac{\varphi \rho_f C_E}{\sqrt{K}} \vec{v} |\vec{v}| \tag{2}$$

$$(1-\varphi)\left(\rho C_p\right)_s \frac{\partial T_s}{\partial t} = (1-\varphi) \nabla \cdot \left(k_{ef-s} \nabla T_s\right) + (1-\varphi) q_s''' + h_i A_s \left(T_f - T_s\right) \tag{3}$$

$$\varphi C_{pf} \frac{\partial \left(\rho_f T_f\right)}{\partial t} + \nabla \cdot \left(C_{pf} \rho_f T_f \vec{v}\right) = \varphi \nabla \cdot \left(k_f \nabla T_f\right) - h_i A_s \left(T_f - T_s\right) \tag{4}$$

Terms on the left hand side in Eqs. (1-4) represent transient and advective transport. The last two terms of Eq. (2) correspond to the resistive force terms and represent the viscous and drag forces resulting from the interaction between the solid and fluid phases in the porous medium. These two terms were adjusted by experimental measurements of pressure drop, where a quadratic relationship to the true velocity was

observed (Table 1). The term associated with the gravity vector in Eq. (2) represents the buoyant force due to the gas density changing with temperature.

During the pyrolysis, heat generation increases and is transferred into the porous bed, creates temperature gradients that promote the gas flow inside the kiln. In the porous media, the flow becomes turbulent when *Re* > 280 (Lesage et al., 2004). In order to account for turbulence fluctuations, Eqs. (1-4) were modified to a time-averaged form (Reynolds-Averaged Navier-Stokes equations), where the Reynolds stress tensor (τ) in Eq. (2) is modeled using an eddy viscosity, μ_t:

$$\nabla \cdot \tau = \nabla \cdot \left(-\rho_f \vec{v}\vec{v}\right) \tag{5}$$

$$-\vec{v}'\vec{v}' = \mu_t \left(\frac{\partial \vec{v}_i}{\partial x_j} + \frac{\partial \vec{v}_j}{\partial x_i}\right) - \frac{2}{3}\delta_{ij}k \tag{6}$$

where δ_{ij} is the Kronecker delta and k is the kinetic energy of the velocity fluctuations. The terms on the right-hand side of Eq. (6) represent the Reynolds shear and normal stresses. To close the system of the governing equations, the Reynolds stress was modeled by the k-ε model (Pedras & Lemos, 2003; Saito & Lemos, 2010):

$$\mu_t = C_\mu \rho_f \frac{{k^T}^2}{\varepsilon} \tag{7}$$

$$\frac{\partial(\rho_f k^T)}{\partial t} + \nabla \cdot (\rho_f \vec{v} k^T) = \nabla \cdot \left[\left(\mu + \frac{\mu_t}{\sigma_k}\right)\nabla k^T\right] + P_k - \rho_f \varepsilon \tag{8}$$

$$\frac{\partial(\rho_f \varepsilon)}{\partial t} + \nabla \cdot (\rho_f \vec{v} \varepsilon) = \nabla \cdot \left[\left(\mu + \frac{\mu_t}{\sigma_\varepsilon}\right)\nabla \varepsilon\right] + \frac{\varepsilon}{k^T}(C_{\varepsilon 1} P_k - C_{\varepsilon 2} P_\varepsilon) \tag{9}$$

$$P_k = \mu_t \nabla\vec{v}(\nabla\vec{v} + \nabla\vec{v}^T) - \frac{2}{3}(\nabla\vec{v})(3\mu_t \nabla\vec{v} + \rho_f k^T) \tag{10}$$

where k^T is the turbulent kinetic energy, ε is the rate of dissipation and σ_k, σ_ε, $C_{\varepsilon 1}$ and $C_{\varepsilon 2}$ are closure parameters with values of 1.0, 1.3, 1.44 and 1.92 respectively (Pedras & Lemos, 2003; Saito & Lemos, 2010).

Eqs. (3-4) describe the energy transport in the solid and fluid phases of porous medium, respectively. The source term q''' in the solid phase represents the energy supplied for the ignition and the consequent energy released during the partial oxidation reactions (reaction heat of pyrolysis). In the pyrolysis reaction, the main components of the wood (hemicellulose, cellulose and lignin) are degraded at different rates following an Arrhenius type reaction kinetic (Mehrabian et al., 2012). Other authors proposed an alternative and complementary approach in which the degradation rate varies as a

function of the reaction product: intermediate solid, char, tar or gas (Park et al., 2010; Grieco & Baldi, 2011; Pan & Kong, 2017).

The reaction heat of pyrolysis, varies in a wide range. Dougaard and Brown (2003) reported values varying from 0.78 to 1.64 MJ kg^{-1} depending on the type of biomass source. A value of 0.93 MJ kg^{-1} was set during the carbonization stage (four days) in order to run the simulations. This term was implemented in CFX acting in the two-point energy sources (shown in Fig 1C) during the first five hours of the process. For the rest of time of carbonization stage, the source term was set to act on the whole porous subdomain. After, for the cooling stage, this value was set to zero. Table 1 presents the model parameters used in the simulation.

Table 1. Model parameters.

Wall (brick fireclay) (Bergman et al., 2011)	value
c_{pw} [J kg^{-1} K^{-1}]	960
k_w [W m^{-1} K^{-1}]	1,0
ρ_w [kg m^{-3}]	2645
Clay floor (Bergman et al., 2011)	
c_{pb} [J kg^{-1} K^{-1}]	880
k_b [W m^{-1} K^{-1}]	1,29
ρ_b [kg m^{-3}]	1450
Porous media (fluid phase) (Saito & Lemos, 2010)	
CO_2 thermophysical properties	Ansys CFX database
N_2 thermophysical properties	Ansys CFX database
Porous media (solid phase) (Bergman et al., 2011; Santos, 2013; Pan & Kong, 2017)	
c_p *wood* [J kg^{-1} K^{-1}]	2385
k wood [W m^{-1} K^{-1}]	0,19
ρ wood [kg m^{-3}]	540
c_p *charcoal* [J kg^{-1} K^{-1}]	1017
k charcoal [W m^{-1} K^{-1}]	0,03
ρ charcoal [kg m^{-3}]	345
l [m]	0.13
ψ	0,9
d_{pore} [μm]	350
Porous media (Santos, 2013; Daugaard & Brown, 2003)	
φ	0,6
A_s [m^{-2}]	65
Nu	$2+(1.1*Pr^{0.33}*Re^{0.6})$
$\Delta P/l$ [Pa m^{-1}]	$24V+343V^2$
q''' [W m^{-3}]	1185
Carbonization time [h]	96
Cooling time [h]	192

The heat transfer by the gas flow through the porous matrix is proportional to the interfacial heat transfer coefficient h_i. These term was assumed to act inside the porous bed locally and it depends on the gas properties, characteristic length of particles (l) and Nusselt number (Nu). This dimensionless number relates the contribution of the convective and conductive mechanisms in the heat transfer phenomena at the fluid-solid interphase. The coupling term (h_i) appears in the two energy equations (Eqs. 3-4) accompanying the interstitial heat exchange specific area (A_s):

$$h_i = k_f \frac{Nu}{l} \tag{11}$$

The interfacial gas flow, driven by the buoyancy force, circulate the porous bed towards the heat space. In this free flow region, which expands as the porous bed shrinks, the gas reaches a higher velocity, resulting in larger Reynolds numbers and increasing convective heat transfer at the bed surface. Because of this, the carbonization front runs from top to bottom of the bed.

Radiation between particles is considered in Eq. (3) within the diffusive term, in which the effective heat transfer coefficient $k_{ef\text{-}s}$ quantifies the conduction and radiation phenomena (Larfeldt et al., 2000):

$$k_{ef-s} = k_c + k_{rad} \tag{12}$$

$$k_{rad} = 4\varphi\sigma\gamma d_p T_s^3 \tag{13}$$

where σ is the Stefan-Boltzmann constant, ψ is the charcoal emissivity and d_p is the average diameter of the charcoal pores. Energy traveling as radiation through the interstitial fluid can be modeled using an additional transfer equation for the porous domain, where the change in intensity is a balance among emission, absorption and scattering (Siegel & Howell, 1992; Modest, 2003):

$$\frac{\partial i_\lambda}{\partial S} = a_\lambda i_{\lambda b}(S) - a_\lambda i_\lambda(S) - \sigma_{s\lambda} i_\lambda(S) + \frac{\sigma_{s\lambda}}{4\pi}\int_{\omega_i}^{4\pi} i_\lambda(S,\omega_i)\phi(\lambda,\omega,\omega_i)d\omega_i \tag{14}$$

The first term on the right side of Eq. (14) represents the gain by emission, followed by the loss terms of absorption and scattering. The last term represents the gain by scattering. The radiation emitted by the wood bed (under carbonization conditions) interacts with the fluid region above it and with the inner surfaces of the kiln. This is known as limit diffusion, because radiant energy is dispersed in all directions. The radiation model P1 was adopted to account for the radiant heat flux, because the medium

inside the kiln is optically dense and approaches the limit diffusion condition. The P1 model simplifies the radiative transfer equation and reduces the required computational effort.

The walls and floor are defined as impermeable with average properties. For these domains, a transport equation is only required for energy, in which the diffusive mechanism is governing:

$$C_{pw}\rho_w \frac{\partial T_w}{\partial t} = k_w \nabla^2 T_w \tag{15}$$

$$C_{pb}\rho_b \frac{\partial T_b}{\partial t} = k_b \nabla^2 T_b \tag{16}$$

3.2.2.3 Boundary conditions and interfaces

The hydrodynamic conditions at the bed-wall and bed-floor interfaces are no-slip, zero speed and thermal energy conservation along the normal direction:

$$-\left[k_b \frac{\partial T_b}{\partial n}\right]_{base} = \left[-k_{ef-s} \frac{\partial T_s}{\partial n} - k_f \frac{\partial T_f}{\partial n}\right]_{porous} \tag{17}$$

$$-\left[k_w \frac{\partial T_w}{\partial n}\right]_{wall} = \left[-k_{ef-s} \frac{\partial T_s}{\partial n} - k_f \frac{\partial T_f}{\partial n}\right]_{porous} \tag{18}$$

$$h_i\left[T_{s-i,t} - T_f\right] = k_w \frac{\partial T_{s-i,t}}{\partial x} \tag{19}$$

Equations 17 and 18 model the heat flux at the bed-wall and bed-floor interfaces. Equation 19 responds by the heat flux between the head space inside the kiln and the inner surface of the walls.

For the carbonization stage, the boundary conditions were established as the following: on the floor, at a depth of 2 m, an adiabatic boundary condition is set; in the symmetry planes, normal gradients are set to zero for all quantities; on the external wall surface, a convective boundary condition is established with outside temperature set to 25 °C:

$$h_{ext}\left[T_{surf,t} - T_\infty\right] = k_w \frac{\partial T_{surf,t}}{\partial x} \tag{20}$$

The convection heat transfer coefficient was calculated considering an average air velocity of 4.5 m/s and outside temperature of 25 °C. Following the experimental

approach proposed by França & Campos (2002), an approximation was made depending on the height of the kiln:

Lateral wall, for $0.3 < Pr < 100$ and $10^{10} < Ra < 10^{13}$:

$$h_{ext} = \left[0.138 \frac{k_{air}}{L_w} Gr^{0.36}\left(Pr_{air}^{0.175} - 0.55\right)\right][1 + (2.237 fv_{air})] \quad (21)$$

Dome, for $Ra > 10^8$:

$$h_{ext} = 0.10 \frac{k_{air}}{L_c} Ra^{1/3}[1 + (2.237 fv_{air})] \quad (22)$$

Where f is a correction factor that depends on the temperature difference between external surface and air (França & Campos, 2002):

f = 0,229 for ΔT = 8.33 °C

f = 0,200 for ΔT = 13.89 °C

f = 0,171 for ΔT = 27.78 °C

f = 0,150 for ΔT = 55.56 °C

f = 0,121 for ΔT = 111.11 °C

As initial conditions for carbonization stages, all temperatures were set to 25 °C. For the cooling stage, the boundary conditions were maintained, except for the adiabatic boundary condition in the floor, which was modified to a depth of 4 m. The simulated conditions at the end of the carbonization stage were used as the initial conditions for the cooling stage, by switching to zero the heat source term in the energy equation (Eq. 3).

The simulation time was set to 96 hours (4 days) for the carbonization stage and 192 hours (8 days) for the cooling stage. The first-order backward Euler and high-resolution discretization schemes were used for the transient and advective terms, respectively. The residual target was set to RMSE < 10^{-6}.

3.3 RESULTS AND DISCUSSION

3.3.1 Model validation

Average of six experimental measurements points of temperature at height of 3.8 m and 11 measurements points of temperature at 1 m height on the inner surface of the

wall were compared with the simulation data (Fig. 2). The CFD predictions are found to be in good agreement with the experimental data, with R^2 of 92% and 95% for the carbonization and cooling stages, respectively. In the highest position (Fig. 2A), as a consequence of the buoyancy forces, a rapid increase in temperature is observed due to the flow of hot gases toward the head space. The internal wall temperature reached almost 300 °C at the end of carbonization stage, and it is a characteristic temperature used by charcoal producers to monitor the behavior of pyrolysis inside the kiln.

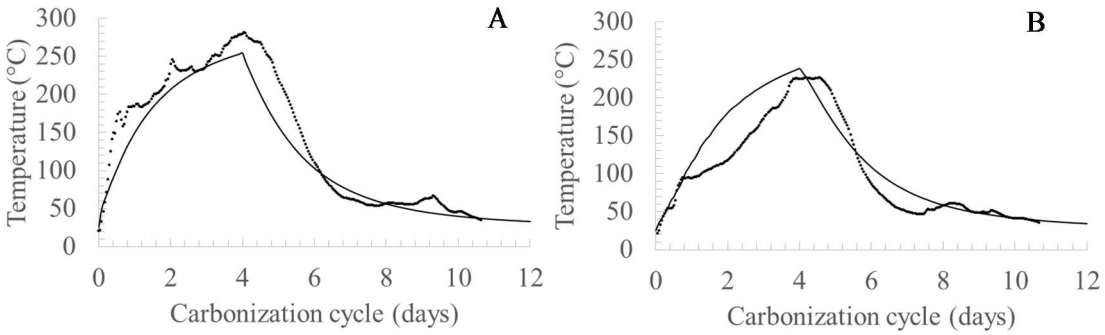

Figure 2. Experimental (dotted line) and simulated (black line) temperature at the internal surface of the wall at a height of 3.8 m (A) and at a height of 1 m (B) during carbonization cycle. Four days for carbonization stage. Eight days for cooling stage.

3.3.2 Simulation

During the carbonization stage (Figure 3), the advance of the carbonization front can be observed from the top to the bottom of the kiln. By having a much lower density compared to wood, stagnant gases at the top of the bed are heated rapidly, creating a convective flow that promote the carbonization front. The simulated Reynolds number varies between 250 for the porous bed and 8,800 for the head space, a condition that justifies the use of a turbulence model. Similarly, during the cooling, the gas phase in the head space releases heat rapidly and therefore decreases its temperature at higher rates than the bed. This phenomenon has been observed in the industry during the opening of the kilns, where apparently cold kilns can undergo combustion breakouts when the air comes into contact with still hot pieces of charcoal lies inside the bed.

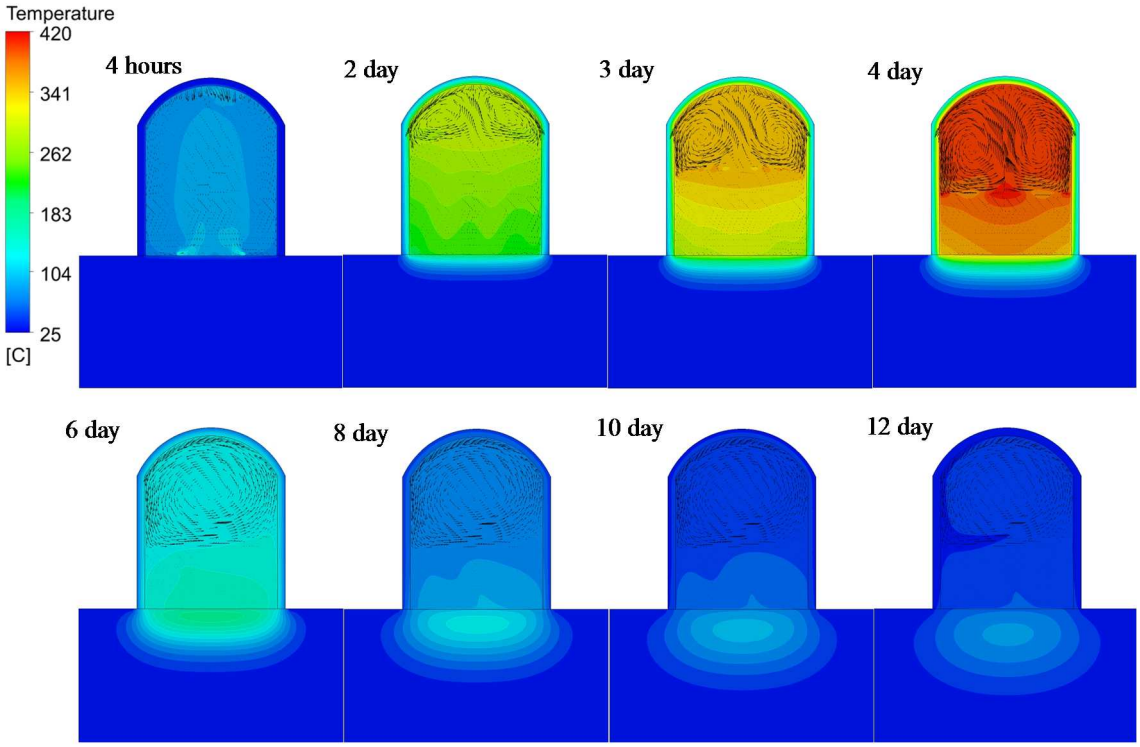

Figure 3. Temperature distribution of the fluid phase of the charcoal bed, walls and floor during the whole carbonization cycle. The arrows indicate the gas flow pattern at the head space.

The heat diffusion through the floor can also be observed in Fig. 3. During the carbonization stage, the heat diffuses from the heated bed to the floor. The diffusion in the depths of the floor continues during the cooling stage, and a zero-temperature gradient can be observed by the boundary condition imposed (4 m depth and 2 m on each side). After the fifth day of processing (first day of cooling), the temperature at the floor is found to exceed the temperature of the bed above the kiln (i.e. interface). This condition results in a reverse heat flux at floor interface, in which the bed begins to absorb energy from the floor (Fig. 4), making it difficult to cool down the bed.

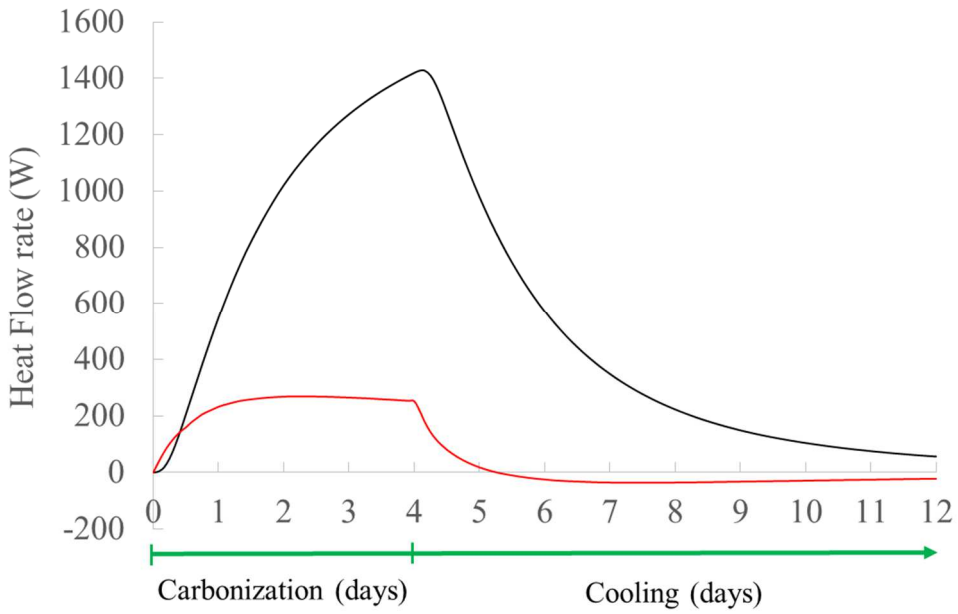

Figure 4. Heat flow rate at walls (black line) and floor (red line) during the carbonization cycle.

The heat flow through the walls is faster than the heat flow at the bed-floor interface (Fig. 4). The walls exchange heat with the environment via convection and radiation, reaching a maximum value of 1427 W at the end of the carbonization stage. At the beginning of the cooling (during the first two days), a higher heat rate can also be observed. Soon after, the heat rate begins to decline exponentially, reflecting a long cooling time. Sixty hours after the process start (the second day of carbonization), the heat flux at the floor interface is 260 W, and presented a tendency to remain stable until the end of the carbonization stage. On the second day of cooling (approximately 32 hours), the heat rate reverses its direction and the bed begins to absorb heat from the floor. The exposed phenomenon highlights the importance of not considering the floor as adiabatic and address new possibilities for different approaches to understand the cooling problem and its further optimization.

The integration of the heat flow rate function shown in Fig. (4) enables estimation of the heat losses during the process. During the carbonization stage, 302.8 MJ are lost through the walls and 69.9 MJ are lost through the floor. These values represent 46.8% of the total energy required in the process (794.8 MJ). Current research in the field of material science evaluating insulation characteristics in bricks (Santos et al., 2015; Witzany et al., 2016; Triantafillou et al., 2017) could be applied in the charcoal industry.

Materials with lower thermal conductivity would minimize losses during carbonization but could extend the cooling time even further.

The temperature distribution at the wall thickness during the carbonization and cooling stages is shown in Fig. 5, at 0.8 m high. The linear profile corresponds to pseudo steady state heat conduction, where the thermal load increase with the pyrolysis time (Fig. 5A). This behavior enables modeling of the wall domain with fewer mesh elements. Additionally, the brick walls can be modeled even without a physical domain, using the thermal resistance approach (Bergman et al., 2011). This approach could result in a lower CPU running time.

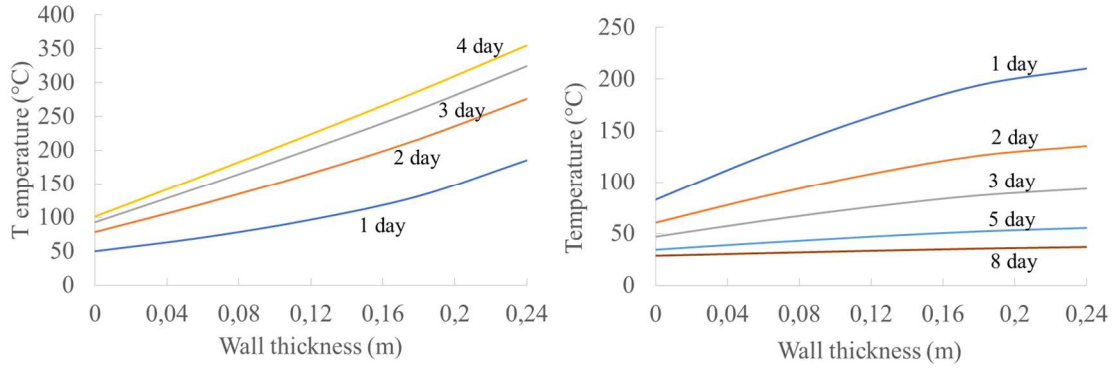

Figure 5. Temperature distribution into the wall during the carbonization (A) and cooling stages (B) at 0.8 m high.

For a one-dimensional plane wall, Fourier's law establishes that the heat flux is proportional to the temperature gradient. After the second day of cooling (Fig. 5B), the temperature gradient decreases considerably, relying on a low heat transfer rate.

Two inlets at the floor provide the heat to start the wood pyrolysis at the beginning of carbonization process. A controlled combustion occurs from the inlet chambers, and then, the process become self-sustaining as the pyrolysis reaction occurs. The floor surface is heated rapidly during the first day when the chambers are active. During the carbonization stage, heat diffusion through the floor starts from the surface and reaches a depth of almost 2 m, where an adiabatic boundary condition can be correctly established (Fig. 6A).

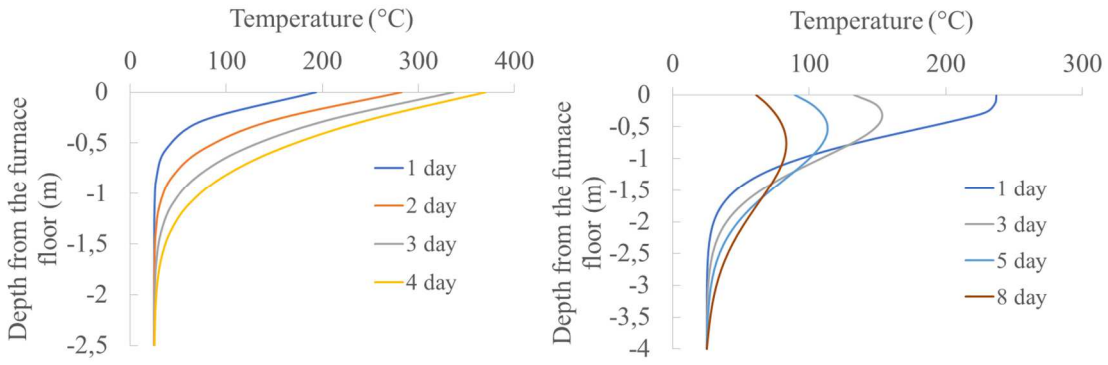

Figure 6. Temperature distribution into the floor during the carbonization stage (A) and during the cooling stage (B).

During the cooling stage, heat diffusion through the floor continues and the adiabatic boundary condition had to be moved to the depth of 4 m(Fig. 6B). After the first day of cooling, the floor's temperature is found to exceed the temperature of the interface (Fig. 6B), thereby inverting the heat flux, as observed in Fig 4. Therefore, the use of an insulation layer at the floor will contribute to a more effective conversion from wood to charcoal, since the heat loss though the kiln floor will be no longer significant. Moreover, with an insulation layer, the cooling stage will be also improved since no heat will be transferred from the clay floor to charcoal.

3.4 CONCLUSIONS

Computational fluid dynamics was presented as a reliable tool for the modeling and simulation of the thermal phenomena involved in the pyrolysis and cooling stages in the production of charcoal in industrial scale kilns.

The thermal inertia of the structural elements of a brick kiln was characterized by determining the temperature profile and heat flux through the walls and floor during the carbonization and cooling stage. The temperature profile in the brick walls showed a pseudo-steady state behavior that allows modeling this subdomain using the thermal resistance method. This approach can reduce computational time in simulations using the CFD method.

The analysis of the heat flux through the structural elements of the kiln allows the quantification of the heat losses in each stage of the process. The bed-floor interface

cannot be considered adiabatic. The floor can be only considered as adiabatic at 2 m depth during the carbonization stage and at 4 m depth during the cooling. The time when the charcoal bed begins to absorb heat from the floor is crucial for the design of carbonization and cooling systems, evaluating different materials and configurations for their optimization.

The simplified model presents an adequate prediction of temperature distribution at walls, floor and porous material. These temperature fields can be used as the initial conditions in the computational model formulation of the cooling process of brick kilns, enabling the simulated conditions to approach the real conditions.

3.5 REFERENCES

Bergman T L, Lavine A S, Incropera F, Dewit D P. Fundamentals of heat and mass transfer. 7th ed. New York: John Wiley & Sons; 2011.

Carneiro A de C O, Vital B R, Oliveira A C, Pereira B L. Pirólise lenta da madeira para produção de carvão vegetal. In: Santos F, Colodette J, Queiroz J, editors. Bioenergia e Biorrefinaria: cana de açúcar e espécies florestais. Viçosa: UFV; 2013. p. 429-458.

Centro de Gestão e Estudos Estratégicos CGEE. Metodologia de estudo e analise de escoamento de gases com transferência de calor por médio de simulação computacional em CFD para otimização do processo de carbonização da madeira em tecnologia DPC. Plano siderurgia MDIC: Modernização de produção de carvão vegetal. 2014.

Coelho M. Desenvolvimento de metodologia para o dimensionamento de câmaras de combustão para gases oriundos do processo de carbonização de madeira [dissertation]. Universidade Federal de Viçosa; 2013.

Daugaard D and Brown R. Enthalpy for pyrolysis for several types of biomass. Energy Fuels. 2003;17(4):934-939.

Empresa de Pesquisa Energética. Balanço Energético Nacional. 2017. 70-1.

França G A C, Campos M B. Análise teórica e experimental do resfriamento de carvão vegetal em forno rectangular. IV Encontro de Energia no Meio Rural; 2002 Oct 28-31; Campinas (SP), Brazil.

Grieco E, Baldi G. Analysis and modelling of wood pyrolysis. Chemical Engineering Science. 2011;66:650-60.

Larfeldt J, Leckner B, Melaaen M. Modelling and measurements of heat transfer in charcoal from pyrolysis of large wood particles. Biomass & Bioenergy. 2000;18:507–14.

Lesage F, Midoux N, Lafiti M A. New local measurements of hydrodynamics in porous media. Experiments in Fluids. 2004;37:257-62.

Mehrabian R, Zahirovic S, Scharler R, Obernberger I, Kleditzsch S, Wirtz S, et al. A CDF model for thermal conversion of thermally thick biomass particles. Fuel Processing Technology. 2012;95:96-08.

Modest M F. Radiative Heat Transfer. 2nd ed. California: Academic Press; 2003.

Oliveira A C, Carneiro A de C, Barcellos D C, Rodriguez A V, Amaral B M, Pereira B L. Resfriamento artificial em fornos retangulares para a produção de carvão vegetal. Revista Árvore. 2015;39(4):769-78. Portuguese.

Pan Y, Kong S. Simulation of biomass particle evolution under pyrolysis conditions using lattice Boltzmann method. Combustion and Flame. 2017;178:21-34.

Park W C, Atreya A, Baum H R. Experimental and theoretical investigation of heat and mass transfer processes during wood pyrolysis. Combustion and Flame. 2010;157:481-94.

Pedras M, de Lemos M. Computation of turbulent flow in porous media using a low Reynolds k-ε model and an infinite array of transversally-displaced elliptic rods. Numerical Heat Transfer, part A. 2003;43(6):585-02.

Peláez-samaniego M R, Garcia-Perez M, Cortez L B, Rosillo-Calle F, Mesa J. Improvements of Brazilian carbonization industry as part of the creation of a global biomass economy. Renewable and Sustainable Energy Reviews. 2008;12:1063–86.

Pereira E G, Martins M A, Pecenka R, Carneiro A de C. Pyrolysis gases burners: Sustainability for integrated production of charcoal, heat and electricity. Renewable and Sustainable Energy Reviews. 2016;75:592–00.

Reis H. Resfriamento de fornos de carbonização por injeção de vapor de água [dissertation]. Universidade Federal de Viçosa; 2009.

Saito M, de Lemos M. A macroscopic two-energy equation model for turbulent flow and heat transfer in highly porous media. International Journal of Heat and Mass Transfer. 2010;53:2424-33.

Santos I. Resfriamento artificial de carvão vegetal em fornos de alvenaria [dissertation]. Universidade Federal de Viçosa; 2013.

Santos P, Martins C,Júlio E. Enhancement of the thermal performance of perforated clay brick walls through the addition of industrial nano-crystalline aluminium sludge. Construction and Building Materials. 2015;101:227-38.

Siegel R, Howell J R. Thermal Radiation heat Transfer. 3rd ed. Whasington: Hemisphere; 1992.

Triantafillou T C, Karlos K, Kefalou K, Argyropoulou E. An innovative structural and energy retrofitting system for URM walls using textile reinforced mortars combined with thermal insulation: Mechanical and fire behavior. Construction and Building Materials. 2017;133:1 – 13.

Witzany J, Zigler R, Kroftová K. Strengthening of compressed brick masonry walls with carbon composites. Construction and Building Materials. 2016;112:1066-79.

4. CHAPTER III: EXPERIMENTAL CHARACTERIZATION OF SELF-HEATING BEHAVIOR OF CHARCOAL FROM EUCALYPTUS WOOD

(Paper under review in Fuel Journal, 2018)

Abstract. The long cooling time of charcoal produced from eucalyptus pyrolysis is due in part to the heat generation in oxidation reactions at low temperatures. The intensity of this reactions depends on complex interactions between the interstitial gas and the solid matrix. The kinetics of the self-heating phenomena due to charcoal oxidation were evaluated. Samples of 230 g of charcoal were subjected to heating in a steel reactor at constant temperature, from 100 to 300 °C, and oxygen concentrations ranging from 20.9 to 10 %. Was evidenced that the rate of oxygen consumption increases with charcoal temperature at rates that depend on the initial concentration of O_2. The beginning of the oxidation reactions was observed at 67 °C in atmospheres with 20.9% O_2. The overall activation energy for the self-heating phenomenon was 17790 J mol^{-1} and its intensity was increased with the temperature and O_2 concentration.

***Keywords**: Biomass, oxidation, kinetic, activation energy.*

4.1 INTRODUCTION

The production of charcoal is based on a thermochemical process known as slow pyrolysis. Wood carbonization consists of concentrating carbon and releasing oxygen by the action of heat, with the consequent increase in the calorific value (Carneiro et al., 2013). This process occurs in four phases according to the temperature reached: wood drying up to 110 °C, roasting up to 250 °C, charring and fixing carbon up to approximately 350 °C (Peláez-Samaniego et al., 2008; Rezende, 2006). Soon after, the charcoal mass has to be cooled, an operation that depending on the configuration of the kiln, can consume the longest time of the production cycle.

In the Brazilian market share, 85% of the production is used in industries as a bio-reducer of iron ore in the pig iron and steel industries (EPE, 2018). Charcoal is a renewable product with advantages over coal because of its higher carbon content, which contributes to the reduction of CO_2 emissions (Alves, 2013). However, the implicit production cost of charcoal is a limiting factor of its use. The charcoal industry in Brazil has been facing and overcoming challenges regarding optimization of the carbonization process and reduction of environmental impact. Usually, the measures adopted to mitigate the environmental impact reflect in a process optimization and vice versa. For instance, the use of gas burners coupled to the carbonization kilns allows the utilization of enthalpy from emissions in the wood drying operation or in power generation, reducing the pollutants releasing to atmosphere (Pereira et al., 2017).

Typical kilns used in charcoal produced by steelmaking companies reach up to 2000 m^3 of wood-capacity. The production cycle in a kiln of 700 m^3 extends on average for 12 days, in which 4 days correspond to the pyrolysis stage and 8 days to the cooling stage. The purpose of this last step is to reduce the temperature of the charcoal bed to a safe handling temperature of 60 °C, which allows the kiln to be opened and charcoal discharged. In this way, the combustion break-outs (generated when the air atmospheric contact with the mass of charcoal) are minimized.

Heat exchangers have been implemented by some companies to reduce cooling time, increasing productivity per kiln. Reductions in cooling time of up to 50% have been achieved using gas-air and gas-water type heat exchangers (França and Campos, 2002; Oliveira et al., 2010; Santos, 2013; Martins, 2014; Oliveira et al., 2015). However, these technologies have been developed by companies and therefore few results have been

published in scientific journals and, despite the advances already made, it could be in fact improved. As verified by Santos (2013) and Martins (2014), the increase in the gas flow rate over the charcoal bed results in an adverse effect on the cooling due to the occurrence of combustion spots, because of the air infiltration caused by the increase of the pressure drop between the suction and the gas injection of the heat exchanger.

The long cooling time of the charcoal bed is due to the insulation characteristics of the kiln building materials and the exothermic oxidation reactions that continue to occur in the charcoal bed during the cooling, depending on the oxygen concentration of the stagnant gases. Therefore, the cooling rate depends on the heat loss by convection and radiation, and the heat generated in the oxidation reactions inside the charcoal bed. Besides the effect on the cooling time, the charcoal oxidation affects its molecular structure and can change its elemental composition, losing up to 15% of its calorific power (Wang et al., 2003; Qi et al., 2010).

Charcoal oxidation begins when the solid matrix is exposed to oxygen, generating gases (CO, CO_2, H_2O and CH_4) and releasing heat (Perdochova et al., 2015). When the rate of energy generation due to the oxidation reaction exceeds the heat transfer rate towards the surroundings, two types of behavior can be identified: a subcritical behavior, which reflects in a limited temperature increase, or a supercritical behavior, characterized by a severe increase of temperature that may cause ignition or explosion (Qi et al., 2010; Cocchi 2015). Experiments in subcritical conditions can provide important information for the determination of the activation energy of the self-heating reactions (Cocchi 2015). The crossing points methods, namely the Chen and Chong method, and the Heat Released method, are oven heating techniques for slow and low-temperature oxidation reactions and can be used to estimate the activation energy in self heating prone substances (Nugroho et al., 1998; Jones et al., 1998; Sujanti and Zhang, 1999; Yuan and Smith, 2012; Cocchi, 2014; Cocchi, 2015).

The kinetics of the oxidation reactions of charcoal, which we call late pyrolysis, still need to be studied. Interestingly, there are no scientific publications regarding this subject for eucalyptus charcoal. Therefore, the aim of this study was to evaluate the kinetics of charcoal self-heating due to the oxidation reactions and their dependence on the oxygen content in the surrounding atmosphere. It is intended to provide information that can be used in mathematical modeling and optimization of the charcoal cooling stage.

4.2 OXIDATION KINETICS

The oxidation reaction of coal involves three phenomena accompanying the temperature increase: the physical adsorption, which starts at low temperatures (<100 °C) when the solid matrix is exposed to oxygen; chemical adsorption, characterized by a heat release (80-420 kJ mol^{-1}), and finally the chemical reaction, characterized by its great exothermicity (Qi et al., 2010). At high temperatures, the heat generated in the chemical reaction can lead to ignition. The oxygen consumption in the oxidation reaction increases with the temperature due to changes in the micro and macrostructure of the coal solid matrix (Qi et al., 2010). At the macro level, water evaporation and gas release develop the porous structure, increasing the internal surface area and pore volume, improving the contact between coal and oxygen. Microscopically, activation constructs increase with temperature and react with oxygen to form coal-oxygen complexes, which once decomposed, release heat and gaseous products (Qi et al., 2010).

Since the internal surface area of coal pores is much larger than the external surface, low-temperature oxidation of coal is a phenomenon occurring predominantly at the internal surface of coal pores (Wang et al., 2003). The oxidation phenomenon is affected by external variables such as temperature, O_2 concentration and moisture, and by internal variables including chemical composition, physical properties, porosity and internal surface area (Wang et al., 2003). Qi et al., (2010) identified the reaction rate, i.e. the rate of oxygen consumption, as the main factor affecting the self-heating rate of coal. Oxidation rate can be modeled as a first-order Arrhenius type reaction for oxygen concentration (Wang et al., 2003; Taraba et al. 2014):

$$r_{ox} = A \cdot C_{O2} \cdot e^{-\frac{E}{RT}} \tag{1}$$

By adopting the thermal equilibrium condition between gaseous and solid matrix, the energy balance in a porous medium with internal heat generation due to reaction can be written as:

$$(\rho c)_m \frac{\partial T}{\partial t} + (\rho c)_f \vec{v} \cdot \nabla T = \nabla \cdot (k_m \nabla T) + q_m''' \tag{2}$$

where

$$(\rho c)_m = (1-\varepsilon)(\rho c)_s + \varepsilon(\rho c)_f \tag{3}$$

$$k_m = (1-\varepsilon)k_s + \varepsilon k_f \tag{4}$$

$$q_m''' = Q_r'''$$ (5)

are respectively, the overall heat capacity per unit volume, overall thermal conductivity, and overall heat production per unit volume due to the oxidation reaction. At the beginning of oven heating test, the sample temperature is lower than the oven temperature. The temperature inside the sample will rise and it will become equal to oven's temperature. Under this condition, the heat-released method can be applied by setting thermal gradients ∇T to zero in eq. 2 and therefore the advective and diffusive terms become negligible. Then, energy accumulation is only a result of the heat generated by the oxidation reaction, which can be expressed as a first-order Arrhenius equation (Jones et al., 1998; Sujanti and Zhang, 1999; Zambra et al., 2011; Cocchi, 2014). Under these assumptions, the heat transfer equation (eq. 2) simplifies to

$$(\rho c)_m \frac{\partial T}{\partial t} = (1-\varepsilon) C_{ox} \rho_s A_0 Q \exp\left(\frac{-E_a}{RT_0}\right)$$ (6)

where C_{ox} is the oxygen concentration, ρ_s is the charcoal apparently density, Q is the heat of reaction, A_0 is the pre-exponential factor, E_a is the activation energy, R is the universal gas constant and T_0 is the cross-point temperature. This last parameter is defined as the equilibrium condition where the temperature at the center of the sample will become equal to the oven temperature. Eq. 6 can be rearranged in a linearized form, which allows the calculation of the activation energy of exothermic reactions that promote self-heating and the reactivity-coupled parameter QA_0C_{ox}:

$$ln\left(\frac{\partial T}{\partial t}\right)_{T_0} = ln\left(\frac{(1-\varepsilon)\rho_s A_0 Q C_{ox}}{(\rho c)_m}\right) - \frac{E_a}{RT_0}$$ (7)

4.3 METHODOLOGY

4.3.1 Charcoal samples

Eucalyptus charcoal obtained from a standardized carbonization process (final temperature of 450 °C) was used. Charcoal particles between 50 and 70 mm were selected for characterization and in further experimental trials. The apparently density of the charcoal was measured according to the hydrostatic method by means of immersion in water as described by Vital (1984). Moisture, volatile matter, ash and fixed carbon content were determined in duplicate and expressed on dry basis according to the procedure established in standard NBR 8112 (ABNT, 1986). The High heating value (HHV) was

determined in duplicates, using a digital calorimeter model IKA C-200, according to Standard NBR 8633 (ABNT, 1984).

4.3.2 Experimental set-up

A furnace equipped with a temperature control system contains the charcoal oxidation apparatus (Figure 1). This system consists on a steel reactor of 4 L capacity that contains the sample of charcoal to be analyzed. The flow and composition of the gas injected into the reactor are controlled by rotameters for air and CO_2. The gas mixture was injected into the reactor using a 1.2 m stainless spiral tube (8.73 mm inner diameter), which works as a preheater. The internal temperature of the furnace and sample center were recorded using two AWG 24 K-type thermocouples linked to an ICP CON 7018 - ICP CON 7520 interface data acquisition module connected to a computer. Gases leaving the reactor were subjected to a clean-up by condensation at 4 ºC, hydrous ethanol (96%) washing for tar retention, drying in silica gel column, and filtration in 0.22 µm membrane (Whatman® Anotop® 25 Plus syringe filter) for particles retention (Coelho, 2012). Therefore, the clean gas composition (O_2, CO and CO_2) was continuously quantified in a real time gas analyzer (Gasboard 3100, Wuhan CUBIC Optoelectronics Co. Ltd., China).

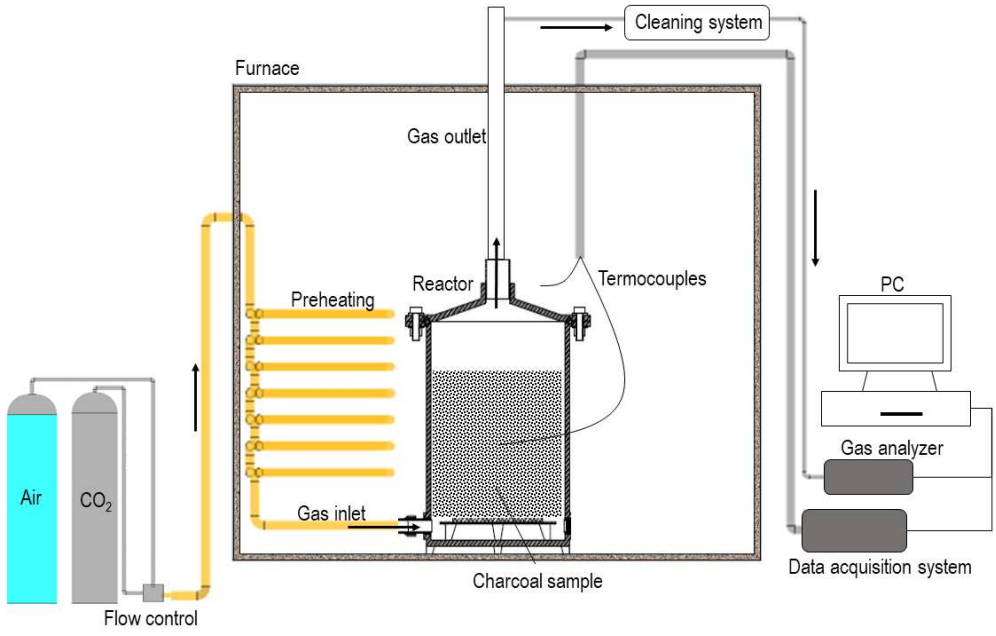

Figure 1. Experimental setup for self-heating experiments.

4.3.3 Procedure

Since the cooling of the kilns by natural convection is a common practice in charcoal companies, the kinetics of the charcoal oxidation in the reactor without any forced gas flow was evaluated in the first part of the experiment. Samples of 230 g of charcoal were heated into the reactor at constant furnace temperatures of 100, 150, 200, 250 and 300°C. The furnace and sample temperature, as well as the gas composition at the reactor outlet, were recorded every second. The temperature heating rate (*dT/dt*) was evaluated using a second order interpolation scheme (Cocchi, 2015) at the vicinity of the crossing point temperature (T_0). The test ended once steady state was reached, i.e. when the sample temperature reached a constant value in time. The activation energy and the reactivity-coupled parameter were determined by regression analysis between the logarithm of the transient heating and the inverse of the temperature (Eq. 7) and attained from the slope of a fitted linear function.

In the second part of the experiment, the influence of gas flow rate on the transient heating rate was evaluated. The furnace was programmed at a constant temperature of 200 °C. Three gas flow rate were tested (1800, 6000, and 8000 $cm^3\ min^{-1}$) with a concentration of 20.9% O_2. For each test, a sample of 230 g of charcoal was placed in the reactor. To ensure that no oxidation occurred before the sample reached the furnace temperature, the oxygen concentration inside the reactor was reduced to less than 1% by injecting a flow of 2000 $cm^3\ min^{-1}$ of CO_2 until the sample temperature became equal to the furnace temperature. Then, the injection of CO_2 was suspended and the injection of gas (air) was started at the different flow rates. The transient heating was continuously recorded and the *dT/dt* value was evaluated. The test ended when the sample temperature reached a constant value.

Finally, the effect of the initial concentration of O_2 in the reactor was evaluated. A mixture of CO_2 and air was injected into the reactor. The flow rate of each gas was adjusted to obtain the desired concentration within the reactor. Concentrations of 20.9, 15, and 10 % of oxygen were tested at a constant flow rate (total air + CO_2) of 1800 $cm^3\ min^{-1}$, previously defined in the second part of the experiment. For each concentration, constant temperature tests of 100, 150, 200, 250, and 300 °C were carried out. The gas flow was injected into the reactor and heating was initiated after the oxygen concentration inside the reactor have been stabilized. Experimental trials were carried using the same procedure described earlier to measure the *dT/dt* value at the crossing-point T_0. Tests ended when the temperature of the sample reached a constant value. The activation energy

and the reactivity-coupled parameter for each oxygen concentration were determined by regression analysis between the logarithm of the transient heating and the inverse of the temperature (Eq. 7) from the slope of a fitted linear function.

4.4 RESULTS

The characterization of the charcoal used in the experiment is presented in Table 1. The values are in the quality range for siderurgic use (Pereira et al., 2012; Santos et al., 2016).

Table 1. Properties of the charcoal samples

Property	Value
Apparently density (kg/m^3)	457.4
Bed porosity	0.60
Moisture content (%db)	5.63
Volatile compounds (kg/kg$_{db}$)	0.234
Ashes (kg/kg$_{db}$)	0.0026
Fixed carbon (kg/kg$_{db}$)	0.763
HHV (kJ/kg)	31859

Figure 2 shows the sample temperature and gas composition profiles inside the reactor during the oxidation tests without gas injection. The *dT/dt* value was observed to increase with temperature up to 250 °C (Fig 2D). At 300 °C the self-heating intensity decreased, and this value dropped to 0.044 K s^{-1} (Fig 2E). This phenomenon is probably due to the limited availability of oxygen above 250 °C (<4%). The maximum temperature increase reached by the sample was 28 K above T_0 for all experimental trials except for the test at 100 °C (Fig 2A), where a slight increase was observed. These results agree with the observations of Van Blijderveen et al. (2010), who reported that the interaction of coal with oxygen changes from endothermic to exothermic only above 150 °C. They are also in agreement with Cocchi (2014), who did not observe self-heating in samples of charcoal in the tests at 100 °C. At the end of each test, the steady-state condition can be observed because of the energy balance between the heat generated inside the sample and the heat transferred to the surroundings.

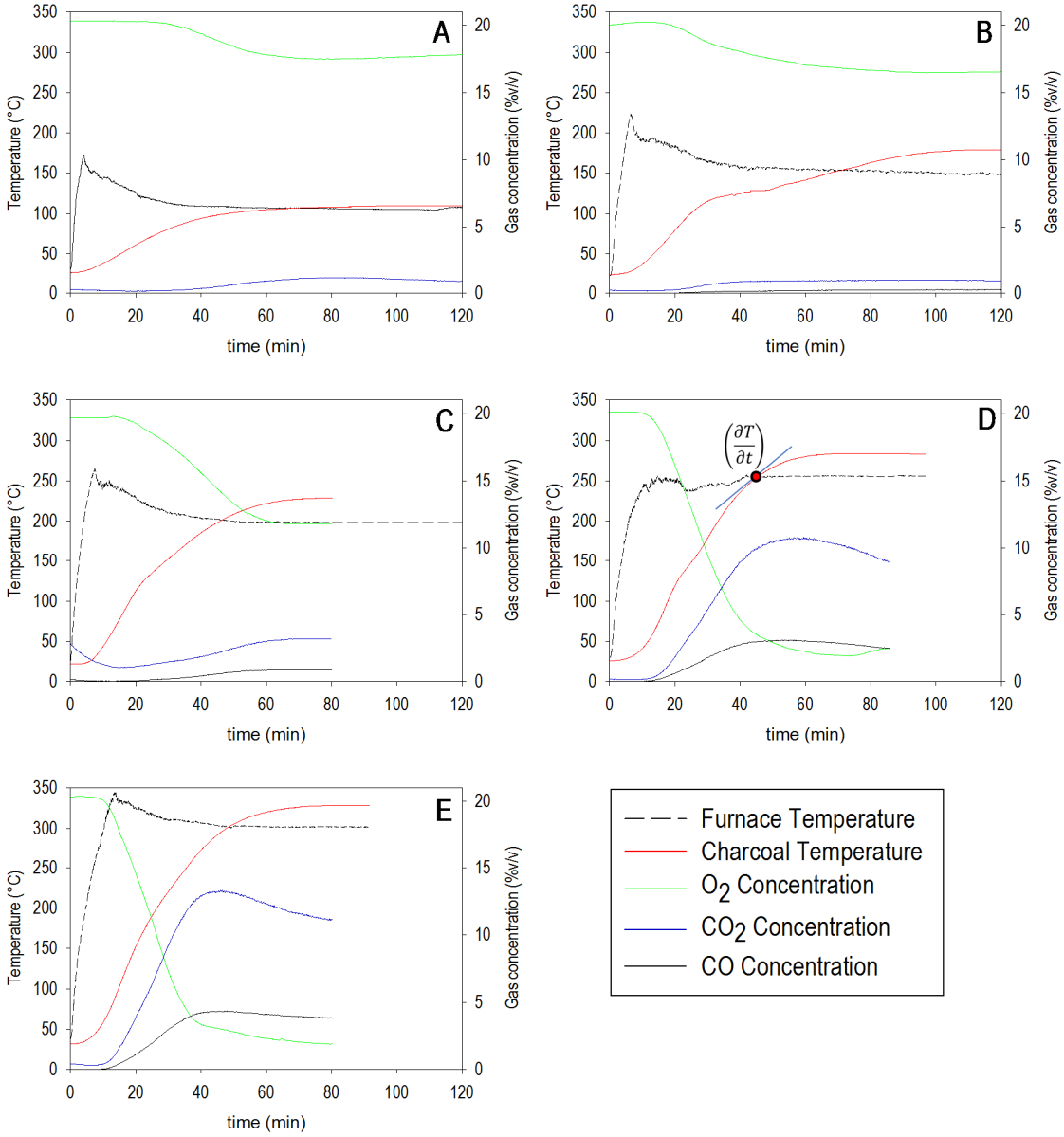

Figure 2. Temperature and gas concentration profiles during the oxidation tests without air injection. A) 100 °C, B) 150 °C, C) 200 °C, D) 250 °C and E) 300 °C. The red dot in Fig. 2D illustrates the crossing point temperature.

The initial temperature of the oxidation reactions was identified as the oxygen concentration began to decrease, corresponding to an average charcoal temperature of 75 °C. A time lag can be observed between the beginning of the oxygen consumption and the beginning of the generation of oxygenated gases (CO_2 and CO). This phenomenon can be explained by the complex interaction between oxygen and charcoal pores. The oxidation reaction that releases gases occurs as a third step, after the phenomena of physical and chemical adsorption of oxygen (Carras and Young, 1994). The generation

of carbon monoxide was only observed above 150 °C, increasing with the temperature until reaching a maximum value of 4.29% at 300 °C. As expected, the rates of O_2 consumption and CO and CO_2 generation increased with temperature, agreeing with experiments reported by Wang et al. (2003) and Yuan and Smith (2013).

Figure 3A shows the exponential increase of the oxygen consumption with the increase of charcoal temperature up to 250 °C. Above this temperature, the consumption tends to stabilize, when the oxygen concentration decreased to 1.96%. The value could indicate the minimum oxygen concentration that would allow the occurrence of oxidation reactions at 250 °C. Evaluating the oxidation of different types of mineral coal, Qi et al. (2010) observed an exponential increase in oxygen consumption at temperatures ranging from 30 to 100 °C, with an 8% decrease in O_2 concentration at 100 °C. For these temperature we observed a decrease of 13.5% in O_2 concentration, indicating, as expected, a higher reactivity of the charcoal due to its higher fixed carbon content.

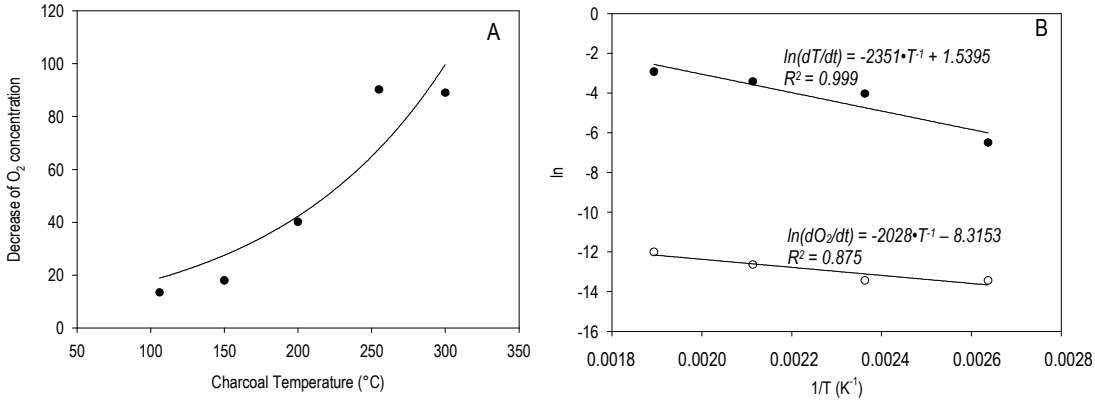

Figure 3. Self-heating testes without air injection. A) Oxygen consumption as a function of charcoal temperature and B) Temperature gradient and rate of oxygen consumption as a function of the inverse crossing point temperature.

Figure 3B shows the regression of the transient linear functions for the self-heating rate and oxygen consumption rate (Eqs. 1 and 7) during the oxidation tests at 100, 150, 200 and 250 °C. The activation energy calculated for the phenomena of self-heating and oxidation (oxygen consumption) was 19.54 kJ mol^{-1} and 16.85 kJ mol^{-1}, respectively. The lower activation energy for the rate of oxygen consumption indicates that this phenomenon occurs before self-heating. Interesting, this behavior can be explained because the oxidation reaction begins with the adsorption of oxygen in an endothermic

step, followed by the exothermic oxidation reaction as such, which generates self-heating (Qi et al., 2010).

Figure 4 shows the temperature profiles of three charcoal samples subjected to heating at 200 °C with different air flow rates. After reach the thermal equilibrium with the furnace, air at different flow rates was injected in injected in the reactor. The heating observed above the furnace temperature is due to the oxidation reactions and reflects a subcritical behavior. A direct relationship was observed between the injected air flow rates and the self-heating rate, which reached values of 0.025, 0.04 and 0.065 K s^{-1} for 1.8, 6.0 and 8.0 L min^{-1}, respectively. The minimum flow rate tested was enough to produce a subcritical behavior in the sample that allowed evaluating the self-heating rate in the cross-point. This minimum value was chosen to evaluate the effect of the gas composition on the next stage of the experiment.

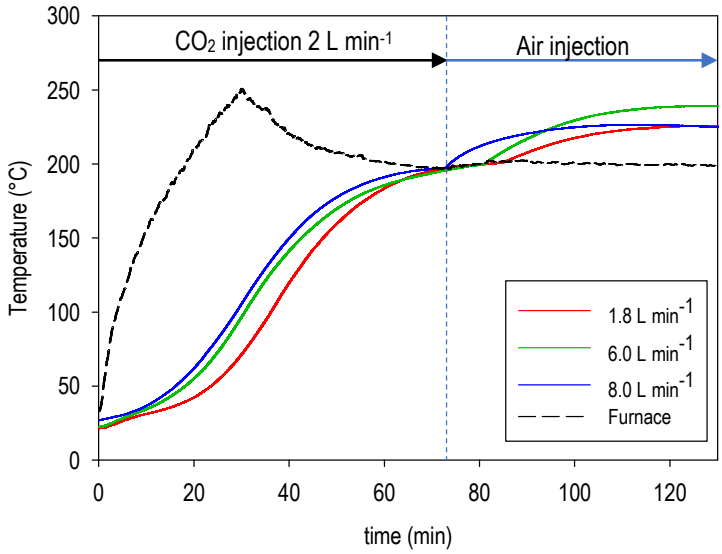

Figure 4. Effect of the air flow rate on the charcoal temperature in samples subjected to oxidation at 200 °C.

Figure 5A shows the temperature profile of charcoal samples subjected to heating at 300 °C and a constant gas flow rate of 1.8 L min^{-1} with 3 different oxygen concentrations. While concentrations of 20.9 and 15% showed close values in the self-heating rate and a maximum charcoal temperature between 401 and 357 °C, respectively, the oxygen concentration of 10% reflected in a low self-heating rate and a maximum charcoal temperature of 309 °C. A similar behavior was observed in the tests at 150, 200, and 250 °C. Figure 5B shows the self-heating rates as a function of temperature for each oxygen

concentration. The linear regression performed shows a nearly constant slope for the three oxygen concentrations reflecting similar values of activation energy at the three concentrations (Fig. 5B). A minimum value of the coupled parameter QA_0C_{ox} for the 10% oxygen concentration was calculated. Table 2 summarizes the calculated kinetic parameters.

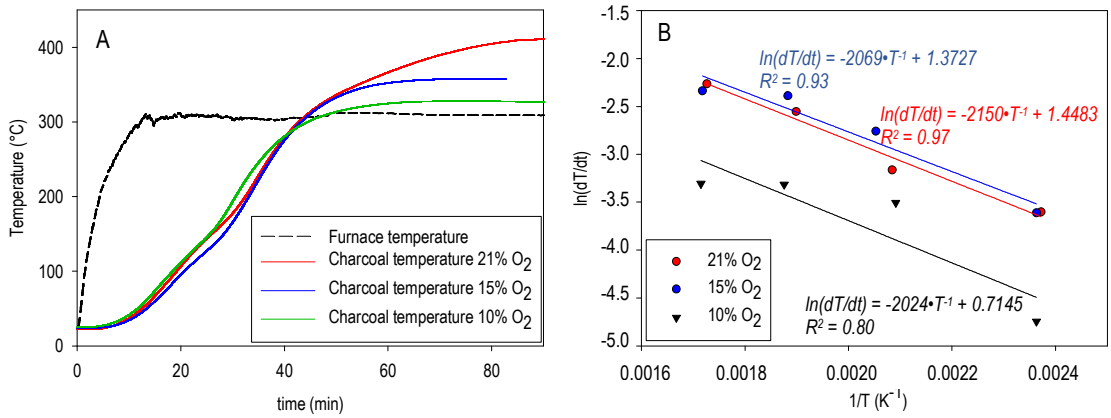

Figure 5. Temperature profile of charcoal samples subjected to oxidation at 300 °C (A) and self-heating rate vs inverse cross point temperature (B), at different concentrations of oxygen.

Table 2. Kinetic parameters calculated for the charcoal self-heating phenomena at different initial concentrations of oxygen (gas flow rate of 1.8 L min^{-1})

Oxygen Concentration (% v/v)	Reaction temperature (°C)	Activation energy (kJ mol^{-1})	QA_0C_{ox} (W kg^{-1})
20.9	67.5	17.87	4328.22
15.0	135.8	17.20	4002.25
10.0	167.7	18.31	2077.89

The activation energy of the charcoal self-heating reactions presented an average value of 17.79 kJ mol^{-1} (Table 2). This parameter was independent of the oxygen concentration in the gas and its value was slightly lower than the value calculated for the tests without air flow injection (19.54 kJ mol^{-1}). These results indicate that the oxidation phenomenon is affected to some extent by the advective mechanism. Although, as also described by Wang et al. (2003), the phenomenon is not limited by O_2 external mass transport, but the O_2 diffusion in the pores. Nugroho et al. (1998), using crossing-point

methods, calculated activation energies of self-heating reactions ranging from 54 to 78 kJ mol^{-1} for three types of Indonesian coal. The higher values of this parameter indicate a lower material reactivity, possibly due to the low fixed carbon content (37 to 49%, Nugroho et al., 1998) as compared to eucalyptus charcoal (73.6 %, Table 1). The coupled parameter QA_0C_{ox} represents the amount of heat released per mass of oxidized charcoal. This value slightly decreases with the reduction of O_2 concentration from 20.9 to 15%, but a great decrease was observed for 10% of O_2, which may indicate a different limiting mechanism at lower O_2 concentrations (Table 2).

The reaction temperature was defined as the temperature reached by the sample in which oxygen consumption began, and was calculated as the average of the values observed in the tests at 150, 200, 250 and 300 °C. Oxygen consumption was imperceptible in the tests at 100 °C. The reaction temperature shows an inverse relationship with the O_2 concentration, presenting high values for 10% of O_2 and being only at 67.5 °C for the tests with atmosphere of 20.9% of O_2. These observations are in accordance with the usual practice in the charcoal industry for kiln opening at the end of the cooling stage. The common practice set the safe temperature of 60 °C for charcoal discharge, which minimize combustion foci.

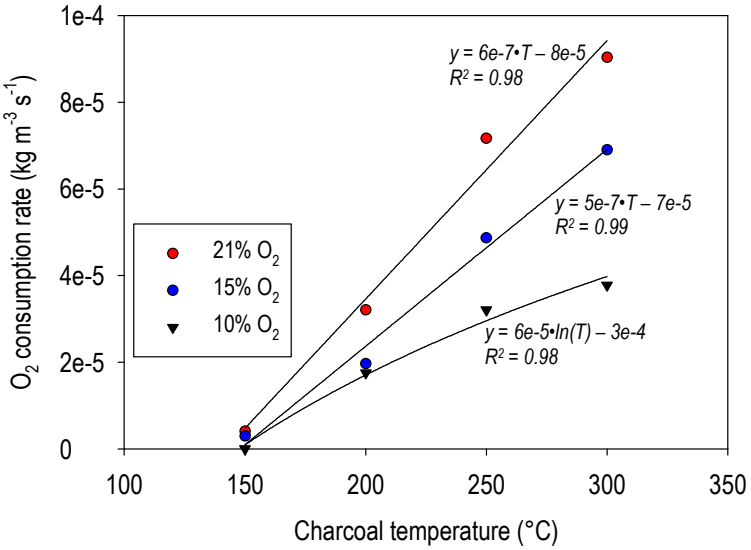

Figure 6. Oxygen consumption rate as a function of charcoal temperature and O2 concentration.

The oxygen consumption rate during the oxidation reactions increased with the charcoal temperature and the oxygen concentration in the gas (Fig. 6) in different ways. At O_2 concentration higher than 15%, the dependence is almost linear. At the lower

concentration a logarithmic dependence is verified. Interestingly, the pronounced and distinct effect of higher oxygen concentration, also observed in Figure 5B, suggest a different limiting oxidation mechanisms for lower concentrations. At 150 °C, the consumption rate for the three concentrations presented close values, being almost negligible for 10% of O_2. Several authors reported a decrease in the rate of oxygen consumption by coal in a batch reactor when the initial concentration of O_2 was reduced (Wang et al., 2003).

4.5 CONCLUSIONS

The charcoal self-heating phenomenon was explored in oven-heating experiments. The higher the temperature and O_2 concentration, the greater the intensity of the oxidation reactions. The activation energy for this phenomenon was independent of the initial oxygen concentration and slightly influenced by the advective mechanism. The oxidation reaction was observed when the charcoal temperature reached 67.5 °C at 20.9% of O_2 and increased to 167.7 °C in atmospheres with 10% of O_2. The rates of heat generation and O_2 consumption derived from these study can be used as energy and chemical species sources in mathematical models that attempt to simulate the heat transfer phenomena during storage and cooling process.

4.6 REFERENCES

ABNT - ASSOCIAÇÃO BRASILEIRA DE NORMAS TÉCNICAS. NBR 8633: Carvão Vegetal – determinação do poder calorífico. Rio de Janeiro, 1984. 13p.

ABNT - ASSOCIAÇÃO BRASILEIRA DE NORMAS TÉCNICAS. NBR 8112: Carvão vegetal: análise imediata. Rio de Janeiro, 1986. 8 p.

Alves I C N. Caracterização tecnológica da madeira e do carvão vegetal em clones híbridos de *Eucalyptus grandis x Eucalyptus urophylla* [dissertation]. Universidade Federal de Viçosa; 2013.

Carneiro A de C O, Vital B R, Oliveira A C, Pereira B L. Pirólise lenta da madeira para produção de carvão vegetal. In: Santos F, Colodette J, Queiroz J, editors. Bioenergia e Biorrefinaria: cana de açúcar e espécies florestais. Viçosa: UFV; 2013. p. 429-458.

Carras J and Young B. Self-heating of coal and related materials: Models, application and test methods. Prog. Energy Combust. Sci. 1994;20:1–15.

Cocchi G. Estimating the activation energy of exothermic reactions in substances that undergo self-heating processes with the Heat Release method: Use of sub critical data. Fuel. 2014;125:152–154.

Cocchi G. The relationship between thermal diffusivity, energy of activation and temperature rise in subcritical self-heating of fuels in sample geometries. Fuel. 2015;158:816–825.

EPE Empresa de Pesquisa Energética. Balanço Energético Nacional. 2018. 70-1.

França G A C, Campos M B. Análise teórica e experimental do resfriamento de carvão vegetal em forno rectangular. IV Encontro de Energia no Meio Rural; 2002 Oct 28-31; Campinas (SP), Brazil.

Jones J C, Henderson K P, Littlefair J, Rennie S. Kinetic parameters of oxidation of coals by heat-release measurement and their relevance to self-heating tests. Fuel. 1998;7719–22.

Martins M A. Desafios da implementação de periféricos na produção de carvão vegetal. In: I SEMINARIO DE CARVÃO VEGETAL. Aperam Bioenergia. Universidade Federal de Viçosa. 2014.

Nugroho Y S, McIntosh A C, Gibbs B M. Using the crossing point method to assess the self-heating behavior of Indonesian coals. Leeds, UK. Twenty-Seventh International Symposium on Combustion/The Combustion Institute. 1998. pp. 2981–2989.

Oliveira D, Teixeira C A, Silva J, Reis H O, Vorobieff C L. Resfriamento rápido de fornos de carbonização. Engenharia Agrícola Jaboticabal. 2010;30(6):1023-1032.

Oliveira A C, Carneiro A de C, Barcellos D C, Rodriguez A V, Amaral B M, Pereira B. L. Resfriamento artificial em fornos retangulares para a produção de carvão vegetal. Revista Árvore Viçosa-MG. 2015;39(4):769-778.

Peláez-Samaniego M R, Garcia-Perez M, Cortez L B, Rosillo-Calle F, Mesa J. Improvements of Brazilian carbonization industry as part of the creation of a global biomass economy. Renewable and Sustainable Energy Reviews. 2008;12:1063–1086.

Perdochova M, Derychova K, Veznikova H, Bernatik A, Pitt M. The influence of oxygen concentration on the composition of gaseous products occurring during the self-heating of coal and wood sawdust. Process Safety and Environmental Protection. 2015;94463-470.

Pereira B L, Oliveira A C, Carvalho A M, Carneiro A C, Santos L, Vital B. Quality of Wood and Charcoal from Eucalyptus Clones for Ironmaster Use. International Journal of Forestry Research. 2012;1-8.

Pereira E G, Martins M A, dos Santos L.F, Carneiro A de C. Energy Assessment of Wood Pyrolysis Coproducts for Drying and Power Generation. Energy & Fuels. 2017;31(12) 13815-13823. DOI: 10.1021/acs.energyfuels.7b02998

Qi X, Wang D, Zhong X, Gu J, Xu T. Characteristics of oxygen consumption of coal at programmed temperatures. Mining Science and Technology. 2010;20:372-377.

Rezende M E. Produção de carvão vegetal – importância do conhecimento fundamental. Curso: Fundamentos e práticas da carbonização da biomassa, ministrado durante o Seminário: Prática, logística, gerenciamento e estratégias para o sucesso da conversão da matéria lenhosa em carvão vegetal para uso na metalurgia e indústria. – Belo Horizonte, novembro 27-28. 2006.

Santos I. Resfriamento artificial de carvão vegetal em fornos de alvenaria. Viçosa, Brasil. [dissertation]: Universidade Federal de Viçosa; 2013.

Santos L C, Freitas F P, Boschetti W, Pereira B, Carvalho A. Produção e caracterização de carvão vegetal a partir de diferentes clones de *Eucalytus spp*. Proceedings of IV Fórum Nacional sobre Carvão Vegetal. Belo Horizonte, Brasil. 2016.

Sujanti W and Zhang D. A laboratory study of spontaneous combustion of coal: the influence of inorganic matter and reactor size. Fuel. 1999;78:549–556.

Taraba B, Michalec Z, Michalcová V, Blejchar T, Bojko M, Kozubková M. CFD simulations of the effect of wind on the spontaneous heating of coal stockpiles. Fuel. 2014;118:107–112.

Van Blijderveen M, Gucho E, Bramer E, Brem G. Spontaneous ignition of wood, char and RDF in a lab scale packed bed. Fuel. 2010;89:2393–2404.

Vital B R. Métodos de determinação da densidade da madeira. Viçosa, MG: Sociedade de Investigações Florestais. 1984; 21 p.

Wang H, Dlugogorski B, Kennedy E. Coal oxidation at low temperatures: oxygen consumption, oxidation products, reaction mechanism and kinetic modelling. Progress in Energy and Combustion Science. 2003;29:487–513.

Yuan L and Smith A. The effect of ventilation on spontaneous heating of coal. Journal of Loss Prevention in the Process Industries. 2012;25(1).

Yuan L and Smith A. Experimental study on CO and CO2 emissions from spontaneous heating of coals at varying temperatures and O2 concentrations. Journal of Loss Prevention in the Process Industries. 2013;26(6):1321-1327. DOI https://doi.org/10.1016/j.jlp.2013.08.002

Zambra C, Rosales C, Moraga N, Ragazzy M. Self-heating in a bioreactor: Coupling of heat and mass transfer with turbulent convection. International Journal of Heat and Mass Transfer. 2011;54:5077–5086.

5. CHAPTER IV: IMPROVEMENTS IN THE THERMAL EFFICIENCY OF CARBONIZATION KILNS: A CFD STUDY

Abstract: In Brazil, wood carbonization process is carried on in brick kilns. Its walls and floor are built using isolation materials that minimize heat losses during the pyrolysis stage but it reflects in long cooling times, decreasing productivity per kiln. The aim of this research was to simulate the thermal performance of a 700 m^3 carbonization kiln in different configurations looking for strategies that allow optimizing the carbonization and cooling stages. A two-dimensional CFD analysis was performed to evaluate the effect of a concrete insulating layer over the bed-floor interface on the thermal performance of the carbonization and cooling stages. A three-dimensional CFD analysis was performed to evaluate the effect of a buoyancy-driven heat exchanger on the cooling time. The results show that a 3 cm layer of insulation concrete over the bed-floor interface could reduce the energy requirement for the carbonization step by 6% and could reduce the cooling time by almost 2 days. The use of a buoyancy-driven flow heat exchanger can reduce the cooling time between 27 and 59%, increasing productivity per kiln per year up to 65%.

Keywords*: biomass energy, heat transfer, natural convection, cooling, buoyancy.*

5.1 INTRODUCTION

Nowadays, the climate change scenario and environmental policies have been driving industries to implement measures to control and reduce pollutant emissions. Despite the efforts, global energy-related CO_2 emissions reached a historic height of 32.5 gigatons in 2017 (IEA 2017). The steel and iron industry accounts for 7 to 9 % of global direct emissions mainly due to the use of coal as a reducer of the iron ore and as an energy source. In addition, 1.83 ton of CO_2 were emitted per ton of steel produced in 2017 (Worldsteel Association, 2018).

In steel production, a carbon source is necessary during the reduction of iron ore. From the technical and environmental points of view, charcoal from biomass is a promising alternative for coke from coal. Besides the higher fixed carbon content, charcoal presents advantages in relation to its low content of sulfur, nitrogen, and heavy metals, elements that may adversely affect the quality of the steel (Nakahara et al., 2014). Biomass, as a renewable carbon resource, could lead to a significant reduction in CO_2 emissions. Kokonya et al. (2013), evaluating the addition of biomass to coking coals, concluded that the addition of 10 % of Scots pine resulted in a significant 3 % reduction in non-renewable carbon emissions. Fick et al. (2013), analyzing the use of biomass for pig iron production, verified that CO_2-equivalent total emissions were reduced in 14.4% and 6.7% in the blast furnace and sintering plant, respectively, when 20% of coke was replaced by charcoal. This saving is around 300 kg of CO_2-equivalent per ton of pig iron produced. Although some metallurgical companies in Brazil have achieved 100% of coal replacement by charcoal from wood (Fick et al., 2013), its cost continues to be a limitation.

With 5.5 million tons in 2016, Brazil is the largest producer and consumer of charcoal from planted forests (EPE, 2017). The slow pyrolysis of wood occurs in four phases according to the temperature reached: wood drying up to 110 °C, roasting up to 250 °C, charring and carbon fixing up to 350 °C (Peláez-Samaniego et al., 2008; Rezende, 2006). In Brazil, the common-use technology for charcoal production consists of masonry kilns in which drying, pyrolysis and cooling are carried out sequentially. The insulating characteristics of masonry walls and clay floor minimize energy losses during wood pyrolysis but hinder the cooling stage. In a kiln of 700 m^3-capacity, the production cycle takes approximately 12 days, in which 4 corresponds to pyrolysis and the 8 days left is taken for cooling. Adding the loading and unloading times, and considering a wood

density of 540 kg m^{-3} and gravimetric yield of 33% (Oliveira et al., 2015), approximately 30 cycles are carried out per year. This equates to an average productivity of 2040 ton of charcoal per kiln per year.

The long cooling time is due in part to the thermal inertia of the kiln structure. During the pyrolysis stage, 8.8% (25221 MJ) of the total energy required in the process is lost through the floor and accumulated in the clay soil (Bustos-Vanegas et al., 2018). Along the cooling stage, this energy is released and then reabsorbed in part by the charcoal bed (Bustos-Vanegas et al., 2018).

During the carbonization stage, wood becomes charcoal and its volume decreases creating a headspace inside the kiln where a flow of hot gases drive the carbonization front from the top to the bottom of the wood bed. At the end of pyrolysis, the headspace could occupy more than 50% of the kiln volume, and the buoyancy force also drive the cooling front upward. This driving force tends to decrease during the cooling due to the decrease in the temperature difference between the bed surface and the inner surface of the walls. The Rayleigh number indicates the intensity of the buoyancy-driven flow inside the kiln headspace. For Rayleigh numbers less than a critical value of 1708, buoyancy forces cannot overcome the resistance imposed by viscous forces and therefor no advection occurs within the cavity (Bergman et al., 2011). Then, conduction and radiation become the dominant mechanisms and the cooling rate decreases.

Natural convection is an economically attractive alternative in several applications since it does not demand an external source of energy. Buoyancy-driven flows within enclosures has been studied in several applications regarding solar energy, building and ventilation, heat exchangers, fuel cells, thermal storage tanks, chemical reactions, cooling and drying process (Lin et al., 2013; Yang et al., 2015; Biswal and Basak, 2017). Although some charcoal companies already had tested prototypes of heat exchangers by natural convection, there is still a lack of information regarding the optimal configuration and operation.

The charcoal producers have been adopting measures to optimize the production process, reducing the charcoal cost and environmental impact. An example is the utilization of enthalpy from carbonization emissions in the wood drying operation or in power generation (Pereira et al., 2017). Also, some research focused on reducing the cooling time by using heat exchangers driven by forced convection (França and Campos,

2002; Oliveira et al., 2010; Santos, 2013; Martins, 2014; Oliveira et al., 2015). Those studies achieved up to 50% savings in cooling time but increasing energy consumption due to the use of fans or pumps. Mathematical modeling could be an important tool to optimize these technologies, perhaps, few studies have addressed this topic (França and Campos, 2002; Santos, 2013; Bustos-Vanegas, 2018) and in some cases using simplifications that facilitate numerical calculations but which may not faithfully represent the physics of the phenomenon. Interestingly, the mathematical approach to the charcoal cooling phenomenon is still an unresolved problem. Therefore, this study aims to improve the carbonization process in brick kilns using a previously validated mathematical model. A two-dimensional CFD analyses was performed to quantify the effect of an insulation layer over the floor. Then, a three-dimensional CFD analyses was used to evaluate the effect of the use of a buoyancy-driven heat exchanger on the cooling process.

5.2 METHODOLOGY

A previously validated mathematical model (Bustos-Vanegas et al., 2018) to quantify the thermal inertia effects of the structural elements of a carbonization kiln (industrial model Vallourec Florestal 700 m^3 nominal capacity) (Fig. 1A) on the carbonization and cooling stages, was used to simulate its thermal performance in different configurations. A two-dimensional approach was used to evaluate the effect of an insulating concrete layer over the clay floor. The effect of a buoyancy-driven flow heat exchanger on the time and homogeneity of cooling was evaluated by means of a three-dimensional analysis. A standard carbonization cycle of 12 days (4 days for the carbonization stage and 8 days for the cooling stage) was simulated for each proposed scenario with the CFD technique using ANSYS CFX v11.0 software.

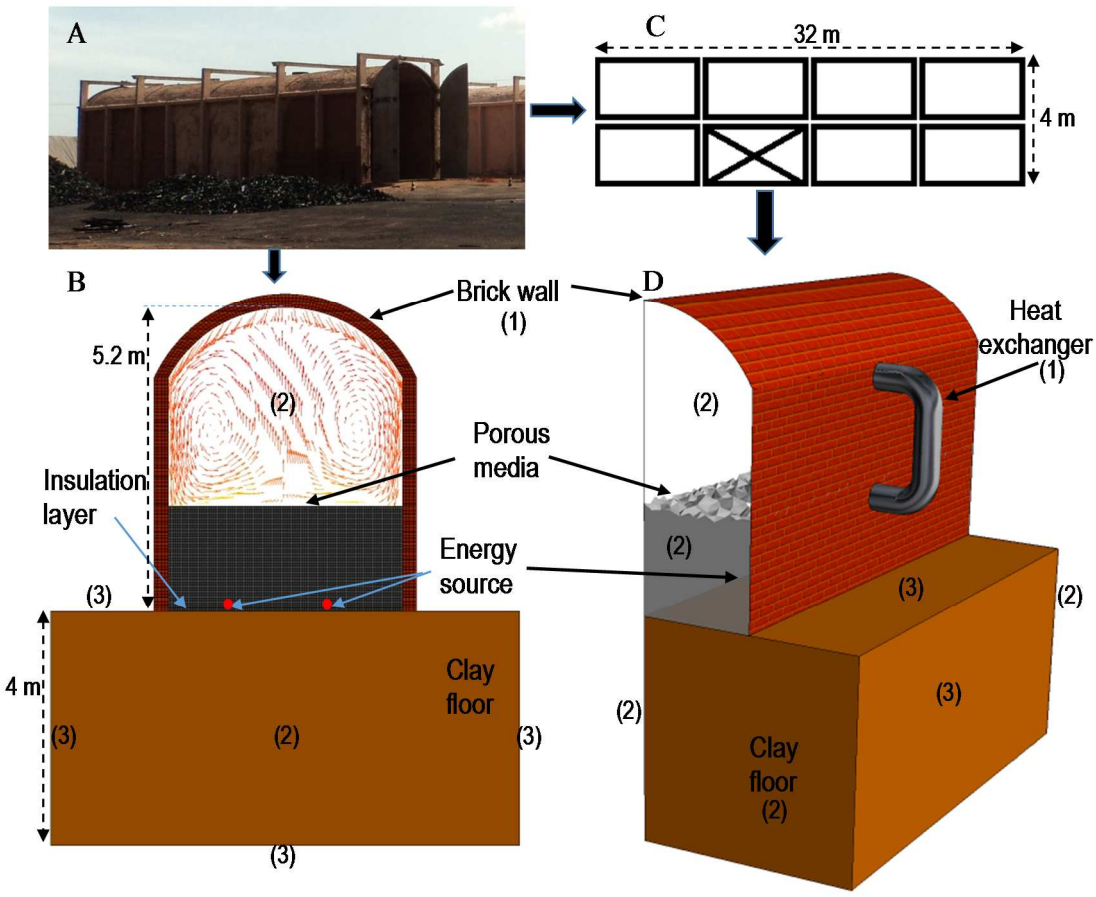

Figure 1. A) Carbonization kiln model (Vallourec Florestal) nominal load capacity of 700 m^3. B) 2D simplification. C) Top view and symmetry condition. D) Kiln segment and heat exchanger coupled for 3D analysis. The numbers in parentheses represent the boundary conditions: (1) mixed condition of convection and radiation, (2) symmetry, (3) adiabatic condition.

5.2.1 Physical model – 2D analysis

As described by Bustos-Vanegas et al. (2018), the two-dimensional approach is a valid simplification to describe the thermal behavior of carbonization kilns under standard operating conditions. Fig. 1B shows in two dimensions, the solid domains of the floor and walls as well as the porous domain (wood bed turning charcoal). As verified by Bustos-Vanegas et al. (2018), during the carbonization stage heat diffuses through the floor and after the first day of cooling, the floor's temperature is found to exceed the temperature of the interface, thereby inverting the heat flux and reheating the charcoal bed. Trying to minimize this problem, a 3 cm layer of ENGECAST -1050® insulation concrete (k = 0.13 W m^{-1} K^{-1}) over the floor was simulated using the resistance method. This material was selected considering its insulating characteristics and its resistance to compression. The

layer should support besides the weight of the wood, the weight of the machinery used to load and unload the kiln. The pressures exerted by this type of machinery ranging between 0.57 and 1 kg-f cm^{-2} (Novak et al., 1992).

After a previous testing of spatial and temporal convergence, a mesh of 13,740 elements (8820 for the porous subdomain, 888 for the wall subdomain and 4032 for the floor subdomain) and a time step of 60 min were chosen. A mesh refinement was applied at the bed-walls and bed-floor interfaces to improve the heat flux conservation and temperature continuity.

5.2.2 Physical model – 3D analysis

A 3D analysis was implemented to evaluate the use of a buoyancy-driven heat exchanger located on the lateral wall of the kiln. The goal was to reduce the cooling time and ensuring homogeneity, without increasing the operating cost. Fig. 1C shows the top view of the kiln divided into 8 symmetrical segments. Because the less area exposed to the convection to the environment, the central region of the kiln will present a lower rate of cooling, that is, it will be the most difficult region to cool. Therefore, one of the central segments was chosen to simulate the cooling stage considering the thermal inertia of the soil and the use of a buoyancy-driven heat exchanger (Fig. 1D). As demonstrated by Bustos-Vanegas et al. (2018), the temperature profile in the brick walls during carbonization and cooling stages show a pseudo-steady state behavior that allows modeling this subdomain using the thermal resistance method. This approach was implemented to reduce computational time.

In addition to decreasing the cooling time, the use of the heat exchanger must guarantee its temperature homogeneity, that is, to minimize possible foci of ignition during the kiln opening. These regions with potential ignition hazards, or breakpoints, were identified as the percentage of charcoal volume with a temperature above 65 °C.

Figure 2 presents the operating principle of the buoyancy-driven heat exchanger and the different simulated configurations. After the carbonization stage, the hot gases in the headspace continue to exchange heat by convection, radiation, and conduction with the inner surface of the walls, the heat diffuses to the outer surface and finally is dissipated in the environment by convection and radiation. The buoyancy force resulting from gas density differences is used as the driving force of the convection phenomenon that directs hot gases to the top of the kiln where the outlet for the heat exchanger is located. The

Rayleigh number was used as an indicator of the transition between the laminar and turbulent regimes (Bergman et al., 2011) of the buoyancy-driven flow inside the kiln:

$$Ra = \frac{g\beta(T_{bs} - T_i)L^3}{\alpha\vartheta} > 1708 \quad (1)$$

where β is the expansion coefficient, T_{bs} is the average temperature of bed surface, T_i is the average temperature of the internal wall, L is the distance from bed surface to the top, α and ϑ are the thermal diffusivity and kinematic viscosity of the gas, respectively.

By integrating the heat exchanger, it is expected to increase and maintain the flow turbulence due to the higher temperature difference (Eq. 1) between the bed surface and the inner surface of the exchanger. The device consists of a carbon steel tube connecting the kiln top with its base. Two retention valves are located at the inlet and outlet of the duct. During the carbonization step, the gas flow is prevented by flooding the valves with water. The details of the valve are shown in Fig 2 in the enlarged box. Once the pyrolysis stage is complete, the valves are drained allowing the passage of gases into the duct (Fig 2). The hot gases entering the exchanger from the top are cooled quickly due to the high thermal conductivity of the steel, which releases the energy as heat to the environment. The "cold" gas becomes denser and runs down the pipe to the base, percolating the bed and exchanging heat with the hot charcoal particles. The cycle repeats as the re-heated gas exits through the bed surface.

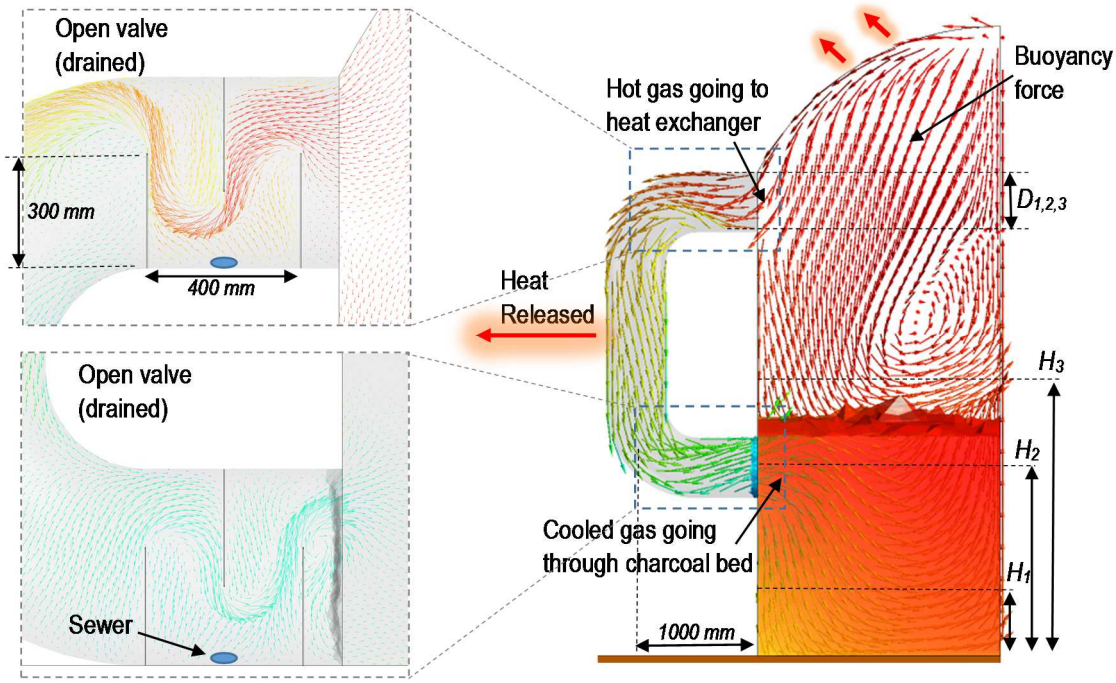

Figure 2. The principle of operation of the buoyancy-driven heat exchanger. The subscripts represent the levels of each factor.

The cooled gas percolating the bed must overcome the pressure drop due to the porous medium (Table 2). It is expected that with a lower injection position (H1) the bed cooling will be faster and more homogeneous since in addition to a larger heat exchange area (greater length of the duct), the gas will be better distributed in the lower parts of the charcoal bed. On the other hand, the lower the injection of the cooled gas, the greater resistance exerted by the bed. In this scenario reverse flow could occur affecting the efficiency of the process. In order to determine the best configuration of the heat exchanger, a 3^2 factorial design was performed. The factors were the exchanger diameter and the injection height of the cooled gas. The levels of each factor are specified in Table 1. The total heat exchange area corresponds to the area of one (1) heat exchanger multiplied by 8 (number of kiln segments).

In each experimental unit, the effect of the configuration was evaluated on the cooling time and on the cooling homogeneity, represented by the percentage of breakpoints at the end of the operation. Due to the need for mesh refinement in the valve region, which increases the computational resource, the valve effect was simulated only in the optimal diameter-height combination resulting from the statistical analysis. Finally, the combined effect of the insulation layer on the floor and the optimized heat exchanger was simulated.

Table 1. Factorial design for the effect of diameter and height of the heat exchanger on the cooling time and cooling homogeneity.

Configuration	Diameter (mm)	Height (mm)	Total heat exchange area (m^2)
C1	150	250	19.02
C2	250	250	31.69
C3	500	250	63.51
C4	150	1550	14.17
C5	250	1550	23.61
C6	500	1550	47.32
C7	150	2050	12.29
C8	250	2050	20.48
C9	500	2050	40.96

After a previous spatial convergence testing, a structured mesh of 60200 hexahedral elements and a non-structured mesh of 1029000 elements were created for the floor and

porous subdomains respectively. A time step of 60 min was chosen for discretization time.

5.2.3 Governing equations

The previously validated model adopts as main simplifications: the charcoal bed as isotropic porous medium in the condition of local thermal non-equilibrium; low-Mach number: density changes only associated with temperature variations; the intergranular gas inside the kiln is an ideal mixture of CO_2 and N_2. The governing equations of the transient model were based on the continuity, momentum and energy equations. For the porous medium:

$$\varphi \frac{\partial \rho_f}{\partial t} + \nabla \cdot \left(\rho_f \vec{v}\right) = 0 \tag{2}$$

$$\frac{\partial \left(\rho_f \vec{v}\right)}{\partial t} + \frac{1}{\varphi} \nabla \cdot \left(\rho_f \vec{v} \vec{v}\right) = -\varphi \nabla P + \mu \nabla^2 \vec{v} + \rho_f \vec{g} - \frac{\varphi \mu}{K} \vec{v} - \frac{\varphi \rho_f C_E}{\sqrt{K}} \vec{v} |\vec{v}| \tag{3}$$

$$(1-\varphi)\left(\rho C_p\right)_s \frac{\partial T_s}{\partial t} = (1-\varphi) \nabla \cdot \left(k_{ef-s} \nabla T_s\right) + (1-\varphi) q_s''' + h_i A_s \left(T_f - T_s\right) \tag{4}$$

$$C_{pf} \frac{\partial \left(\rho_f T_f\right)}{\partial t} + \nabla \cdot \left(C_{pf} \rho_f T_f \vec{v}\right) = \varphi \nabla \cdot \left(k_f \nabla T_f\right) - h_i A_s \left(T_f - T_s\right) \tag{5}$$

The transient and advective transport are represented by terms on the left-hand side in Eqs. (2-5). The last two terms of Eq. (3) correspond to the resistive force and represent the viscous and drag forces resulting from the interaction between the solid and fluid phases in the porous medium. Buoyancy force, due to the gas density changing with temperature, is represented by the term associated with the gravity vector in Eq. (3).

During the pyrolysis, heat is increasingly generated and transferred into the porous bed creating temperature gradients that promote the gas flow inside the kiln. In the porous media, the flow becomes turbulent when Re > 280 (Lesage et al., 2004). Bustos et al. (2018) calculated values of Re number varying between 250 for the porous bed and 8800 for the headspace. Then, the turbulence phenomenon was modeled using the Reynolds-Averaged Navier-Stokes (RANS) approach. In the 2D analyses, turbulence fluctuations were modeled using the standard k-ε model (Pedras and de Lemos, 2010; Saito and de Lemos, 2010).

When the heat exchanger is coupled to the kiln in the 3D analyses, the near-wall region will experience high-temperature gradients. The wall modeling strategy for this

scenario requires solving the viscous sublayer (y+ values about 1), whereby a first layer thickness of $5x10^{-4}$ m was defined and the SST k-ω model was implemented. These model has shown good performance in similar applications (Wu and lei, 2015; Miroshnichenko and Sheremet, 2018).

The diffusive term in Eq. (4) quantifies radiation and conduction between the particles (Larfeldt et al., 2000). Energy traveling as radiation through the interstitial fluid was modeled by P1 model available in CFX solver. Model parameters, including the source term of reaction heat of pyrolysis in Eq. (4), are listed in Table 2. The condition of local thermal non-equilibrium is defined by the interfacial heat transfer coefficient hi. This term was assumed to act inside the porous bed locally and it depends on the gas properties, characteristic length of particles and Nusselt number (*Nu*).

$$h_i = k_f \frac{Nu}{l} \tag{6}$$

Heat flow released through the heat exchanger is related to the convective heat transfer coefficient hHE for the internal flow in the pipe. This coefficient is dependent on the Nusselt number (NuHE), fluid properties and pipe's diameter (Eq. 7), and was calculated using the Dittus-Boelter correlation (Eq. 8) (Bergman et al., 2011).

$$h_{HE} = k_f \frac{Nu_{HE}}{D} \tag{7}$$

$$Nu_{HE} = 0.0265 Re^{4/5} Pr^{0.3} \tag{8}$$

Fourier's law defines energy transport (Eq. 9 – 10) in the walls and floor subdomains for the 2D approach. In the 3D approach Eq. (9) is suppressed since wall subdomain is modeled as a boundary condition.

$$C_{pw}\,\rho_w \frac{\partial T_w}{\partial t} = k_w \nabla^2 T_w \tag{9}$$

$$C_{pb}\,\rho_b \frac{\partial T_b}{\partial t} = k_b \nabla^2 T_b \tag{10}$$

5.2.4 Boundary conditions and interfaces– 2D analysis

No-slip condition and thermal energy conservation along the normal direction were setting as hydrodynamic conditions at the bed-wall, bed-insulation and insulation-floor interfaces (Eq. 11-13). Heat flux between the headspace inside the kiln and the inner surface walls is defined by Eq. (14).

$$-\left[k_{is}\frac{\partial T_{is}}{\partial n}\right]_{is} = \left[-k_{ef-s}\frac{\partial T_s}{\partial n} - k_f\frac{\partial T_f}{\partial n}\right]_{porous} \quad (11)$$

$$-\left[k_b\frac{\partial T_b}{\partial n}\right]_{base} = \left[-k_{is}\frac{\partial T_{is}}{\partial n}\right]_{is} \quad (12)$$

$$-\left[k_w\frac{\partial T_w}{\partial n}\right]_{wall} = \left[-k_{ef-s}\frac{\partial T_s}{\partial n} - k_f\frac{\partial T_f}{\partial n}\right]_{porous} \quad (13)$$

$$h_i\left[T_{s-i,t} - T_f\right] = k_w\frac{\partial T_{s-i,t}}{\partial x} \quad (14)$$

On the floor, an adiabatic boundary condition is set at 2 m depth and 4 m depth for the carbonization and cooling stages respectively. In the symmetry planes, normal gradients are set to zero for all quantities; on the external wall surface, a mixed boundary condition is established with outside temperature set to 25 °C. The external heat transfer coefficient hext accounts for the convection, following the experimental approach proposed by França and Campos (2002), and for the radiation, by Stefan Boltzmann law:

$$h_{ext-w}\left[T_{surf,t} - T_{\infty}\right] = k_w\frac{\partial T_{surf,t}}{\partial x} \quad (15)$$

$$h_{ext-w} = h_{conv} + h_{r-w} \quad (16)$$

$$h_{r-w} = \sigma\gamma_w T^3 \quad (17)$$

where σ is the Stefan Boltzmann constant and Υ_w is the wall emissivity. The simulation time was set to 96 hours (4 days) and 192 hours (8 days) for the carbonization and cooling stage, respectively. The first-order backward Euler and high-resolution discretization schemes were used for the transient and advective terms, respectively. The residual target was set to RMSE < 10^{-6}.

5.2.5 Boundary conditions and interfaces– 3D analysis

In the simulations of the kiln cooling with the coupled heat exchanger, the boundary conditions were the same as those adopted for the two-dimensional case. Only Eq. (15) was omitted and Eq. (14) was modified by replacing the heat diffusion through the physical wall with a global heat transfer coefficient U_w:

$$h_i\left[T_{s-i,t} - T_f\right] = U_w\left[T_{surf,t} - T_{\infty}\right] \quad (18)$$

$$U_w = 1/R_w \tag{19}$$

$$R_w = \frac{L_w}{k_w} + \frac{1}{h_{ext-w}} \tag{20}$$

where R_w is the total resistance at wall boundary and L_w is the wall thickness. In a similar approach, heat flow rate through the heat exchanger wall was modeled using a global heat transfer coefficient U_{HE} using the Churchill relation for Nusselt number (Bergman et al., 2011):

$$h_i\left[T_{s-i,t} - T_f\right] = U_{HE}\left[T_{surf,t} - T_\infty\right] \tag{21}$$

$$U_{HE} = 1/R_{HE} \tag{22}$$

$$R_{HE} = \frac{r_o ln(r_o/r_i)}{k_{HE}} + \frac{1}{h_{ext-HE}} \tag{23}$$

$$h_{ext-HE} = h_{conv-HE} + h_{r-HE} \tag{24}$$

$$h_{r-HE} = \sigma \varepsilon_{HE} T^3 \tag{25}$$

$$\mathrm{h_{conv-HE}} = \mathrm{k_{air}} \frac{\mathrm{Nu_{ex-HE}}}{\mathrm{D}} \tag{26}$$

$$\mathrm{Nu_{ex-HE}} = 0.3 + \frac{0.62 \mathrm{Re_{ex}}^{1/2} \mathrm{Pr_{air}}^{1/3}}{[1 + (0.4/\mathrm{Pr_{air}})^{2/3}]^{1/4}} \left[1 + \left(\frac{\mathrm{Re_{ex}}}{282000}\right)^{5/8}\right]^{4/5} \tag{27}$$

$$\mathrm{Re_{ex-HE}} = \frac{\mathrm{v_{air}} \mathrm{D}}{\vartheta_{\mathrm{air}}} \tag{28}$$

where R_{HE} is the total resistance at the heat exchanger external boundary, r_o and r_i are the external and internal diameter of the heat exchanger and ε_{HE} is its emissivity. v_{air} and ϑ_{air} are the velocity and kinematic viscosity of the air respectively. The first-order backward Euler and high-resolution discretization schemes were used for the transient and advective terms, respectively. The residual target was set to RMSE < 10-6. The simulation time was set until the charcoal bed reached an average temperature of 60°C.

Table 2. Model parameters

Wall (brick fireclay) (Bergman et al, 2011)	value
c_{pw} [J kg^{-1} K^{-1}]	960
k_w [W m^{-1} K^{-1}]	1,0
ρ_w [kg m^{-3}]	2645
ε_w	0.94
L_w [m]	0.24
Clay floor (Bergman et al, 2011)	
c_{pb} [J kg^{-1} K^{-1}]	880
k_b [W m^{-1} K^{-1}]	1,29
ρ_b [kg m^{-3}]	1450
Insulation layer (Engecast1050®)	
k_{is} [W m^{-1} K^{-1}]	0,13
Thickness [mm]	30
Porous media (fluid phase) (Saito and de Lemos, 2010)	
CO_2 thermophysical properties	Ansys CFX database
N_2 thermophysical properties	Ansys CFX database
Porous media (solid phase) (Santos, 2013; Pan and Kong, 2017; Bergman et al, 2011)	
c_p *wood* [J kg^{-1} K^{-1}]	2385
k wood [W m^{-1} K^{-1}]	0,19
ρ *wood* [kg m^{-3}]	540
c_p *charcoal* [J kg^{-1} K^{-1}]	1017
k charcoal [W m^{-1} K^{-1}]	0,03
Apparently density of charcoal [kg m^{-3}]	457
l [m]	0.13
Ψ	0,9
d_{pore} [μm]	350
Porous media (Santos, 2013; Daugaard and Brown, 2003)	
Φ	0,6
A_s [m^{-2}]	65
Nu	$2+(1.1*Pr^{0.33}*Re^{0.6})$
$\Delta P/l$ [Pa m^{-1}]	$24V+343V^2$
q'''[W m^{-3}] (standard configuration)	1185
Heat exchanger – Carbon steel layer (Bergman et al, 2011)	
k_{HE} [W m^{-1} K^{-1}]	55
L_{HE} [mm]	3.2
ε_{HE}	0.65
Carbonization time [h]	96
Cooling time (standard configuration) [h]	192

5.3 RESULTS

5.3.1 2D simulations

Figure 3A shows the temperature profile of the kiln operating in standard condition at the end of the carbonization stage. In Fig 3B it is shown the effect of application of a 30 mm insulation layer over the floor at the end of the carbonization stage (4 days). When the insulation layer is coupled to the kiln, the heat source in Eq. (4) can be adjusted to a 6% lower value. A temperature difference of approximately 100 °C can be noticed in the first floor's layers between the two cases compared. Eq. (11) and (12) defines the heat flux through the bed-floor interface as depending on the thermal conductivity of the insulation layer. Since this value is ten times lower than the thermal conductivity of the clay floor (Table 2), the energy released from the charcoal bed under pyrolysis hardly crosses the interface, reflecting in a lower heat diffusion through the floor (Fig. 3B and 4A).

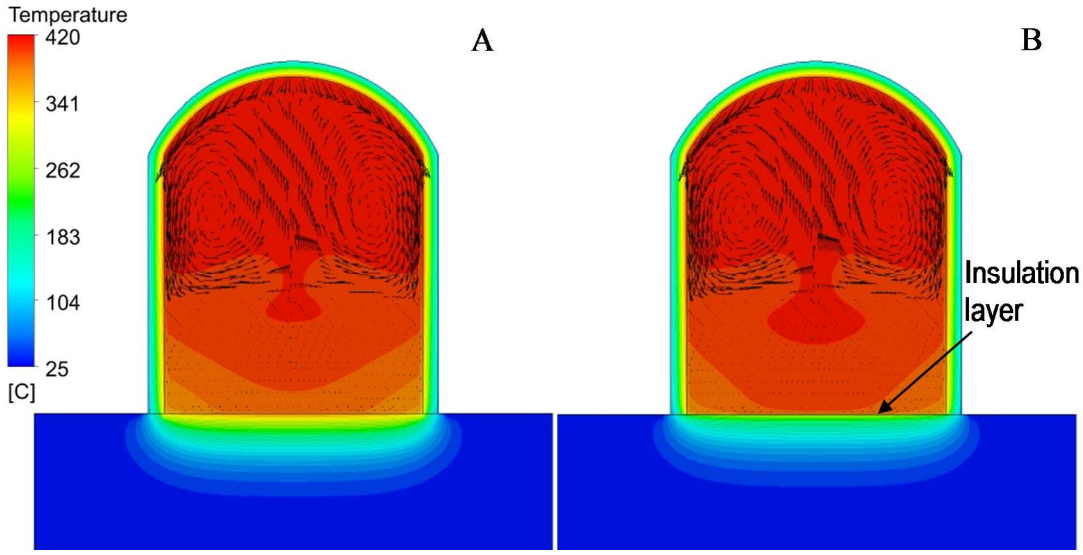

Fig 3. Temperature distribution of the fluid phase of the charcoal bed, walls and floor at the end of carbonization stage (4 days). A) standard configuration B) insulation layer over the floor.

The heat losses during the process can be observed in Fig 4A. When the insulation layer is used, the heat flows through the floor and walls during carbonization stage are reduced by 56.5% and 18.5%, respectively. During the second day of cooling under standard conditions, the heat flow reverses its direction and the bed begins to receive heat from the floor. As observed in Fig 4A, this phenomenon is minimized and delayed with the insulation layer application. The heat flow rate through the walls declines

exponentially during the cooling for both configurations. Perhaps a slightly higher decline is noticed when the insulation layer is adopted (Fig 4A), the less heat re-absorbed from the floor reflects in a reduction of 25.5% (approximately 2 days) in the cooling time (Fig 4B). Furthermore, with the application of the insulation layer, the breakpoints were reduced from 17.4% to 7.6%, considering a target cooling temperature of 60 °C.

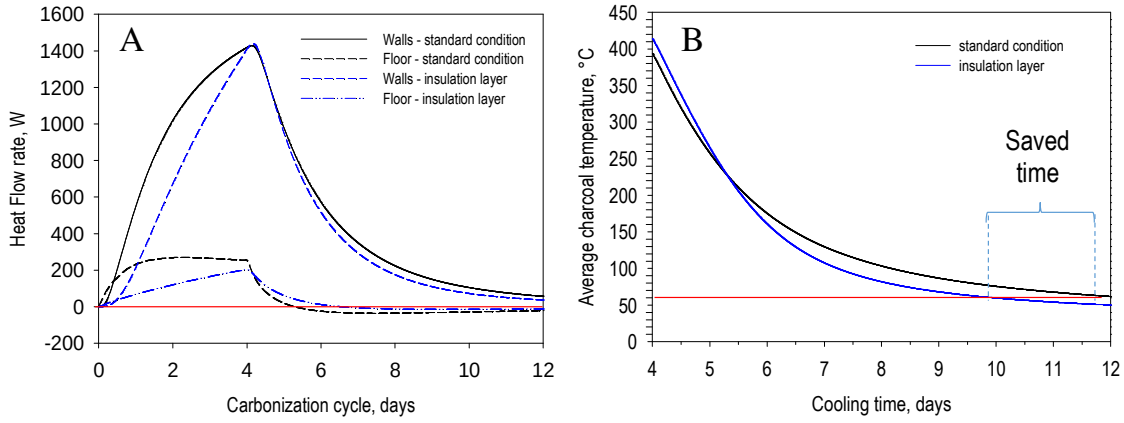

Fig. 4. A) Heat flow rate at walls and floor during the carbonization cycle. Red line demarcates the time when heat flow reverse from floor to the bed. B) Kiln cooling profile. Red line is the average target temperature of charcoal at the end of cooling stage (60°C).

5.3.2 3D simulations

Fig. 5A shows the temperature distribution of a kiln segment (Fig. 1D) under standard conditions at the end of the cooling stage (8 days). At this point, the kiln is ready to open for charcoal discharge. It could be noticed the cooling front advancing from top to the bottom as the gases in the headspace dissipate heat through the walls and becomes cold. As a consequence of the heat diffusion through the floor during the carbonization stage, a hot region can be observed in the underground. The reversed heat flow from the floor impedes the cooling of the charcoal bed in regions close to the ground. As depicted in Fig. 5B, a considerable volume of charcoal (17.4%) closed to the kiln floor remains with a high risk of ignition (temperature above 65°C) during the product discharge. This result agrees with observations in practice when some regions of the charcoal bed burn during the kiln opening.

As the cooling proceeds, the temperature of the bed surface decreases and the Rayleigh number drops to a critical value (1708) around the fifth day of cooling (Fig. 6). Then, the buoyancy force cannot overcome the viscous forces and the advection becomes

negligible. This condition hampers the operation, resulting in long cooling times as reported in Table 3.

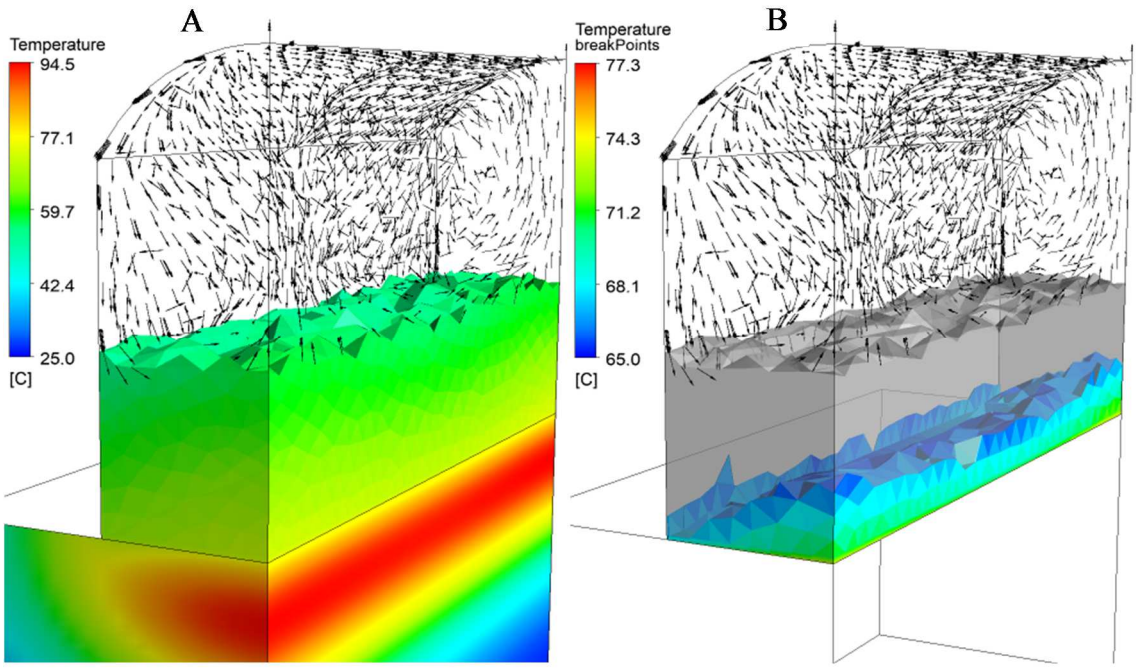

Fig 5. (A) Temperature distribution of a standard configuration kiln at the end of cooling stage (192 h) and (B) charcoal bed volume (in color) above the breakpoint temperature (65 °C).

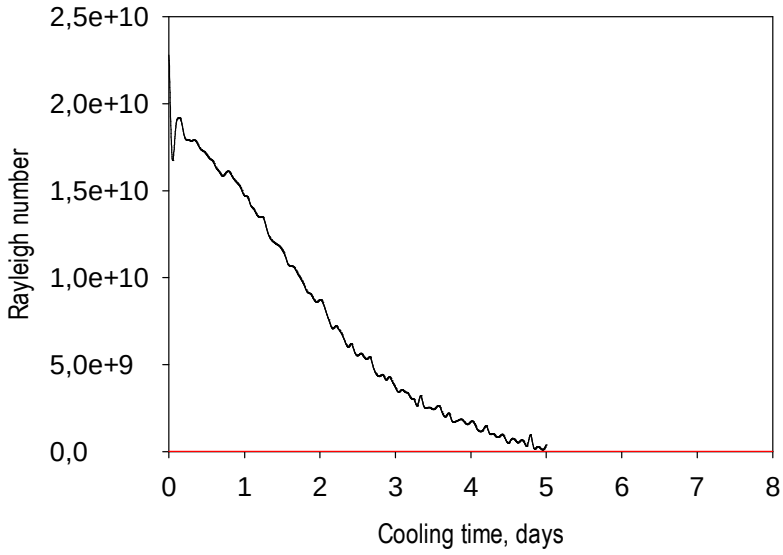

Figure 6. Raylegh number during kiln cooling under standard conditions. Red line demarcates the critical value (1708).

With the coupling of the heat exchanger driven by natural convection, the buoyancy force inside the kiln was increased, maintaining a turbulent regime throughout the cooling ($Ra > 5x10^{10}$). That reflected in higher heat transfer rates and consequently lower cooling times. Table 3 summarizes the main results of 3D simulations for kiln cooling under standard conditions and by using the heat exchanger, according to the factorial design (Table 1). The simulations were stoped when the average temperature of charcoal bed reacheed 60°C.

Table 3. Simulation results for cooling until average charcoal temperature of 60 °C

Configuration	Heat Exchange size (mm)		Cooling time	Temperature (˚C)		Saved time (%)	Breakpoints (%)
	Diameter	Height	(days)	Var.	Max.		
Standard condition	--	--	8.00	19.20	77.00	0.00	17.43
C1	150	250	7.38	40.80	73.30	7.81	0.42
C2	250	250	6.63	42.90	76.60	17.19	5.15
C3	500	250	4.75	46.50	79.90	40.63	9.17
C4	150	1550	7.58	40.20	72.90	5.21	0.44
C5	250	1550	6.83	41.30	74.90	14.58	0.72
C6	500	1550	5.13	43.10	78.90	35.94	6.86
C7	150	2050	7.54	24.00	72.50	5.73	0.43
C8	250	2050	6.92	26.00	73.60	13.54	0.50
C9	500	2050	5.67	34.40	75.80	29.17	0.61

Results in Table 3 indicate both cooling time and homogeneity depending on the heat exchanger configuration (diameter and height). In all configurations, cooling time reductions were achieved ranging from 5 to 40%. Santos (2013), Martins (2014) and Oliveira et al. (2015) achieved reductions in cooling time ranging from 12.5 to 70% using forced convection heat exchangers operating between 5 and 10 hp. The significance of the effects observed in Table 3 is shown in Figures (7) and (8).

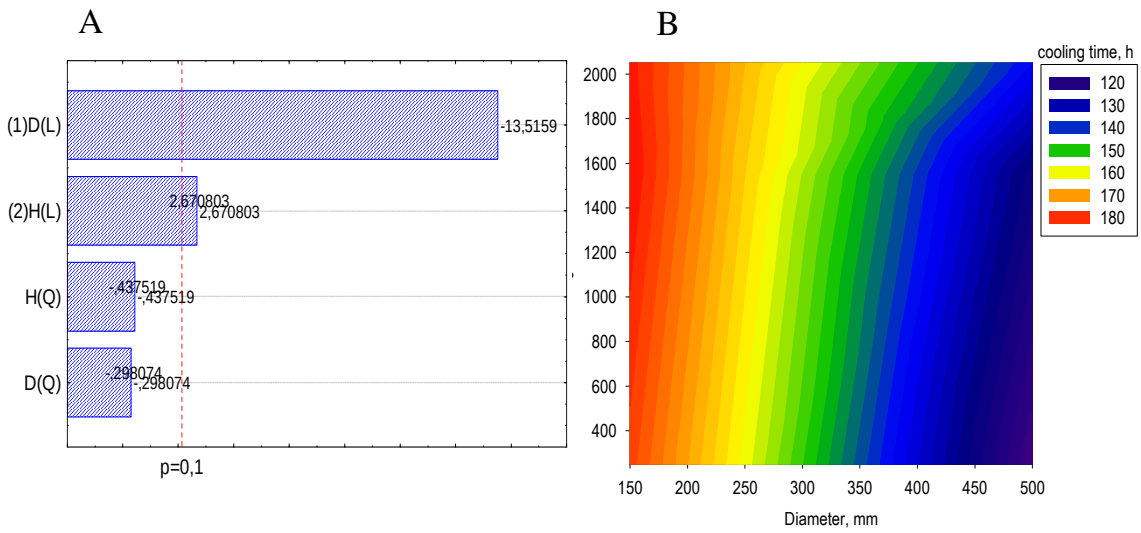

Fig. 7. Effect of Diameter (D) and Height (H) on the cooling time A) Pareto chart. B) Surface chart.

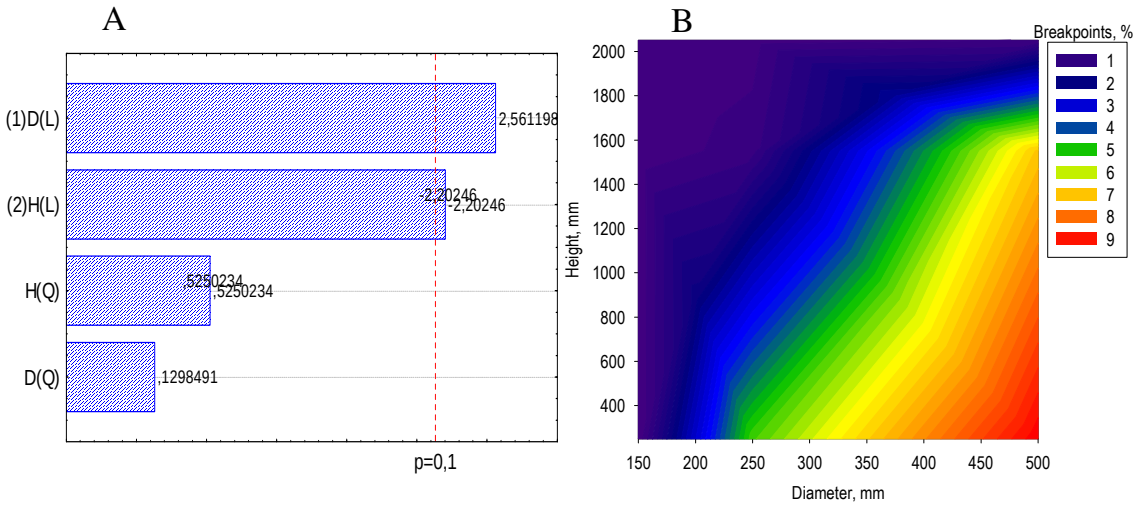

Fig. 8. Effect of Diameter (D) and Height (H) on the homogeneity of the cooling process (breakpoints). A) Pareto chart. B) Surface chart.

As seen in Fig. 7A, at 90% probability, the diameter and height of the heat exchanger have a significant effect on the cooling time. The diameter showed the main effect and as expected, because of the increase of heat exchange area, the bigger the diameter, the less cooling time (Fig 7B). The injection of cooled gas through the bottom contributes to the reduction of the cooling time (Fig 7B) by increasing the heat exchange area (length of the exchanger) and by rapidly cooling the low-central region of the bed. These results are in agreement with Martins (2014), who observed better results when the gas cooled in a forced convection heat exchanger was injected at the bottom of the

charcoal bed, although requiring a ventilation power 33% higher than required for the top injection.

In relation to homogeneity, the effect was significant and opposite to the effect on cooling time (Fig 8A). The largest charcoal volume with high ignition risk (breakpoints) was observed when the cooled gas was injected through the bottom using the largest diameter (Fig 8B). This is because the gas stream from the exchanger rapidly cools the low-central region of the bed and rises to the bed surface once reheated in the heat exchange with the charcoal particles. Thus, the advective flow does not reach the particles located in the corners, which cool slowly since only conduction and inter particle radiation occurs.

Critical values resulting from the factorial analyses indicate a point of minimum for the effect on cooling time (D = 2140 mm, H = -82 mm) and a point of maximum for the effect on breakpoints (D = 1114 mm, H = 302 mm). It is evident that the larger the diameter and the smaller the height, the shorter the cooling time, but also the less homogeneity. Before proceeding with the optimized configuration, the effect of the retention valve was evaluated on the configuration that resulted in lower cooling time (Configuration C3, Table 3).

As shown in Fig. 9, the inlet and outlet valves modified the flow pattern affecting the pressure and velocity field, and consequently the heat transfer phenomena. As expected, a pressure drop can be observed in the posterior region of the valves, where the gases tend to recirculate. Reduction in the gas flow rate at the inlet valve causes a reduction of the Reynolds number along the duct. Therefore, the Nusselt number and consequently the internal heat transfer coefficient (h) were also reduced, which decreases by more than 50%. As expected, the gas flow rate through the duct tends to decrease with the progress of cooling. Without the effect of valves, its value dropped from 0.37 to 0.13 kg s^{-1}. Considering the valves in simulation runs, the mass flow was reduced considerably varying between 0.1 and 0.03 kg s^{-1}. Besides that, the pressure drop after the outlet valve decreased the penetration of cooled gas into the charcoal bed. As a consequence, the cooling time increased by 16 hours and the breakpoints increased to 12.94% (Table 4).

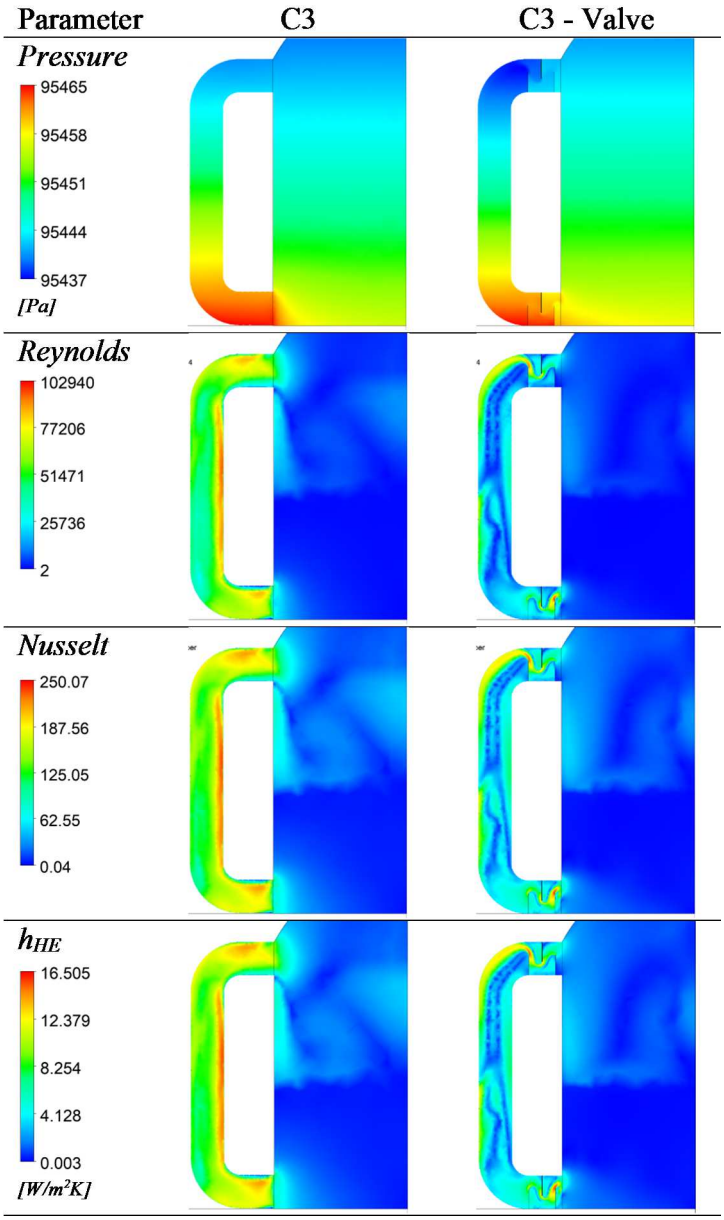

Figure 9. Effect of the retention valves on the heat exchanger performance after 12 hours of cooling. Left: configuration C3. Right: configuration C3 with retention valves.

Table 4. Retention valves effect on the cooling process. Cooling stops when average charcoal temperature reached 60 °C.

Configuration	Cooling time (days)	Temperature (˚C)		Saved time (%)	Breakpoints (%)
		Var.	Max.		
C3	4.75	46.50	79.9	40.63	9.17
C3 + valve	5.42	47.40	80.20	32.29	12.94

The internal heat transfer coefficient in the duct operating with the valves shows an average value of 4 W m^{-2} K^{-1} during the cooling, while the value for the external side was defined as constant (air flowing at 4.5 m s-1 and 25 °C) hext = 13.40 W m-2 K-1. These values indicate that the greatest resistance to heat transfer occurs at the internal side. Internal fins could decrease this resistance, but in the absence of mechanical force, the pressure drop caused by such extended surfaces could stagnate even more the gases inside the duct, hindering the heat transfer. External fins or larger diameters of the duct could increase the heat transfer area increasing the heat transfer rate. Although this condition will result in shorter cooling times, it can also result in significant volumes of the bulk with a high risk of ignition. To overcome this problem in the optimized configurations, the increase in heat exchange area was achieved by using 2 equidistant pipes. The position for the cooled gas injection was fixed at the kiln bottom (H1), the diameter was fixed to 500 mm, and the cooling time was extended until the volume of breakpoints reached a value less than 2%.

Table 5 summarized the setup of four optimized configurations. The retention valve was simulated at the inlet and outlet of the heat exchanger. The combined effect of the heat exchanger and the insulation layer on the floor was simulated in cases C11 for one pipe and C13 for two pipes.

Table 5. Configuration of optimized buoyancy-driven heat exchanger

Configuration	Diameter (mm)	Height (mm)	Number of pipes	Total Heat exchange area (m^2)	Insulation layer
C10	500	250	1	63.51	No
C11	500	250	1	63.51	Yes
C12	500	250	2	127.02	No
C13	500	250	2	127.02	Yes

Fig. 10 ilustrates the progress of the cooling front using one pipe (C10) and two pipes (C12). Near the gas injection at the bottom, regions of faster cooling can be observed. When a central pipe is used (Fig. 10A and 10B), the gas quickly cools the central region starting from the base, but breakpoints remain at the lower corners of the kiln segment. Ten hours before finishing the cooling with C10 configuration (Fig. 10A), the breakpoints correspond to 14.28% of the charcoal volume. Using two pipes, the

breakpoints 10 hours before the end of the cooling correspond to 9.94% of the volume of the charcoal (Fig. 10C). Figure 10 also shows a significant reduction of cooling time using two pipes: 37 hours less to guarantee breakpoints < 2% (Fig 10D). Table 6 displays the main results of cooling simulations for optimized cases presented in Table 5.

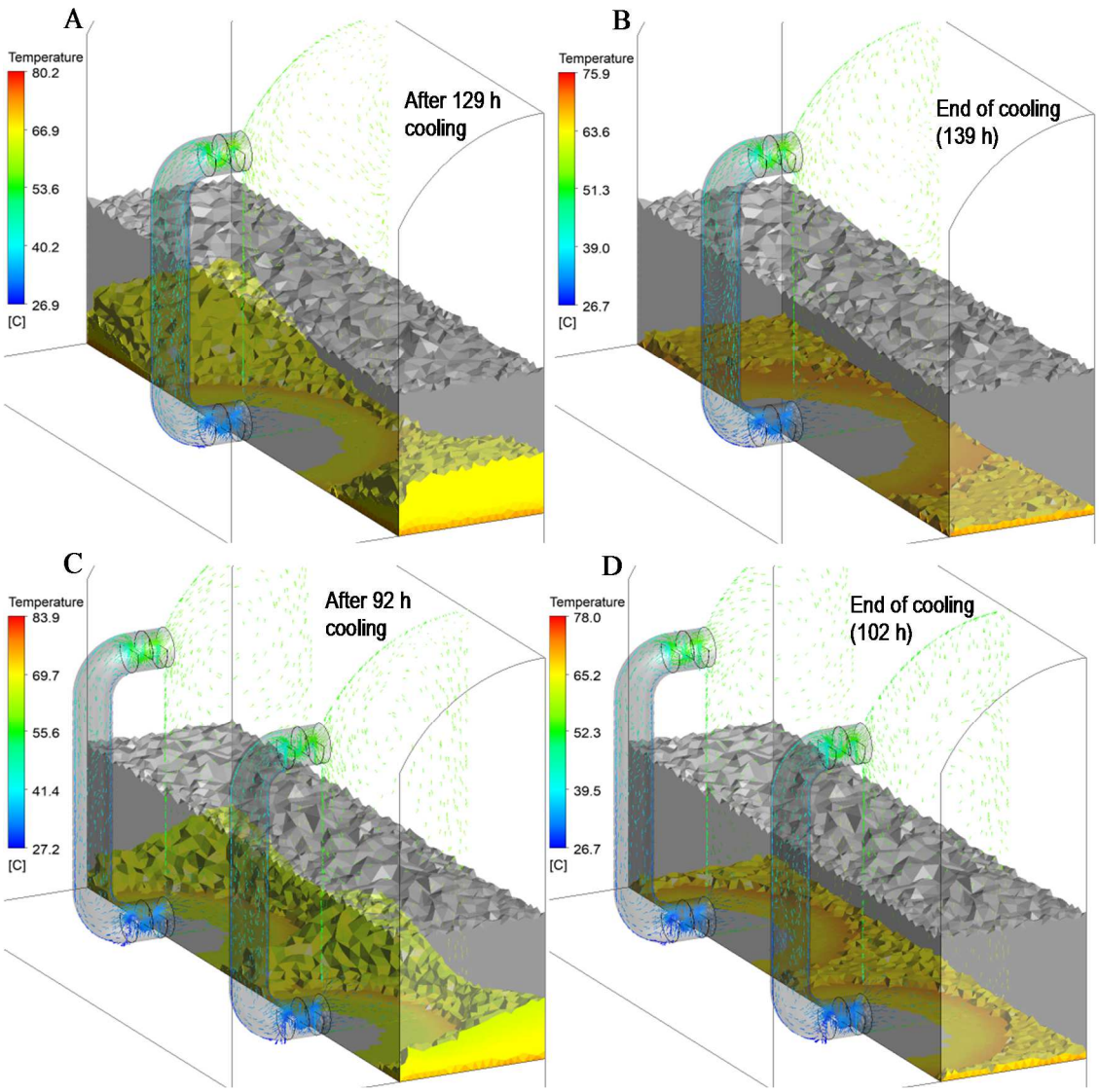

Figure 10. Kiln cooling performance in C10 configuration (A-B) and C12 configuration (C-D). The colored regions in the charcoal bed represent charcoal particles above 65 °C. The vectors indicate the gas flowing on a central plane in the heat exchanger.

Table 6. Results of kiln cooling simulations with optimized heat exchangers. Increased in productivity based on an average charcoal production of 2040 ton in a standard conditions kiln (time cooling = 192 h).

Config.	Time cooling (days)	Tmax (˚C)	T gas (°C)	Saved time (%)	Breakpoints (%)	Increase in productivity per kiln (%)
C10	5.79	75.80	54.70	27.60	1.74	22.5
C11	4.58	74.30	54.10	42.71	1.39	39.8
C12	4.25	78.00	54.00	46.88	1.63	45.4
C13	3.25	76.77	54.00	59.38	1.75	65.5

As can be seen in Table 6, the use of one heat exchanger per kiln segment (63.51 m2 of total heat exchange area) results in 27.6% reduction of cooling time. Using a forced convection gas/air type heat exchanger with 125 m2 of total heat exchange area, Oliveira et al. (2015) obtained 12.5% reduction of the cooling time. The low efficiency of this configuration is due in part to the fact that the exchanger operated with a single suction point and a single injection point at the top of the kiln. The authors slightly increased efficiency (38% reduction time) by defining a central suction point and two injection points at the upper edges of the kiln and adding a gas-water thermal exchange area (35 m2). The maximum reduction of cooling time (43%) was achieved when the authors were increased the heat exchange area to 360 m2 (330 m2 for water-gas area) and using a ventilation power of 10 hp. Comparing these results with those presented in Table 6, it is possible to verify the higher efficiency of the system proposed in this research. The vertical flow pattern created by the buoyancy-driven heat exchanger and the higher number of suction and injection points result in shorter cooling times and less risk of ignition at the opening of the kiln.

The data in Table 6 also indicates that the insulation layer improves the process by 14.5%, while the use of the double pipe increases the process efficiency by 19%. The most significant time reduction (59.38%) was achieved when the insulation layer and double pipe heat exchanger were coupled to the kiln (C13). The potential increment in the charcoal production by implementing one of the proposed cooling systems varies between 24 and 68% and is directly related to the number of heat exchangers coupled to

the kiln. The average gas temperature at the end of the cooling for the four cases was 54°C. This value can be used as a safety indicator for the kiln opening.

5.4 CONCLUSIONS

Using Computational Fluid Dynamics it was possible to simulate alternative configurations of a carbonization kiln that allowed optimizing the stages of pyrolysis and cooling in the charcoal production. The use of a 3 cm layer of insulation concrete in the bed-floor interface reduces ignition energy consumption by 6% and resulted in a time saving of 23% for the whole cycle.

The buoyancy-driven heat exchanger is an efficient alternative that does not add operational costs and allows a significant reduction of the cooling time of carbonization kilns. The retention valves necessary to avoid heat losses during the pyrolysis stage affect the overall efficiency of the heat exchanger because the increasing in the pressure drop.

The use of 8 buoyancy-driven heat exchangers (4 on each side) coupled to a carbonization kiln of 700 m^3 capacity, allows reducing the cooling time from 8 to 5.7 days. By doubling the number of coupled heat exchangers, the cooling time can decrease up to 4.6 days. The maximum time reduction (3.25 days) results from the conjugate effect of the heat exchanger (16 per kiln) and the insulation layer. Such decreases of the cooling time allow increasing the number of carbonization cycles per kiln per year, resulting in production increases of up to 65%. The results of this research allow minimizing time and costs in the development of physical prototypes of buoyancy-driven heat exchangers for carbonization kilns.

5.5 REFERENCES

Bergman T L, Lavine A S, Incropera F, Dewit D P. Fundamentals of heat and mass transfer. 7th ed. New York: John Wiley & Sons; 2011.

Biswal P, Basak T. Entropy generation vs energy efficiency for natural convection based energy flow in enclosures and various applications: A review. Renewable and Sustainable Energy Reviews. 2017;80:1412-1457.

Bustos-Vanegas J D, Martins M A, Carneiro A de C, Freitas A G, Barbosa R C. Thermal inertia effects of the structural elements in heat losses during the charcoal production in brick kilns. Fuel. 2018;226:508-515.

Daugaard D and Brown R. Enthalpy for pyrolysis for several types of biomass. Energy Fuels. 2003;17(4):934-939.

Empresa de Pesquisa Energética. Balanço Energético Nacional; 2017: 70–1.

Fick G, Mirgaux O, Neau P, Patisson F. Using Biomass for Pig Iron Production: A Technical, Environmental and Economical Assessment. Waste Biomass Valor. 2013. DOI 10.1007/s12649-013-9223-1

França, G. A. C. and Campos, M. B., 2002. Análise teórica e experimental do resfriamento de carvão vegetal em forno retangular. In: Anais do IV Encontro de Energia no Meio Rural, Campinas (SP).

IEA International Energy Agency. Global energy & CO_2 status report 2017. https://www.iea.org/publications/freepublications/publication/GECO2017.pdf (accessed November 2018).

Konkonya S, Castro-Díaz M, Barriocanal C, Snape C. An investigation into the effect of fast heating on fluidity development and coke quality for blends of coal and biomass. Biomass and Bioenergy. 2013;56:295-306.

Larfeldt J, Leckner B, Melaaen M. Modelling and measurements of heat transfer in charcoal from pyrolysis of large wood particles. Biomass & Bioenergy. 2000;18:507–14.

Lesage F, Midoux N, Lafiti M A. New local measurements of hydrodynamics in porous media. Experiments in Fluids. 2004;37:257-62.

Lin Y J P, Huang J J, Li J S. A study on buoyancy-driven flows in two series-connected chambers. Experimental Thermal and Fluid Science. 2013;48:37-48.

Martins, M. A., 2014. Desafios da implementação de periféricos na produção de carvão vegetal. In: I SEMINARIO DE CARVÃO VEGETAL. Aperam Bioenergia. Universidade Federal de Viçosa.

Miroshnichenko IV and Sheremet MA. Turbulent natural convection heat transfer in rectangular enclosures using experimental and numerical approaches: A review. Renewable and Sustainable Energy Reviews. 2018;82:40-59.

Nakahara T, Yan H, Ito H, Fujita O. Study on one-dimensional steady combustion of highly densified biomass briquette (bio-coke) in air flow. Proceedings of the Combustion Institute 35 (2) (2015) 2415-2422.

Novak L, Mantovani E, Martyn P J, Fernandes B. Efeito to tráfego de trator e da pressão de contato pneu/solo na compactação de um latossolo vermelho-escuro álico, em dois níveis de umidade. Pesquisa Agropecuaria Brasileira. 1992;27(12):1587-1595.

Oliveira, D., Teixeira, C. A., Silva, J., Reis, H. O., Vorobieff, C. L., 2010. Resfriamento rápido de fornos de carbonização. Engenharia Agrícola Jaboticabal 30 (6), 1023-1032.

Oliveira, A. C., Carneiro, A. de C., Barcellos, D. C., Rodriguez, A. V., Amaral, B. M., Pereira, B. L., 2015. Resfriamento artificial em fornos retangulares para a produção de carvão vegetal. Revista Árvore Viçosa-MG 39 (4), 769-778.

Peláez-Samaniego, M. R., Garcia-Perez, M., Cortez, L. B., Rosillo-Calle, F., Mesa, J., 2008. Improvements of Brazilian carbonization industry as part of the creation of a global biomass economy. Renewable and Sustainable Energy Reviews 12, 1063–1086.

E. G. Pereira, M. A. Martins, L. F. dos Santos, A. de C. Carneiro, Energy Assessment of Wood Pyrolysis Coproducts for Drying and Power Generation, Energy & Fuels 31 (12) (2017) 13815-13823. DOI: 10.1021/acs.energyfuels.7b02998

Pan Y, Kong S. Simulation of biomass particle evolution under pyrolysis conditions using lattice Boltzmann method. Combustion and Flame. 2017;178:21-34.

Pedras M, de Lemos M. Computation of turbulent flow in porous media using a low Reynolds k-ε model and an infinite array of transversally-displaced elliptic rods. Numerical Heat Transfer, part A. 2003;43(6):585-02.

Rezende, M. E., 2006. Produção de carvão vegetal – importância do conhecimento fundamental. Curso: Fundamentos e práticas da carbonização da biomassa, ministrado durante o Seminário: Prática, logística, gerenciamento e estratégias para o sucesso da conversão da matéria lenhosa em carvão vegetal para uso na metalurgia e indústria. – Belo Horizonte, novembro 27-28.

Saito M, de Lemos M. A macroscopic two-energy equation model for turbulent flow and heat transfer in highly porous media. International Journal of Heat and Mass Transfer. 2010;53:2424-33.

Santos I. Resfriamento artificial de carvão vegetal em fornos de alvenaria [dissertation]. Universidade Federal de Viçosa; 2013.

Worldsteel Association. 2018. Steel Facts. https://www.worldsteel.org/about-steel/steel-facts.html (accessed November 2018).

Wu T and Lei C. On numerical modelling of conjugate turbulent natural convection and radiation in a differentially heated cavity. International Journal of Heat and Mass Transfer. 2015;91:454-466.

Yang X, Zhong K, Kang Y, Tao T. Numerical investigation on the airflow characteristics and thermal comfort in buoyancy-driven natural ventilation rooms. Energy and Buildings. 2015. http://dx.doi.org/10.1016/j.enbuild.2015.09.071

6. GENERAL CONCLUSIONS

In order to achieve a sustainable production of charcoal, a close interaction between the producing companies and the academy is indispensable. In addition to the improvements already achieved in the use of carbonization gases for energy cogeneration, there is a window to optimize the production cycle, making the cooling stage more efficient. To fulfill this is necessary a deep knowledge regarding the physical-chemical phenomena occurring simultaneously within the charcoal bed and its interaction with the structural elements of the kiln.

The systems based on forced convection heat exchangers are presented as a viable alternative to reduce cooling time by about 50% without affecting the charcoal quality. However, the additional cost due to the operation of pumps or fans must be taken into account in calculating the kiln's operating efficiency.

The thermal inertia of the structural elements of the brick kilns has a big impact on the thermal performance of the carbonization and cooling stages. The temperature profile in the brick walls showed a pseudo-steady state behavior that allows modeling this subdomain using the thermal resistance method. This approach can reduce computational time in simulations using the CFD method. The analysis of the heat flux through the structural elements of the kiln allows the quantification of the heat losses in each stage of the process. The bed-floor interface cannot be considered adiabatic. The floor can be only considered as adiabatic at 2 m depth during the carbonization stage and at 4 m depth during the cooling. The time when the charcoal bed begins to absorb heat from the floor is crucial for the design of carbonization and cooling systems, evaluating different materials and configurations for their optimization.

The charcoal oxidation during the cooling is a phenomenon that due to its exothermicity, has a significant effect on the cooling time. The higher the temperature and O_2 concentration, the greater the intensity of the oxidation reactions. The activation energy for this phenomenon was independent of the initial oxygen concentration and slightly influenced by the advective mechanism. The oxidation reaction was observed when the charcoal temperature reached 67.5 °C at 20.9% of O_2 and increased to 167.7 °C in atmospheres with 10% of O_2.

The buoyancy-driven heat exchanger is an efficient alternative that doesn’t demand operating costs and allows a considerable reduction of the cooling time of

carbonization kilns. The use of 8 buoyancy-driven heat exchangers (4 on each side) coupled to a carbonization kiln of 700 m^3 capacity, allows reducing the cooling time from 8 to 5.7 days. Doubling the number of coupled heat exchangers, the time can decrease up to 4.6 days. The maximum time reduction (3.25 days) results from the conjugate effect of the heat exchanger (16 per kiln) and the insulation layer over the floor. Such decreases in the cooling time allow increasing the number of carbonization cycles per kiln per year, reflecting on production increases of up to 65%.

Since the buoyancy-driven heat exchanger does not require an external force (fan) to direct the gas flow, a smaller pressure difference between suction and injection is created. This condition should result in less air infiltration by cracks and consequently lower ignition risk when compared to systems based on forced convection. For future studies, it is recommended to couple the rates of heat generation and O_2 consumption derived from these study to mathematical models that attempt to simulate the heat transfer phenomena during storage and cooling process.